Universitetet i Stavanger

FACULTY OF SCIENCE AND TECHNOLOGY

MASTER'S THESIS

Study programme/specialisation: Petroleum Engineering/ Drilling Engineering	Spring semester, 2017 Open
Author: Morten Lund Olsen	……... (signature of author)
Programme coordinator: Supervisor: Dr. Jan Aage Aasen	
Title of master's thesis: **Modelling of Slurry Transport in Horizontal Openhole Gravel Packing**	
Credits: 30 ECTS	
Keywords: Openhole gravel pack Sediment in work string Alpha wave modelling Critical velocity Full-scale experiment	Number of pages: 126 + supplemental material/other: 19 Stavanger, June 28/2017

(This page intentionally left blank)

Modelling of Slurry Transport in Horizontal Openhole Gravel Packing

Morten Lund Olsen

June 28, 2017

(This page intentionally left blank)

ABSTRACT

The objective of this work is to study slurry transport in horizontal openhole gravel packing and to investigate the process of sedimentation, both inside work string and for alpha wave.

An attempt to quantify the amount of gravel deposited in the work string is made, since control of the gravel consumption is vital for the outcome of the operation, and uncontrolled sedimentation can cause unnecessary confusion during the packing process. A practical and straightforward method to quantify the gravel deposition in horizontal section of the work string is presented. Sedimentation is strongly affected by internal pipe diameter and pump rate, and these parameters should be carefully evaluated through operational planning. The utilization of the presented model could aid in designing the slurry transport, by selecting the ideal pump rate and work string specifications. Modelling for typical pipe sizes shows a lower limit for the pump rate where sedimentation arises.

Alpha wave design is a key factor for successful gravel packing, and the models typically used are either based on small-scale experiments or not specifically developed for gravel packing. Gruesbeck et al., Penberthy et al. and Oroskar and Turian models were used in this thesis to find the critical flow velocity. Estimating the actual flow velocity above alpha dune was performed using Gruesbeck et al. pressure drop balance and a proposed method for describing the flow rate split between the annuli. This allowed finding the corresponding alpha dune gravel fill for the distinct models. The true volumetric gravel fill percent was found based on data from the actual field case and compared to the modelled. Gruesbeck et al. showed the best fit. Oroskar and Turian model was not developed for gravel packing purpose, and results showed that it may not be suitable for the eccentric annular configuration encountered.

Modelling of flow velocity was done using friction loss based on wall roughness, and it is believed to represent the overall friction, rather than characterize the borehole wall. Results from the work string modelling suggest that the phenomenon of bed surface friction needs to be investigated further for alpha wave. It is a considerable contributor to the frictional pressure loss, especially for higher gravel fill percentages. Using borehole wall roughness to calculate friction factor might not give the best representation of the reality. To verify the flow rate split and investigate the bed friction influence, a full-scale experiment involving true diameters of screens and washpipe should be conducted, and a proposal for this is given in the thesis.

(This page intentionally left blank)

TABLE OF CONTENTS

(This page intentionally left blank)

LIST OF FIGURES

(This page intentionally left blank)

LIST OF TABLES

(This page intentionally left blank)

NOMENCLATURE

A	area of pipe cross-section	[m^2]
A_{ab}	cross-sectional area influenced by bed	[m^2]
A_{aw}	cross-sectional area influenced by pipe wall	[m^2]
A_b	cross-sectional area of bed	[m^2]
A_g	cross-sectional area of gravel fill	[m^2]
A_o	cross-sectional discharge area above bed	[m^2]
A_p	cross-sectional area of pipe	[m^2]
A_{pw}	area of pipe wall	[m^2]
A_{sector}	area of circle sector	[m^2]
A_{so}	cross-sectional area of screen/openhole annulus	[m^2]
$A_{triangle}$	area of triangular section of pipe cross-section	[m^2]
A_{wp}	cross-sectional area of screen/washpipe annulus	[m^2]
C	volumetric solids concentration	[-]
C_b	volumetric bed concentration	[-]
C_D	drag coefficient	[-]
C_{vab}	mean spatial concentration in area A_{ab}	[-]
C_{vabc}	contact-load portion of C_{vab}	[-]
C_{vd}	mean delivered concentration	[-]
C_μ	uniformity coefficient	[-]
C_*	gravel concentration above bed at equilibrium	[-]
dL	incremental length	[m]
dP	differential pressure	[Pa]
$\left(\frac{dP}{dL}\right)$	pressure drop gradient	[Pa m^{-1}]
$\left(\frac{dP}{dL}\right)_a$	acceleration pressure drop gradient	[Pa m^{-1}]
$\left(\frac{dP}{dL}\right)_f$	frictional pressure drop gradient	[Pa m^{-1}]
$\left(\frac{dP}{dL}\right)_h$	hydrostatic pressure drop gradient	[Pa m^{-1}]
d_p	particle diameter	[m]
d_{50}	median particle diameter	[m]
d_{85}	particle diameter larger than 85 weight percent of distribution	[m]
D	internal diameter of pipe	[m]
D_e	external diameter of pipe	[in]
D_h	hydraulic diameter	[m]
D_{ho}	hydraulic diameter screen/openhole annulus	[m]

D_{hwp}	hydraulic diameter screen/washpipe annulus	[m]
D_{h*}	hydraulic diameter screen/openhole annulus at equilibrium	[m]
D_i	outer diameter of inside conduit	[m]
D_o	inner diameter of outside conduit	[m]
D_p	internal diameter of pipe	[m]
D_s	outer diameter of screen	[m]
D_{si}	inner diameter of screen	[m]
D_w	wellbore diameter	[m]
D_{wp}	outer diameter of washpipe	[m]
D_{50}	median formation particle diameter	[m]
f	Fanning friction factor	[-]
F_B	buoyant force	[N]
F_D	drag force on particle	[N]
F_{DW}	frictional drag force on pipe wall	[N]
F_G	gravitational force	[N]
g	acceleration due to gravity 9.81 m s^{-2}	
g_f	acceleration due to gravity 32.2 ft s^{-2}	
h	hydraulic head	[m]
i	hydraulic gradient	[m.w.c/m]
i_m	mixture hydraulic gradient	[m.w.c/m]
k_s	hydraulic roughness of top of bed	[m]
K	empirical coefficient	[-]
L	characteristic length	[m]
L_p	pipe length	[m]
m_b	mass of sediment bed	[kg]
m_{fso}	mass of fluid in screen/openhole annulus	[kg]
m_{fwp}	mass of fluid in screen/washpipe annulus	[kg]
m_g	mass of gravel	[kg]
m_{gf}	mass of gravel and fluid	[kg]
m_s	mass of sand sample	[kg]
$\dot{m}$	mass rate of solids	[kg s^{-1}]
n	empirical coefficient	[-]
N_{Re}	Reynolds number	[-]
O	wetted perimeter	[m]
O_b	wetted perimeter of bed surface	[m]
O_w	wetted perimeter of pipe wall	[m]
P_{dyn}	dynamic pressure	[Pa]
q_s	solids flux	[m^2 s^{-1}]
Q_f	flow rate of carrier fluid	[m^3 s^{-1}]
Q_{fl}	rate of fluid loss to formation	[m^3 s^{-1}]
Q_{lpm}	pump rate	[lpm]

Q_m	initial injection flow rate of mixture	[$m^3 s^{-1}$]
Q_s	flow rate of solids	[$m^3 s^{-1}$]
Q_{wp}	fluid flow rate in screen/washpipe annulus	[$m^3 s^{-1}$]
Q_*	mixture flow rate above bed at equilibrium	[$m^3 s^{-1}$]
Re_p	particle Reynolds number	[-]
$\mathrm{Re}_{p'}$	particle Reynolds number used in Eq. 3-24 and 3-25	[-]
R_{ha}	hydraulic radius of discharge area A_a	[m]
R_{hb}	hydraulic radius of sub-area A_{ab}	[m]
R_{hw}	hydraulic radius of sub-area A_{aw}	[m]
R_{sd}	relative submerged density of particle	[-]
t	wall thickness pipe	[in]
T_p	pumping time	[s]
u_{*b}	bed shear velocity	[m s^{-1}]
v	fluid velocity	[m s^{-1}]
v_a	mean velocity in discharge area	[m s^{-1}]
v_b	bed velocity	[m s^{-1}]
v_c	critical velocity of slurry	[m s^{-1}]
v_{ls}	line speed	[m s^{-1}]
v_m	mean velocity in entire cross-section of pipe	[m s^{-1}]
v_o	mixture velocity in screen/openhole annulus	[m s^{-1}]
v_t	terminal settling velocity of particle	[m s^{-1}]
v_{wp}	fluid velocity in screen/washpipe annulus	[m s^{-1}]
v_*	mixture velocity above bed at equilibrium	[m s^{-1}]
v_α	alpha wave velocity	[m s^{-1}]
v_1	critical velocity according to Penberthy et al.	[m s^{-1}]
v_2	critical velocity according to Penberthy et al.	[m s^{-1}]
V_s	volume of sand particles	[m^3]
V_{so}	volume of screen/openhole annulus	[m^3]
V_t	total volume occupied by sand sample	[m^3]
V_w	internal volume of work string	[m^3]
V_{wp}	volume of screen/washpipe annulus	[m^3]
x	fraction of eddies according to Oroskar and Turian	[-]
x_1, x_2, x_3, x_4	empirical coefficients	[-]
y_b	bed height, vertical position of bed in pipe cross-section	[m]
α	empirical coefficient	[-]
β	empirical coefficient	[-]
γ	angle of vertical position of top of bed in pipe cross-section	[rad]
ε	absolute roughness	[m]
ε_{OH}	absolute wall roughness screen/openhole annulus	[m]
ε_{wp}	absolute wall roughness screen/washpipe annulus	[m]
η	packing density	[-]
Θ	Shields parameter	[-]

Θ_{cr}	critical Shields parameter	[-]
κ	Kármán constant	[-]
λ	Darcy-Weisbach friction factor	[-]
λ_a	Darcy-Weisbach friction factor for area A_a	[-]
λ_b	Darcy-Weisbach friction factor for area A_{ab}	[-]
λ_o	Darcy-Weisbach friction factor of screen/openhole annulus	[-]
λ_w	Darcy-Weisbach friction factor for area A_{aw}	[-]
λ_{wp}	Darcy-Weisbach friction factor of screen/washpipe annulus	[-]
λ_*	Darcy-Weisbach friction factor of screen/openhole annulus at equilibrium	[-]
μ	fluid viscosity	[kg $m^{-1}s^{-1}$]
μ_d	median value of distribution	
μ_f	dynamic viscosity of fluid	[kg $m^{-1}s^{-1}$]
μ_m	viscosity of mixture, corrected for solids concentration	[kg $m^{-1}s^{-1}$]
μ_r	relative viscosity of mixture	[-]
ν_f	kinematic viscosity of fluid	[m^2 s^{-1}]
ρ	density	[kg m^{-3}]
ρ_{bulk}	bulk density of solids	[kg m^{-3}]
ρ_f	density of fluid	[kg m^{-3}]
ρ_m	density of mixture	[kg m^{-3}]
ρ_s	density of solid particles	[kg m^{-3}]
σ	standard deviation of distribution	
σ_y	yield stress	[psi]
τ_b	bed surface shear stress	[Pa]
τ_w	wall shear stress	[Pa]
φ	solids internal friction angle	[deg]
Φ	Einstein transport parameter	[-]
ψ	incremental pressure drop from presence of solids	[Pa m^{-1}]
ω	empirical coefficient	[-]
ϕ	porosity	[-]

SI METRIC CONVERSION FACTORS

To convert from	To	Multiply by	
bar	psi (lbf/in^2)	1.45037744	E + 01
bar	pascal (Pa)	1.0	E + 05
centipoise	pascal second (Pa-s)	1.0	E – 03
foot	meter (m)	3.048	E – 01
inch	meter (m)	2.54	E – 02
minute	second (s)	6.0	E + 01
pound (lbm)	kilogram (kg)	4.5359237	E – 01
gallon	$meter^3$ (m^3)	3.875	E – 03

(This page intentionally left blank)

ABBREVIATIONS

DC	Drill Collar
DIF	Drill-in fluid
DP	Drill Pipe
HWDP	Heavy Weight Drill Pipe
ID	Internal Diameter
lpm	liters per minute
LPS	Laser Particle Size
LDV	Limit Deposit Velocity
OD	Outer Diameter
OH	Open Hole
OHGP	Openhole gravel pack
RCP	Random Close Packing
RLP	Random Loose Packing
TVD	True Vertical Depth
WWS	Wire-wrapped screen

(This page intentionally left blank)

ACKNOWLEDGEMENTS

I am now at the end of my studies in petroleum technology, and it has been a most meaningful and interesting time of my life. I am grateful for the service I have been given from the lecturers and other employees at the Institute of Petroleum Technology during my years at the University of Stavanger. They have been very helpful, as I have worked full-time offshore and sometimes have needed adaption of my studies.

I want to thank Dr. Jan Aage Aasen, my academic supervisor, for his help and guidance during my work on this Master's thesis. His door has always been open, both when I have been in need for aid in the technical matters and also when I have needed motivation through tough times.

Thanks to my fellow students. You have inspired me and given me many good memories and laughs. I will miss our frequent matches of table tennis.

I am grateful for the support I have gotten from my parents during the time of studies. You have been most helpful and encouraged me when needed.

Finally, I would like to express gratitude to my wife for making the studies possible, as she has taken care of home and family over these years. Her patience has been immense when I have been away for longer periods, alternating between offshore work and the university. After finishing the Bachelor's studies, we have brought two children into this world. They have given me a world of joy and happiness, and there has not been a bad day they could not lighten up with their smiles. You are my true motivation.

(This page intentionally left blank)

1 BACKGROUND OF THESIS

Gravel packing can be a cost-effective completion method for sand control in unconsolidated reservoir formations and ensures high productivity in long horizontal wells. The gravel pack operation is normally done with circulating pack and alpha-beta wave propagation for horizontal OHGP.

Several models describing the gravel pack process exist and have been used, but only some of them were made solely for this purpose. They are in general empirical, based on experiments in smaller than reality scale models. Gruesbeck et al. and Penberthy et al. presented models for calculating the critical velocity of gravel transport based on such experiments[1, 2]. Other critical velocity models, not specifically made for gravel packing, have also been used for this purpose in other theses. Oroskar and Turian model is an example of this; a semi-mechanistic model made for the general slurry transport in circular conduits[3]. The gravel packing involves geometries and fluid rheology that might be outside the intended purpose of such models, and caution has to be made utilizing them for gravel packing.

Critical flow velocity is a vital parameter of the alpha wave model presented in this thesis, so comparison will be made for the three different and normally encountered critical velocity models.

1.1 Study objectives and methodology

The objective of this work is to study slurry transport in horizontal OHGP and to investigate the process of sedimentation, both in work string and in alpha dune outside the sand screens. Gravel will settle out of the fluid if the energy needed for transportation is not attained. In the work string, this deposition is not preferred as the operational goal is to transport the gravel to the area between the screens and the borehole wall. For the alpha dune, the settling and deposition of gravel is the objective, and one would try to control the process to achieve a successful gravel pack.

Only horizontal configuration will be considered for both these cases. This is the overall limitation of the thesis. First the problem of sedimentation inside the work string during gravel displacement will be addressed, as this was experienced by a NCS operator during their gravel packing operations. By making use of a slurry transport model made for practical engineering purposes, the amount of gravel accumulation in the work string is quantified and recommendations on the pump rate and work string diameter can be given.

Control of the amount of gravel pumped is important for the overall operational success, and avoidance of gravel deposition in the work string is preferred.

For the gravel packing process itself, a method for modelling and designing the alpha dune height is proposed, using Gruesbeck et al. model for balancing the frictional pressure losses in both involved annuli. The flow rate split between the annuli will be handled as varying with the alpha dune height throughout the iteration, and not like in earlier work in other Master's theses on the subject. Operational data from an NCS operator is used to quantify the alpha fill percent of the gravel pack operation. The modelled mixture flow velocity above the sediment bed will be compared to the critical velocity of Gruesbeck et al., Oroskar and Turian and Penberthy et al. to give a qualitative evaluation of the accuracy of the different models.

A proposal for a real full-scale experimental set-up, with true-size diameters for drillpipe, wellbore, screens and washpipe will be presented. It can be used to verify how well the critical velocity models correspond to full-scale configuration. Experiments using realistic diameters are not known to have been conducted.

1.2 Report structure

General information of sand control and OHGP is presented in Chapter 2. It includes sand production issues, gravel pack design and theories of the circulating pack and alpha/beta wave model.

Chapter 3 contains the necessary supporting theory to set a stage for modelling of slurry transport. Terminal particle settling velocity, particle Reynolds number, drag coefficient equations for different flow regimes, basic geometry of pipe and eccentric annulus, gravel fill calculations, pressure drop theory and related equations, Reynolds number, friction factor equations and particle packing theory are presented and discussed.

The case of sedimentation inside the work string is addressed in Chapter 4, and the slurry transport model of Matoušek is used to quantify sedimentation[4]. It is intended to propose a practical method to aid in the design of gravel pack operation for eliminating the work string sedimentation.

Chapter 5 is presenting modelling of the alpha wave dune height and quantification of the gravel fill percent. Modelling using Gruesbeck et al. model is compared to other critical velocity models. The iteration method for balancing the pressure losses in the annuli with the flow rate splitting is presented, and results are compared to different critical velocity models. Verification of the modelling is done by comparison to data from a real gravel

pack job on the background of deduced actual gravel fill. An alternative approach to the proposed model is presented, showing a method to design the alpha dune to a specific gravel fill. The proposed model is then examined for sensitivity to wellbore diameter, washpipe size and fluid viscosity. To conclude the chapter, the friction factor used in the modelling is discussed.

Chapter 6 is presenting a proposal for a full-scale diameters experimental set-up, where the data and parameters from Chapter 4 and 5 will make the foundation, and calculations of the fluid and gravel requirements are shown. Experiments for both sedimentation in work string and alpha dune are proposed.

Chapter 7 presents the conclusions made from the work.

(This page intentionally left blank)

2 INTRODUCTION

Several methods to avoid and control sand production exist. Sand production can have a negative impact on the productivity of a well and should be avoided to the extent possible, either by prevention based on mechanical methods or by production strategy. In general, the different lower completion types can be divided into the following:

- Barefoot/openhole
- Cased and perforated
- Openhole screens
- Gravel pack (Cased hole and openhole)

All of these completion types can deal with sand production if the completion is adequately designed for its purpose and premises.

2.1 Sand control

Sand production is often associated with unconsolidated and poorly consolidated reservoir formations. There are several methods to cope with and prevent sand production, involving completion methods and production strategy. Production of sand can be a costly affair, leading to reduction in productivity. Costly maintenance and workovers to both surface and downhole equipment may be the outcome. Erosion from impingement of sand particles can ultimately cause equipment failure. High productivity wells with high flowing velocities are especially vulnerable to erosion problems, and premature failure of wellbore and well equipment may be encountered.

As the reservoir is depleted, there may be necessary to reduce the drawdown to avoid troublesome sand production, which in turn impacts the economy. When a well fills with sand there could be limitations to well intervention options. Removal involves wireline bailing or coiled tubing circulation. For subsea wells, well intervention and workover can be particularly expensive, as it involves vessel or rig operations. Accumulation of produced sand in surface equipment like separators and flowlines can reduce the production capabilities of the facility, and shut-in of the well may be necessary for sand removal. If the sand production is severe or is progressing over long time, the formation could collapse. In worst case, the entire well can be lost.

Sand production is dependent on rock strength, regional stresses on the wellbore and local loads on the wellbore from the presence of the hole, flow, reduced pore pressures and the presence of water[5]. The factors influencing the tendency of sand production in a well is[6]:

- Degree of formation consolidation
- Reduction in pore pressure throughout the life of the well
- Production rate
- Increase in drawdown pressure
- Reservoir fluid viscosity
- Increase of water production

In a well with no sand control equipment installed, drawdown pressure must be kept above a critical pressure to avoid production of sand. As a reservoir is depleted and the reservoir pressure decreases, the maximum available drawdown eventually reduces until there is sand production regardless of the drawdown.

2.2 Openhole gravel pack - OHGP

Originally, gravel packing was used in horizontal and deviated wells, but gained popularity for horizontal wells because of the potentially high productivity. Long horizontal reservoir sections enable a large reservoir contact area, which in many cases is preferable to drainage strategy and economics. Gravel packing is often preferred over openhole screen completion when the formation is less consolidated, due to the risk of sand production and the risk of later borehole collapse. The installation of a gravel pack will stabilize and prevent collapse of the formation, and hence control fines production. Standalone screens are prone to plugging and erosion under such conditions and may not be very well suited if high amount of fines are expected. Compared to cased hole gravel pack, the OHGP is believed to give lower skin factors than the cased hole counterpart. Additionally, the cost of installing could potentially be less because of eliminating liner running, cementing and perforating[5]. On the other hand, OHGP gives minimal opportunities for zonal isolation within the reservoir. For cased hole gravel pack, the packs can be stacked to isolate contribution from unwanted intervals.

The idea behind gravel packing is to fill the annulus between the borehole and the screens with sized gravel to hinder sand production and help stabilize the formation. The screens are sized to stop gravel from being produced. Gravel is sized to stop sand production. To prevent plugging of the pack itself, the gravel size may be designed to let fines pass through. Altogether, the installation of a gravel pack “removes” the annulus and aids in controlling the sand production.

2.2.1 Gravel selection

The selection of gravel size is a delicate balance between stopping the sand and risking plugging of the gravel pack. Saucier's criterion is much used for gavel design [7]. It states that the median formation grain diameter D_{50} should between 5 and 6 times the median gravel particle diameter d_{50}.

$$5 < \frac{D_{50}}{d_{50}} < 6 \tag{2-1}$$

Saucier advised to use median formation particle diameter to represent the ratio as a practical approach, as it is a more readily available value. His sizing criterion was indicating selection of finer gravel than what was normally used on the time. Saucier considered it to be more effective for screening the formation particles, because fines can affect the pack permeability by plugging and reduce production if the gravel particles are larger. His experiments indicated that finer packs had higher permeability than coarser packs. Also, well-rounded gravel particles showed higher permeability and less risk of plugging.

Both gravel size and formation grain size determinations are done by either sieve or laser particle size analysis (LPS). Sieve analysis uses a set of stacked sieves of different mesh sizes, where the grain sample is passed through the shaking sieves. The weight percent of particles resting on each sieve will give a cumulative size distribution of the sample. LPS analysis is quicker and more representative of the finer particles. From the cumulative size distribution the degree of sorting can be deduced. Sorting factor is given by Eq. 2-2. It is also referred to as uniformity coefficient.

$$C_{\mu} = \frac{D_{40}}{D_{90}} \tag{2-2}$$

Here, D_{40} indicates the particle diameter larger than 40 weight percent of the distribution and D_{90} is representing a diameter larger than 90 weight percent of the distribution. A uniformity coefficient greater than five is said to indicate bad sorting[6]. The sorting factor will be one of the deciding factors for gravel size.

The gravel size is given for the range of sieves used for the analysis. A 20/40 US mesh gravel sample contains particles that will go through a 20 mesh, but not a 40 mesh. This ensures a narrow range and more uniform distribution of diameters, which gives improved control to sand production. Typical mesh sizes used and the corresponding opening dimensions are given in Table 2-1[5].

Table 2-1 Typical mesh sizes and openings[5]

US mesh	Opening	
	(in)	(μm)
10	0.0787	2000
12	0.0661	1680
14	0.0555	1410
16	0.0469	1190
18	0.0394	1000
20	0.0331	841
25	0.0280	707
30	0.0232	595
35	0.0197	500
40	0.0165	400
45	0.0138	354
50	0.0117	297

Methods of measurements of the quality of gravel and minimum specifications can be found in ANSI/API Recommended Practices 19C[8]. An example of the grain size distribution, showing the difference in sorting of two samples of equal median particle diameter, is presented in Figure 2-1[6].

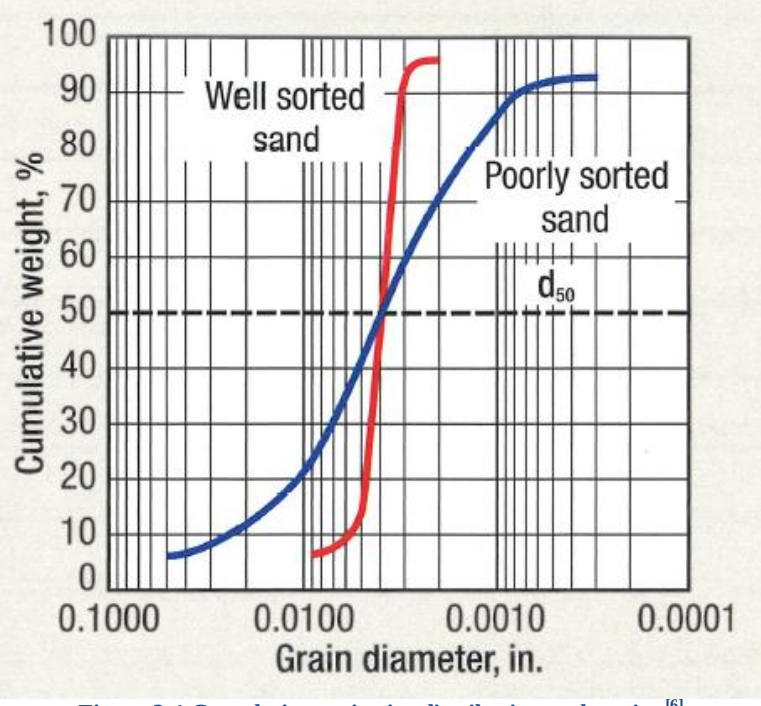

Figure 2-1 Cumulative grain size distribution and sorting[6]

2.2.2 Screen selection and screen opening design

Screen openings should be selected to hold back all the gravel in the annulus. Depending on the gravel size, fines can be transported through the pack and should not plug the screen openings. Typically, either wire-wrapped or premium screens are used. Wire-wrapped screens (WWS) consist of a base pipe with longitudinal rods welded to it, and a wedge shaped wire wrapped around and spot-welded to the rods. The opening size is determined by the gap between the consecutive rounds of wire. Premium screens are constructed with multiple woven meshes around the base pipe and a protective shroud that covers the outer mesh. Premium screens are in general more robust and therefore likely the preferred option for running in long deviated/horizontal openhole wells, which are harsher installation environments than WWS might be designed for.

2.2.3 Fluids

The reservoir can be drilled using a water-based drill-in fluid (DIF) system, consisting of sized salt brine and additives for desired functionalities. The fluid should keep the borehole stable, prevent formation damage, give filtration control, ensure adequate cuttings transportation and be compatible with reservoir and completion fluids. Additionally, the filter cake must be able to be broken down and removed. An oil based system might be used instead, as it is naturally more inhibitive with respect to shale present in the reservoir and has better lubricity than its water-based counterpart.

For horizontal OHGP, the carrier fluid for gravel transportation is normally a low viscous Newtonian brine. Additives for shale control, friction reduction and fluid loss can be added. Examples of brines used are sodium chloride, potassium chloride and sodium bromide. The brine will have a lower and upper achievable density, and the proper type must be chosen to ensure well control. The carrier fluid must be able to transport the gravel to its desired location by ensuring sufficient lift throughout transportation to prevent bridging off the annulus and associated premature screen-out. Secondly, it should separate itself from the gravel to form a compact and highly permeable pack. It must also be compatible with the formation and reduce the permeability as little as possible.

Breakers are used to break down the filter cake during or after gravel packing, to secure optimal well productivity. Acids or slow acting enzymes are used for this purpose. Breaker can be added to the carrier fluid or spotted through the pack, either through the washpipe or later by coiled tubing. There is a concern of risk of fluid loss related to breaking the filter cake, and if planned to be performed during or at the end of gravel packing, a slow acting breaker is advisable.

2.2.4 Circulating pack

There are in general two methods of installing the gravel pack in a horizontal well; circulating pack and alternate path pack. This thesis is only considering the former and alternate path pack will only be given a limited introduction. A description of the sequences for a generic horizontal circulating pack is given by Bellarby in his book "Well completion Design"[5], and is here slightly modified:

- Drill reservoir with water-based mud and displace to solids-free water-based completion brine.
- Run screens with washpipe and cross-over tool, and set gravel pack packer. It is also possible to run screens and then displace the mud to brine.
- Circulate low concentration gravel (0.5 to 2 ppa) into the annulus between the screens and formation. Gravel concentration is given as pounds of proppant added per gallon of clean fluid (ppa). The gravel will settle out and form a dune (alpha dune).
- At a critical dune height (designed at 70 to 90 percent of openhole area), the water flow above the dune is fast enough to turbulently transport the gravel.
- The dune extends along the well by dune action (alpha wave) until it reaches the toe of the well. Meanwhile, fluids are returning via the screen/openhole annulus and screen/washpipe annulus and entering the washpipe at the toe of the well for returning to surface. The alpha wave may stall or multiple waves can be created if the rate is reduced either by surface or by losses. Lower rates lead to higher, slower dunes.
- The fluid is circulated, and hence any space (rathole) beyond the end of the washpipe will receive very little gravel, and the alpha wave will stop at the end of the washpipe.
- Pressure will increase because fluid now has to travel through the pack and the screen to reach the washpipe. Gravel is then progressively packed back towards the heel of the well (beta wave).

To ensure a successful pack, the filter cake needs to stay intact during packing to prevent dehydration of the slurry and possible premature alpha wave stall. Also, rathole from previously drilled section can reduce slurry velocity and pose an increased risk of screen-out. A ratio of screen ID to washpipe OD of 0.8 is an industry rule-of-thumb to warrant the necessary flow in screen/openhole annulus to reduce risk of bridging[5].

The alternate path gravel pack is used when losses to formation are expected to be severe and cannot be avoided. Carrier fluid is viscous to limit leak-off to formation, and the gravel concentration is much higher than for circulating pack. Pump time for gravel placement is shorter and saves operational time, but the fluid system used is more expensive due to its complexity. Gravel placement does not require full returns and can be done without returns at all. The alternate path pack uses screens with shunt tubes that allow the slurry to bypass obstacles like bridged-off areas and aids in squeezing and dehydrating the gravel pack.

2.2.5 Alpha-Beta wave model

Gravel packing of horizontal OHGP with circulating pack technique can be explained by the alpha-beta wave principle. In the screen/openhole annulus, a stationary bed (dune) of settled out particles is created, and the slurry flows as a heterogeneous mixture above this bed. The dune builds and propagates along the open area for flow (alpha wave). A critical velocity for gravel transport governs this process, the velocity at which the slurry transport is in a dynamic equilibrium and the net deposition is zero. When the flow velocity of the mixture is lower than the critical velocity, the amount of particles that settle out is higher than the amount of particles picked up from the bed, and the bed height increases until the velocity eventually reaches the critical velocity. At this critical velocity, the system attains an equilibrium, and the dune moves forward from the heel to the bottom of the well. A mixture of carrier fluid and gravel flows in the screen/openhole annulus. Some fluid leaks radially through the screens and into the screen/washpipe annulus, before it is returned to surface through the washpipe. The alpha wave eventually reaches the toe of the well, and the area above the bed will pack back towards the heel in what is called the beta wave. During the propagation of the beta wave, carrier fluid will leak through the screens and the pack itself to enter the screen/washpipe annulus before returning to surface via the washpipe. Figure 2-2 shows a representation of the alpha and beta wave.

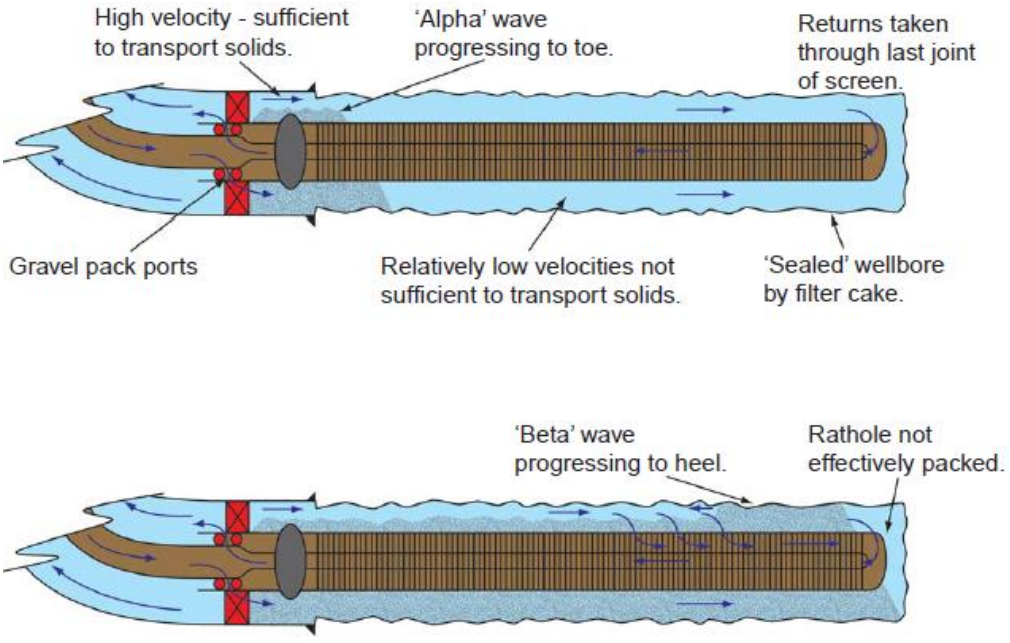

Figure 2-2 Alpha and beta wave[5]

During alpha wave, the pumping pressure will steadily increase because more and more flow is forced through the screen/washpipe annulus. There is also a contribution from increasing bed height along the wellbore, due to pack dehydration from fluid loss to formation. Pumping pressure will increase more rapidly during beta wave because even more flow is forced into screen/washpipe annulus and pack before returning through the washpipe. Eventually, the pressure increases abruptly when the annulus is completely filled with gravel. This is known as screen-out. A typical pumping chart is shown in Figure 2-3, plotting surface treatment pressure (pump pressure) against time.

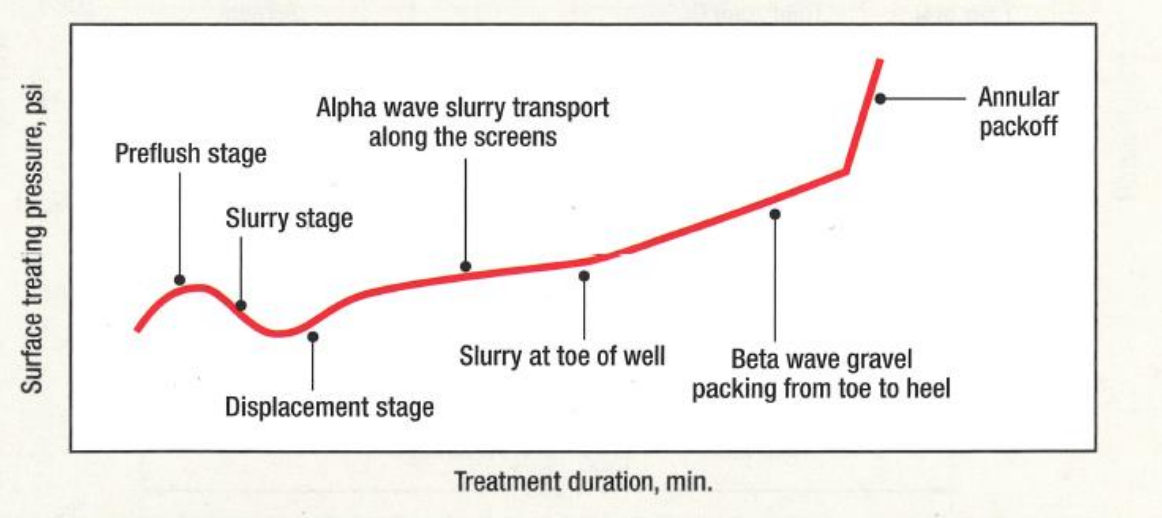

Figure 2-3 Typical pumping chart for gravel pack job[6]

3 SUPPORTING THEORY

This chapter presents the basic theory that builds up the models used in this thesis. First, particle settling will be presented with related equations for force balance, particle Reynolds number and settling velocity. The differentiation between flow regimes and their associated drag coefficients will be discussed. Geometry needs attention, since the slurry transport takes place through a variety of pipe and annulus configurations. Basic pressure drop and friction factor equations are given, as they are vital for the modelling of particle transportation. Lastly, particle packing structures and porosity calculations are outlined.

3.1 Particle settling

The settling velocity of particles is an important parameter in slurry transport. A particle transported by a carrier fluid will settle in the liquid if not imposed to upward forces much larger than the gravitational force on the particle. Settling velocity is influenced by particle size, particle density, particle shape, fluid density, viscosity and the settling process being laminar or turbulent. Numerous models are available and only some will be presented in this thesis. Models are in general divided in two groups; those based on a single particle settling in quiescent fluid and those accounting for particle-particle interaction (hindered settling). Only the former of the two will be considered in this thesis.

3.1.1 Force balance

A particle released from rest in a still fluid will settle under the influence of gravitational force. The fall velocity of the particle will increase until the upward drag force and buoyant force acting on the particle equals the downward gravitational force. This steady-state velocity is called the terminal settling velocity. Forces acting on the particle are shown in Figure 3-1.

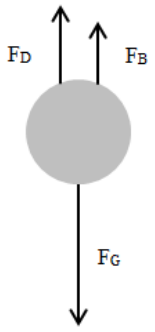

Figure 3-1 Forces acting on settling particle

At terminal velocity the upward acting force is in equilibrium with the downward forces, and the drag force can be expressed with Eq. 3-1 and 3-2, where F_G denotes gravitational force, F_D the drag force and F_B the buoyant force.

$$F_D = F_G - F_B \tag{3-1}$$

Equation 3-2 is then derived from the force balance:

$$\frac{1}{2}\rho_f C_D v_t^2 \frac{\pi d_p^2}{4} = (\rho_s - \rho_f) g \frac{\pi d_p^3}{6} \tag{3-2}$$

Where ρ_f is fluid density, ρ_s is particle density, C_D is drag coefficient, d_p is particle diameter, v_t is terminal settling velocity and g is the gravitational acceleration. Rearranging the expression yields for terminal velocity:

$$v_t = \sqrt{\frac{4}{3}\frac{R_{sd} d_p g}{C_D}} \tag{3-3}$$

Here R_{sd} is the relative submerged density of the particle given by:

$$R_{sd} = \frac{\rho_s - \rho_f}{\rho_f} \tag{3-4}$$

3.1.2 Particle Reynolds number

The settling velocity is a function of the particle Reynolds number, which is indicating the fluid turbulence arising from the settling process.

$$\mathrm{Re}_p = \frac{v_t d_p}{\nu_f} = \frac{\rho_f v_t d_p}{\mu_f} \tag{3-5}$$

Here ν_f is the kinematic viscosity of the fluid, d_p the particle diameter, ρ_f the fluid density, μ_f the dynamic fluid viscosity and v_t the terminal settling velocity. Drag coefficient is dependent on the flow regime around the settling particle. The flow is considered to be laminar when $\mathrm{Re}_p < 1$ and turbulent for $\mathrm{Re}_p \geq 2000$. Between these there exists a transitional region.

3.1.3 Drag coefficient for laminar region

For low Reynolds number, drag force is given by Stokes formula[9]. It is valid for $Re_p << 1$, but agrees with experiments up to $Re_p = 1$. At these low Reynolds numbers, the flow condition is referred to as being creeping. The total drag force on the spherical body according to Stoke is given by Eq. 3-6.

$$F_D = 3\pi\mu_f v_t d_p \tag{3-6}$$

The drag coefficient can now be derived from Eq. 3-7:

$$C_D = \frac{2F_D}{\rho_f v_t^2 \frac{\pi d_p^2}{4}} = \frac{24}{\mathrm{Re}_p} \tag{3-7}$$

Substituting drag force in Eq. 3-2 (left-hand side) with Stokes drag force yields an expression for the terminal settling velocity of particle:

$$v_t = \frac{1}{18}(\rho_s - \rho_f)\, g\, d_p^2 \tag{3-8}$$

3.1.4 Drag coefficient for turbulent region

For higher Reynolds number, $Re_p > 2000$, the drag coefficient is near constant up to a point where the flow reaches a critical point. This region is called the Newton's regime, and the drag coefficient is in the range from 0.4 to 0.445 [10, 11]. Drag coefficient will then be independent of Re_p. The critical point is governed by the separation of the boundary layer around the particle, which will lead to a sudden decrease in the friction between the particle surface and fluid at $Re_p \approx 2.5*10^5$, depending on the roughness of the surface [9].

3.1.5 Drag coefficient for transitional region

The determination of drag coefficient is more unclear for the transitional region. It is difficult to approach this analytically, and the available models are based on curve fitting of experimental data. Typically, the drag coefficient is found to be on the Kaskas equation form[12] (Eq. 3-9) and other variations of this.

$$C_D = \frac{a}{\mathrm{Re}_p} + \frac{b}{\sqrt{\mathrm{Re}_p}} + c \tag{3-9}$$

The parameters *a*, *b* and *c* are chosen to give a best fit to the experimental data. As an example, Rouse's equation is presented in Eq. 3-10[13].

$$C_D = \frac{24}{\mathrm{Re}_p} + \frac{3}{\sqrt{\mathrm{Re}_p}} + 0.34 \tag{3-10}$$

Another variation is Schiller-Naumann, which will be used in this thesis for deriving the terminal settling velocity (Eq 3-11).

$$C_D = \frac{24}{\mathrm{Re}_p}(1 + 0.15\,\mathrm{Re}_p^{0.687}) \tag{3-11}$$

The Schiller-Naumann equation is valid for $1 < \mathrm{Re}_p < 800$, showing good correlation with experimental data within this range[14]. Figure 3-2 shows the drag coefficient relation for a spherical body, at a range of Reynolds numbers, in comparison with the Stoke drag coefficient. Separation of the two graphs can be seen at a Re_p value just below 1, and the Newton's region of nearly constant drag coefficient above 10^5.

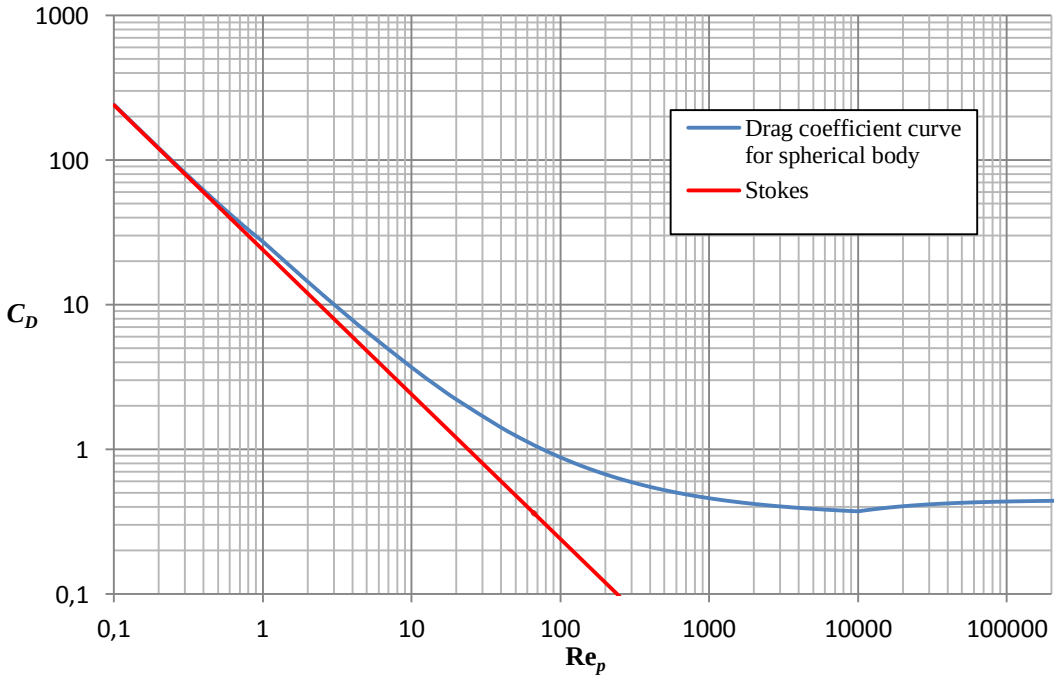

Figure 3-2 Drag coefficient and Reynolds number relationship for spherical body compared to Stokes

3.1.6 Calculating the terminal settling velocity

The settling velocity is a function of the particle Reynolds number, through the drag coefficient. Then the calculation of the settling velocity calls for an iterative approach, because of the implicit nature of the equation (Eq. 3-3). One should make an initial guess for v_t and calculate Re_p. This will indicate if the settling process is laminar, turbulent or in the transitional region, and a suitable drag coefficient equation can be chosen based on this. The guessed value for settling velocity is checked to be within an appropriate error range. If not, an average between the guessed and calculated value should be chosen, and the process started over until the guessed value for settling velocity is found.

3.2 Basic geometry

Pipe and annulus geometries need some attention. They are important to the model structure in this thesis for describing areas and diameters involved when transporting gravel slurry. The thesis differentiates between two distinct areas of the gravel pack system; the inside of the work string, which is a transport conduit for slurry, and the wellbore area. Particularly, the annulus configuration is complicating the calculations.

3.2.1 Hydraulic diameter and wetted perimeter

In conduits with geometries more complex than the simple circular conduit configuration, the effective area open to flow and its fluid-contact perimeters must be accounted for. For this effective area, the equivalent diameter must be calculated and it is called the hydraulic diameter D_h[9]. Wetted perimeter O is the length of the geometry in contact with the fluid for the cross-section of the duct, and A is the area open to flow. For flow through a circular duct, the hydraulic diameter will obviously be equal to the internal diameter, and the wetted perimeter will be equal to the inner circumference. For a circular conduit, the cross-sectional area is in general:

$$A = \frac{\pi D^2}{4} \tag{3-12}$$

And this can also be expressed as:

$$A = \frac{DO}{4} \tag{3-13}$$

Hydraulic diameter is defined as:

$$D_h = \frac{4A}{O} \tag{3-14}$$

And wetted perimeter as:

$$O = \frac{4A}{D} = \pi D \tag{3-15}$$

3.2.2 Work string geometry

Presented in Figure 3-3 is the geometry for pipe with a sediment bed. The inner pipe diameter is denoted D_p, y_b is the bed height and γ is the angle of vertical position of top of bed in the pipe cross-section. The next three sub-chapters will give the equations needed to calculate the areas, hydraulic diameters and wetted perimeters involved when a deposited gravel bed is present.

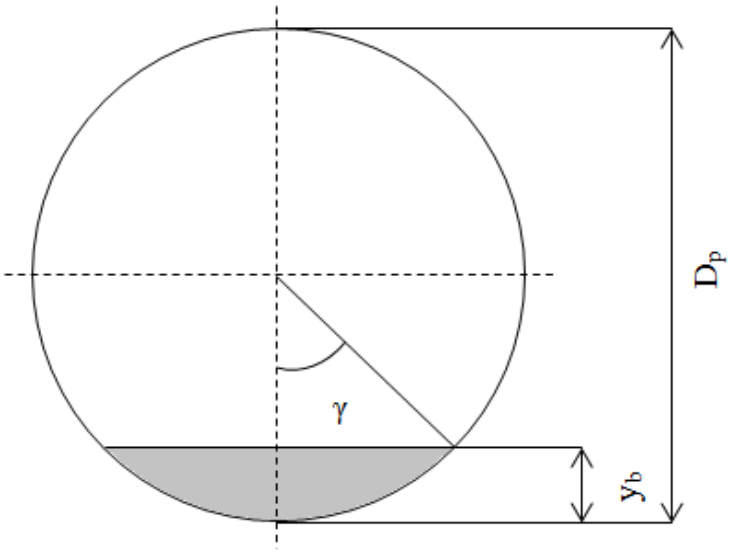

Figure 3-3 Cross-section of pipe with bed and associated position angle

3.2.2.1 Calculation of areas

The position angle γ from the vertical can be expressed as:

$$\cos\gamma = 1 - \frac{2y_b}{D_p} \tag{3-16}$$

Area of the full cross-section is given by:

$$A_p = \frac{\pi D_p^2}{4} \tag{3-17}$$

The circle sector from the position angle:

$$A_{sector} = \gamma \frac{D_p^2}{4} \tag{3-18}$$

The area of the triangular section above bed:

$$A_{triangle} = \frac{D_p^2}{4} \sin\gamma\cos\gamma \tag{3-19}$$

Now the area of the circular segment formed by the bed becomes:

$$A_b = A_{sector} - A_{triangle} \tag{3-20}$$

$$A_b = \frac{D_p^2}{4} (\gamma - \sin\gamma\cos\gamma) \tag{3-21}$$

Area open to flow:

$$A_o = A_p - A_b \tag{3-22}$$

$$A_o = \frac{D_p^2}{4} ((\pi - \gamma) + \sin\gamma\cos\gamma) \tag{3-23}$$

3.2.2.2 Calculation of wetted perimeters for work string

Fluid will come in contact with both the surface of the sedimentation bed, $O_{b,}$ and the open pipe wall above this bed O_w. Figure 3-4 shows the wetted perimeter for pipe flow with sediment bed.

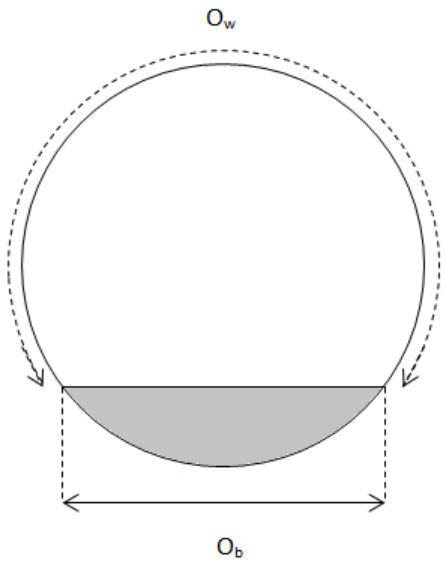

Figure 3-4 Cross-section of pipe with bed and associated wetted perimeters

Equations for calculating wetted perimeters:

$$O_b = D_p \sin\gamma \tag{3-24}$$

$$O_w = D_p (\pi - \gamma) \tag{3-25}$$

3.2.2.3 Calculation of hydraulic diameter for work string

For the case of work string geometry, the expression of hydraulic diameter will consider the sum of the perimeters related to the wall and the bed, and be a combination of Eq. 3-23 through 3-25:

$$D_h = \frac{4A_o}{O_b + O_w} = \frac{D_p((\pi - \gamma) + \sin\gamma\cos\gamma)}{((\pi - \gamma) + \sin\gamma)} \tag{3-26}$$

3.2.3 Wellbore geometry

The geometry for screen section inside open hole and washpipe inside screen is more complicated than for the circular duct. There will be two annuli for fluid flow; screen/washpipe annulus and screen/openhole annulus. For both annuli, a fully eccentric configuration is assumed, with screen and wash pipe lying on the low side as shown in Figure 3-5. In this thesis, only bed heights above screen diameter will be considered, as the gravel fill above screens is an assumption for the scope of work. As an operational goal, the dune height for the alpha wave should be designed to be 70 to 90% of the openhole area, according to Bellarby[5]. For simplicity, the bed height is assumed to be higher than outside diameter of the screens, as shown later in Figure 3-6 and 3-7.

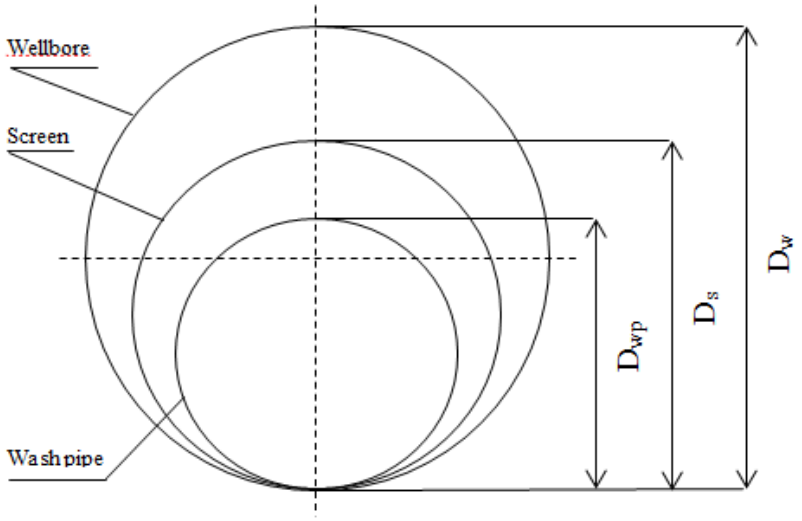

Figure 3-5 Simplified geometric configuration for gravel pack operation

3.2.3.1 Calculation of wetted perimeter for annulus

For flow of fluid in an annulus, the fluid will be in contact with both the inner wall of the outside tube and the outside wall of the inner tube. The wetted perimeter can in this case be expressed as in Eq. 3-27. This equation will be valid for the screen/washpipe annulus, where no sedimentation is assumed to take place.

$$O = \pi D_{si} + \pi D_{wp} \tag{3-27}$$

For the screen/openhole annulus with sediment bed, the equation will be more complex and needs to differentiate between different scenarios of bed height compared to outside screen

diameter to work over the full diameter of the wellbore. Methods for calculating hydraulic diameter and wetted perimeter with bed height below screen diameter have been presented in other theses[15, 16]. Figure 3-6 shows the simplified geometry of the screen/openhole annulus with bed height above screens, and its related position angle. This is in fact a mirrored image of Figure 3-1. Now, the same approach as for the work string example can be used. An expression for wetted perimeter O_w at pipe wall needs to be worked out. O_b is still given by the same equation as for the work string example.

Wetted perimeters:

$$O_b = D_w \sin\gamma \tag{3-28}$$

$$O_w = D_w\gamma \tag{3-29}$$

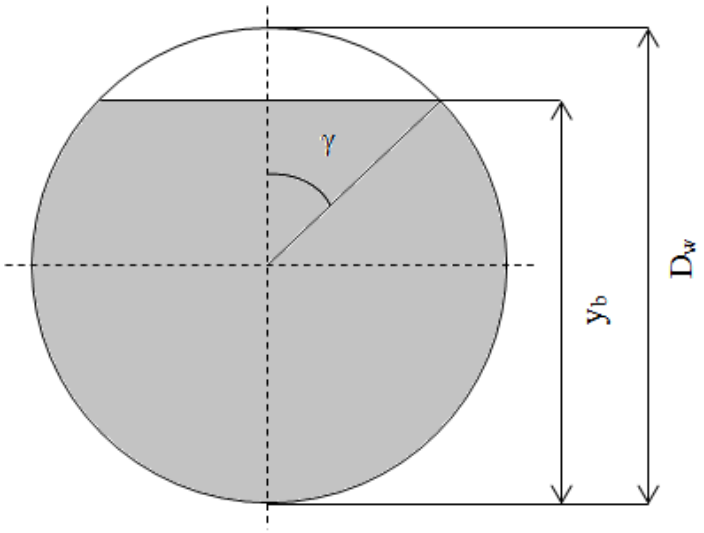

Figure 3-6 Simplified geometry of screen/openhole annulus and position angle

3.2.3.2 Gravel fill calculations

The amount of gravel placed outside the screens defines the degree of success for the gravel packing operation. Obviously, a totally filled annular space is preferred for sand control. Figure 3-7 shows the cross-section of screen/openhole annulus, divided in an area filled with gravel and an area open for flow. The figure represents an alpha dune covering the screen diameter.

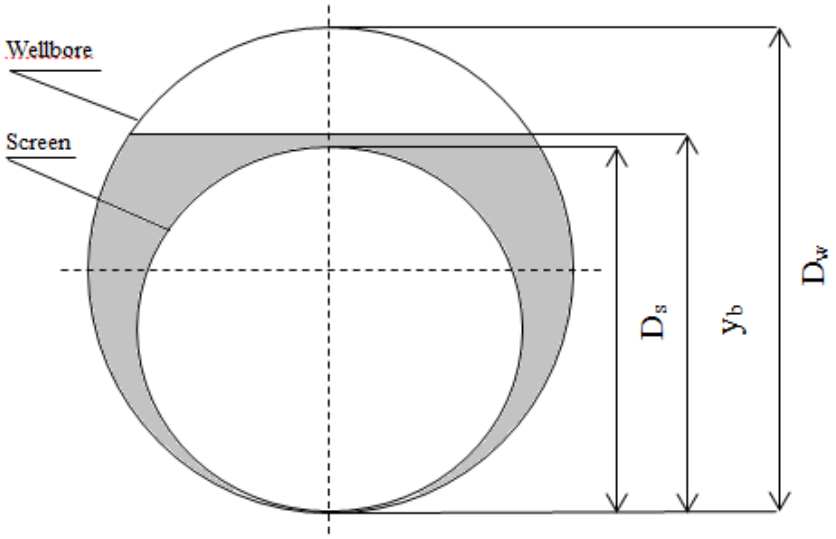

Figure 3-7 Geometry of screen/openhole annulus with gravel fill above screens

The area of the entire screen/openhole annulus A_{so} is equal to the difference in cross-sectional areas of screen and wellbore.

$$A_{so} = \frac{\pi}{4}(D_w^2 - D_s^2) \tag{3-30}$$

The size of the wellbore is a matter of uncertainty, since the wellbore could be subjected to hole-enlargement from issues related to drilling and rock mechanics. The hole can be drifted to a certain diameter to make sure the screens can be run safely, but the true diameter is rarely known until after the gravel pack operation, when volume of gravel pumped is estimated.

Area open to flow A_o is now:

$$A_o = \frac{D_w^2}{4}(\gamma - \sin\gamma\cos\gamma) \tag{3-31}$$

Area of annulus filled with gravel A_g is then the area of the entire annulus minus the open area for flow, under the assumption that gravel is covering the screen:

$$A_g = A_{so} - A_o = \frac{D_w^2}{4}((\pi - \gamma) + \sin\gamma\cos\gamma) - \frac{\pi D_s^2}{4} \tag{3-32}$$

Gravel fill percent:

$$Gravel\ Fill = \frac{A_g}{A_{so}} * 100\% \tag{3-33}$$

Example:
With 8.5 in OH and 6.625 in screens, the gravel fill at bed height flush with screen can be found. Table 3-1 shows the values calculated from aforementioned equations.

Table 3-1 Calculated values of areas and gravel fill for example case

Parameters	Values
D_w	0.2159 m
D_s	0.1923 m
y_b	0.1923 m
γ	0.6668 rad
A_w	0.03661 m^2
A_s	0.02919 m^2
A_b	0.03450 m^2
A_o	0.00211 m^2
A_{so}	0.00742 m^2
A_g	0.00531 m^2
Gravel fill%	**71.6**

Considering the design suggestion of 70 to 90% gravel fill during alpha wave, the calculated value supports the assumption that covering the screens is a sound design criteria for the gravel pack operation, for the given screen and openhole diameters.

3.2.3.3 Calculation of hydraulic diameter for annulus

The hydraulic diameter for the area open for flow in an annulus can in general be expressed as:

$$D_h = \frac{4A}{O} = \frac{\pi D_o^2 - \pi D_i^2}{\pi D_o + \pi D_i} = D_o - D_i \tag{3-34}$$

Where
D_o = inner diameter of outside conduit
D_i = outer diameter of inside conduit

And for wash screen/washpipe annulus:

$$D_{hwp} = D_{si} - D_{wp} \tag{3-35}$$

Where
D_{hwp} = hydraulic diameter of screen/washpipe annulus
D_{si} = inner diameter of screen base pipe
D_{wp} = outer diameter of wash pipe

Now for screen/openhole annulus, the hydraulic diameter for the open area above the bed takes the same form as Eq. 3-26 for the work string case with bed and is derived from combining Eq. 3-28, 3-29 and 3-31:

$$D_{ho} = \frac{4A_o}{O_b + O_w} = \frac{D_w(\gamma - \sin\gamma\cos\gamma)}{(\gamma + \sin\gamma)} \tag{3-36}$$

3.3 Pressure drop

The pressure loss in a conduit with flowing slurry will be three-parted. There is loss due to friction at the flow boundaries, the conduit wall and sediment bed surface. For inclined sections, hydrostatic loss will occur. In addition, there is pressure loss from acceleration of the slurry. The models used in this thesis will solely implement horizontal configuration, and hence the hydrostatic pressure drop is not considered. Also, the contribution from acceleration is neglected, as the fluid is assumed to be incompressible. The full pressure gradient balance is given by Eq. 3-37.

$$\left(\frac{dP}{dL}\right) = \left(\frac{dP}{dL}\right)_f + \left(\frac{dP}{dL}\right)_h + \left(\frac{dP}{dL}\right)_a \tag{3-37}$$

In this sub-chapter, D denotes the characteristic diameter of the conduit, making the equations valid for flow both in circular pipes and geometries characterized by the hydraulic diameter.

3.3.1 Frictional pressure drop

The frictional pressure loss in fluid transported through a conduit is the change in kinetic energy resulting from the interaction with the conduit surface. Dynamic pressure P_{dyn} is the kinetic energy per volume of fluid, and is proportional to the fluid density and flow

velocity squared, here referred to as line speed v_{ls} (Eq. 3-38).

$$P_{dyn} = \frac{1}{2}\rho_f v_{ls}^2 \tag{3-38}$$

The shear stress at the pipe wall τ_w is expressed as the frictional drag force F_{DW} over the pipe wall area, where dL is the incremental length.

$$\tau_w = \frac{F_{DW}}{A_{pw}} = \frac{F_{DW}}{\pi D dL} \tag{3-39}$$

Remembering the expression for drag force on a settling particle (Eq. 3-2), the drag force can now be expressed for the pipe wall area as:

$$F_{DW} = f\,\frac{1}{2}\rho_f v_{ls}^2 \pi D dL \tag{3-40}$$

The Fanning friction factor f is related to the pipe wall surface. Now, a new expression for wall shear stress can be derived.

$$\tau_w = f\,\frac{1}{2}\rho_f v_{ls}^2 \tag{3-41}$$

Substituting for Darcy-Weisbach friction factor as $\lambda \equiv 4f$ yields:

$$\tau_w = \lambda\,\frac{1}{8}\rho_f v_{ls}^2 \tag{3-42}$$

Pressure loss is related to the pipe wall stress and can be derived from a force balance for the fluid flow through a circular conduit, and the following force balance is found in literature[17].

$$dP\left(\frac{\pi D^2}{4}\right) = \tau_w \pi D dL \tag{3-43}$$

Combining Eq. 3-42 and 3-43, and solving for the frictional pressure gradient yields:

$$\left(\frac{dP}{dL}\right)_f = \frac{2f\rho_f v_{ls}^2}{D} = \frac{\lambda \rho_f v_{ls}^2}{2D} \tag{3-44}$$

The energy loss in a flowing system is often referred to as head loss or hydraulic head *h*. It can be viewed as the loss of an equivalent hydrostatic column of the fluid. Hydraulic gradient *i* is head loss per incremental length of the flow conduit (Eq. 3-45). The unit of hydraulic gradient is m.w.c/m (meter water column per meter) and represents the loss of an equivalent hydrostatic column per unit length of pipe.

$$i = \frac{dh}{dL} \tag{3-45}$$

Pressure differential can be expressed in terms of head loss and hydraulic gradient as:

$$dP = \rho_f g\, dh = \rho_f g\, i\, dL \tag{3-46}$$

The relationship between hydraulic gradient and the frictional pressure gradient is then:

$$\left(\frac{dP}{dL}\right)_f = \rho_f g\, i \tag{3-47}$$

Combining Eq. 3-44 through 3-46 yields an expression for the hydraulic gradient:

$$i = \frac{2 f v_{ls}^2}{g D} = \frac{\lambda v_{ls}^2}{2 g D} \tag{3-48}$$

3.3.2 Reynolds number

The frictional pressure drop is largely dependent on the flow regime. A way of discriminating between laminar and turbulent flow is the use of Reynolds number. This dimensionless number is representing the ratio of inertial and viscous forces on the fluid. The inertial force is the fluid's resistance to motional change, and the viscous force is resisting deformation from shear stress. Laminar flow occurs at low Reynolds numbers and is dominated by viscous forces, causing smooth flow. At higher Reynolds numbers the inertial forces are dominating and characterized by eddy currents and flow instabilities. Reynolds number is defined in Eq. 3-49, with fluid density ρ, fluid velocity v, fluid viscosity μ and characteristic length L.

$$N_{\mathrm{Re}} = \frac{\rho v^2}{\frac{\mu v}{L}} = \frac{\rho v L}{\mu} \tag{3-49}$$

For flow in non-circular geometries, the hydraulic diameter can be used to express the characteristic length. To distinguish between the different flow regimes, the following Reynolds numbers marks the transitions:

$N_{\mathrm{Re}} \leq 2300$	Laminar flow
$2300 > N_{\mathrm{Re}} \leq 4000$	Transition from laminar to turbulent flow
$N_{\mathrm{Re}} > 4000$	Turbulent flow

3.3.3 Friction factor

The Hagen-Poiseuille equation gives the frictional pressure loss for laminar flow[17].

$$\left(\frac{dP}{dL}\right)_f = \frac{32\mu v}{D^2} \tag{3-50}$$

Combining this equation with Eq. 3-44 yields:

$$\frac{\lambda \rho_f v_{ls}^2}{2D} = \frac{32\mu v_{ls}}{D^2} \tag{3-51}$$

Then friction factor is:

$$\lambda = \frac{64}{N_{\mathrm{Re}}} \tag{3-52}$$

Friction factor for laminar flow is then dependent on Reynolds number alone. For other flow regimes, the friction factor is related to the absolute wall roughness ε of the flow conduit, and hence impacts the pressure drop in the system. Absolute roughness is an expression for the surface irregularities and is expressed in units of length. It is not physically measured, but is rather the equivalent sand grain roughness that will yield the same friction factor. For smooth pipes, Blasius' friction factor is valid for Reynolds numbers up to 10^5 and is given by[18]:

$$\lambda = 0.3164 N_{\mathrm{Re}}^{-0,25} \tag{3-53}$$

Most pipes used in drilling and completion operations are not smooth. For turbulent flow, the roughness then strongly affects the friction factor, and thus the pressure loss. Wall roughness is influenced by type of material and manufacturing, as well as environmental

exposure and service time. Dimensional analysis indicates that the effect of wall roughness is due to its dimensions relative to the pipe diameter, rather than the absolute dimensions[19]. Typical values for pipe wall roughness are presented in Table 3-2 and values for rock surfaces in Table 3-3.

Table 3-2 Absolute surface roughness for steel pipe[20]

Condition	Absolute Roughness (ε)
New clean pipe	$1.5*10^{-5}$ ft ($4.572*10^{-5}$ m)
Moderately corroded pipe	$1.3*10^{-3}$ ft ($3.9624*10^{-4}$ m)
Heavily corroded pipe	$1.0*10^{-2}$ ft ($3.048*10^{-3}$ m)

Table 3-3 Absolute surface roughness for rock formation types[21]

Rock Formation Types	Absolute Roughness (ε)
Competent, low fracture Igneous (e.g., granite, basalt) Sedimentary (e.g., limestone, sandstone) Metamorphic (e.g., gneiss)	0.003 to 0.006 m
Competent, medium fracture Igneous (e.g., granite, basalt) Sedimentary (e.g., limestone, sandstone) Metamorphic (e.g., gneiss)	0.006 to 0.009 m
Poor competence, high fracture Igneous (e.g., breccia) Sedimentary (e.g., sandstone, shale) Metamorphic (e.g., schist)	0.009 to 0.012 m

The relative roughness of a surface is the ratio of its absolute roughness to the pipe diameter, ε/D. Equations used for turbulent and transitional regime use this relation. An explicit expression for friction factor in rough pipe at turbulent flow was proposed by Nikuradse[22]:

$$\frac{1}{\sqrt{\lambda}} = 1.74 - 2\log_{10}\left(\frac{2\varepsilon}{D}\right) \approx -2\log_{10}\left(\frac{\varepsilon}{3.7D}\right) \tag{3-54}$$

For this equation, the friction factor is not dependent on the Reynolds number, as the thickness of the laminar boundary layer towards the pipe wall becomes smaller with increasing degree of turbulence. At high enough turbulence, the boundary layer thickness is smaller than the wall irregularities, leading to turbulence throughout the entire flow. The

most commonly used equation is the Colebrook and White formula[23] (Eq. 3-55). It fills the gap between laminar and turbulent regions for both smooth and rough pipes.

$$\frac{1}{\sqrt{\lambda}} = -2\log_{10}\left(\frac{\varepsilon}{3.7D} + \frac{2.51}{N_{\mathrm{Re}}\sqrt{\lambda}}\right) \tag{3-55}$$

Note that for high Reynolds numbers, this equation approaches the Nikuradse as the viscous forces become less dominant. The Colebrook and White equation is implicit on the friction factor, therefore requiring numerical iteration to solve. Explicit equations are also available. They are simpler to use for practical purposes One of these is the Swamee-Jain formula[24] (Eq. 3-56), which will be used for friction factor calculations in this thesis. It is valid for the whole transitional and turbulent range, and shows good approximation to Colebrook-White.

$$\frac{1}{\sqrt{\lambda}} = -2\log_{10}\left(\frac{\varepsilon}{3.7D} + \frac{5.74}{N_{\mathrm{Re}}^{0,9}}\right) \tag{3-56}$$

The famous Moody chart gives the Darcy-Weisbach friction factors for different relative roughness over the range of Reynolds numbers, from laminar to turbulent flow (Figure 3-8).

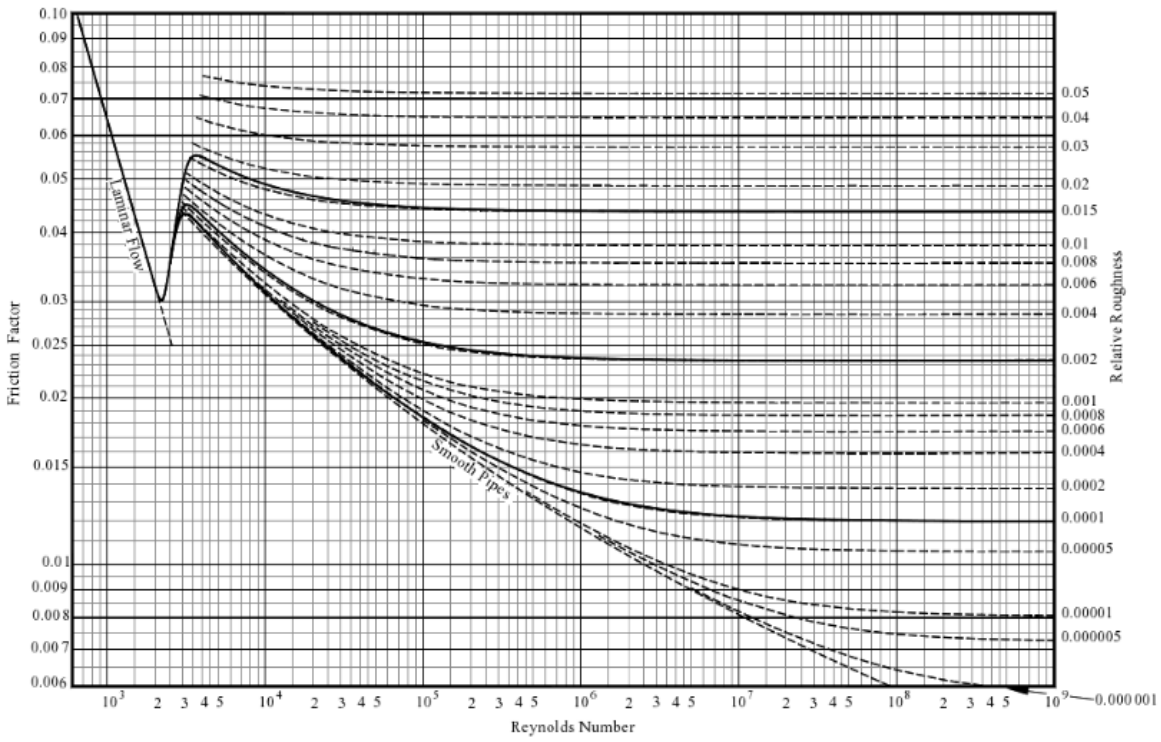

Figure 3-8 Moody diagram for Darcy-Weisbach friction factors[19]

3.4 Packing of particles

Particles can arrange themselves in several packing structures. The variations will give different packing densities and porosities. Spherical particles are assumed for the scope of this thesis, as the gravel sand grains are normally well rounded and have high sphericity. One can also look at monodisperse (uniform sized) or polydisperse (different sized) distribution of particles.

3.4.1 Porosity and bulk density

Porosity ϕ is defined as the void volume fraction of a material over the total volume. The packing of particles will leave an empty space in between, which can be occupied by gas, liquid or other smaller particles. The packing density η is defined as the volume fraction of the system occupied by particles, where V_s is the volume of the sand particles themselves and V_t is the total volume occupied by the particles.

$$\eta = 1 - \phi = \frac{V_s}{V_t} \tag{3-57}$$

Bulk density of particles is the mass of the particles to the total volume of the system, where m_s represents mass of sand sample and ρ_s is density of the solid particles:

$$\rho_{bulk} = \frac{m_s}{V_t} = \frac{\rho_s V_s}{V_t} \tag{3-58}$$

Combining Eq. 3-57 and Eq. 3-58 yields an expression for the bulk density based on the porosity:

$$\rho_{bulk} = \eta \rho_s = (1 - \phi)\rho_s \tag{3-59}$$

3.4.2 Packing structures

A presentation of different structures of spherical packing and their related porosities can be found in literature. Figure 3-9 is an overview of the different general arrangements spheres can order during packing[25]. The Kepler's Conjecture states that the highest density spherical particles can have is $\pi/\sqrt{18} \approx 0.74$[26]. This is considered to be the upper limit for the packing density of spheres. Other packing arrangements and related porosities are presented in Table 3-4[25].

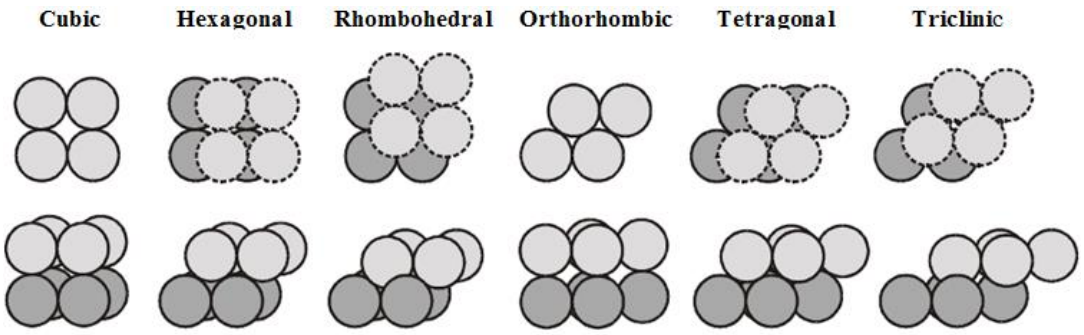

Figure 3-9 Packing structures[25]

Note that both rhombohedral and triclinic structures potentially give the highest density as stated by Kepler's Conjuncture. The general arrangements of packing are idealistic representations, and it is reasonable to assume random packing to be more realistic for sedimentation during gravel pack operations. The calculated porosity can though show a best fit. Bear in mind that the stated values for porosity are the maximum theoretically achievable values.

Table 3-4 Packing structures and related porosities[25]

Packing Structure	Maximum Porosity ϕ
Cubic	0.476
Hexagonal	0.395
Orthorhombic	0.395
Tetragonal	0.302
Rhombohedral	0.260
Triclinic	0.260
Random	≥0.399

Considering random packing of equal hard spheres, the lower and higher limits are referred to as RLP (Random Loose Packing) and RCP (Random Close Packing), respectively. Packing density for RLP is ~ 0.555 and ~ 0.64 for RCP[27, 28]. The related porosity range for random packing is then from 0.36 to 0.445. However, the gravel sand consists of a distribution of grain sizes and not equally sized grains. A solution for a polydisperse grain mixture makes use of the sieve analysis data for the gravel sand. The median particle size d_{50} can be found from the cumulative grain size distribution diagram, and the mean grain size is calculated based on the sieve analysis data set. A mixture of different grain sizes will pack denser than a mixture of equally sized grains, since voids between larger grains can be occupied by smaller grains. Statistical analysis yields the standard deviation of the

particle distribution, which is directly linked to the porosity according to Santiso and Müller[29]. They presented tables of packing densities of polydisperse hard spheres based on the standard deviation, for both Gaussian and lognormal distributions. They suggest that for natural sand, the lognormal distribution is more realistic. Their findings are in between the values of RLP and RCP for uniformly sized spheres. Table 3-5 shows the values for lognormal distribution.

Table 3-5 Packing density and standard deviations[29]

Standard deviation σ	Packing density η
0	0.602
0.01	0.603
0.025	0.604
0.05	0.605
0.075	0.608
0.1	0.611
0.125	0.614
0.15	0.617
0.175	0.621
0.2	0.624

(This page intentionally left blank)

4 SEDIMENTATION IN WORK STRING

From an operational perspective, there is assumed that the gravel pumped during the packing process will end up filling the annulus made up by the open hole and screen joints. However, this may not always be the case, since the successful placement of gravel also depends on the flow behavior in the work string. The flow of gravel slurry will be affected by the flow rate, and thus the line speed of the mixture for a given open area for flow. A critical velocity for deposition of particles must be exceeded to transport particles to their preferred destination. This is known as the *Limit Deposit Velocity* (LDV). A bed formed from the sedimentation of particles will start to dissolve at velocities above the LDV, and disappear if the velocity is sufficiently high. It is also referred to as *critical velocity*, which will be used in this thesis. Unsuspected deposition of particles in the work string will cause confusion to the amount of gravel fill during the packing process. Pre-job planning takes into account uncertainties in borehole diameter, and there will be enough gravel for a given over-displacement in case of washouts and hole enlargement. The degree of work string sedimentation will give additional uncertainties to the gravel volume needed to perform a successful gravel pack job. To address these uncertainties, a model for slurry transport in the work string needs to be implemented.

4.1 The Matoušek model

While there are numerous models describing the phenomena of slurry transport in pipelines, many of these are intricate and overly complicated for practical engineering purposes. In general, slurry transport models are describing how to transport particles without settling, for the use in operations where a sediment-free conduit is preferred. The Matoušek model is a predictive model for frictional pressure drop in settling slurries transported in pipes with a stationary bed[4]. It is chosen for its ease of implementation and use in practical engineering. Frictional pressure drop and height of sedimentation bed are the outputs, which will indicate the magnitude of gravel fill in the pipe for given geometry and flow rate. The weight of gravel settled out in the work string can then be quantified. The implementation of a slurry transport model for the work string will aid in optimizing the gravel pack job.

Input parameters for the model are mean delivered solids concentration C_{vd}, median diameter of particle d_{50}, internal diameter of pipe D_p, mean velocity in entire cross-section of pipe v_m, density of solid particle ρ_s and density of fluid ρ_f. The median particle diameter is found from the sieve analysis.

The model is valid for a certain range of average flow velocities through the cross-sectional pipe area. The lower limit is governed by the velocity at which the Shields parameter reaches the critical Shields value for initiation of particle motion on the bed surface. These parameters will be discussed later in the chapter. The upper limit is the deposit limit threshold velocity at which the bed starts to slide and dissolve (LDV). Matoušek validated the model with experimental data from his own work and others[30-33]. The experiments included both circular pipe of 100 to 150 mm and enclosed rectangular conduit of 98 times 98mm. The particles in the experiments were sand or bakelite, with median diameter 0.3 to 1.1 mm and specific gravities of 1.53 to 2.67 sg.

The model is a 3-layer model, with a bed layer and a combined upper layer. The upper layer is further divided in an area associated by the bed and the area influenced by the pipe wall. The distribution of flow velocity and concentration in slurry flow in pipe cross-section is shown in Figure 4-1.

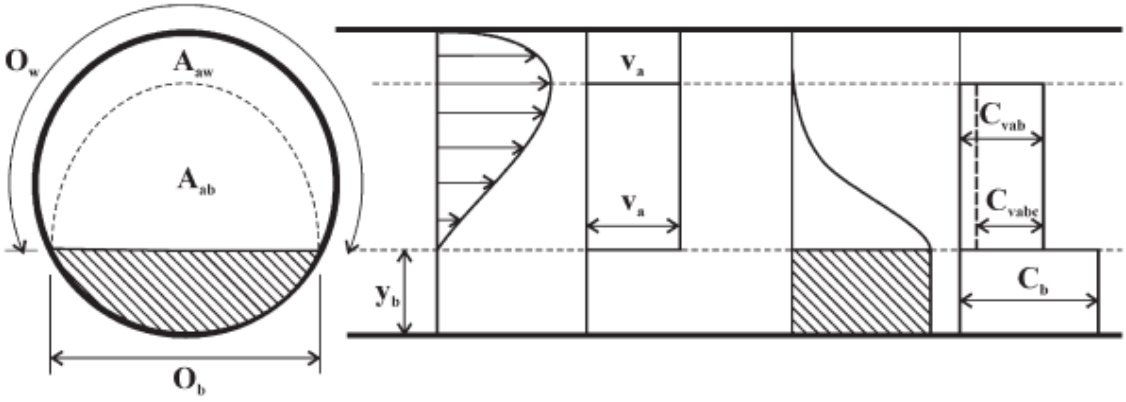

Figure 4-1 Schematic of velocity and concentration distribution of slurry in pipe cross-section[4]

The total area open for flow over the bed, or discharge area, will be referred to as A_a. The sub-area A_{ab} is influenced by the bed friction, while sub-area A_{aw} is influenced by pipe wall friction. Wetted perimeters O_w and O_b are the boundaries against the pipe wall and the bed surface, respectively. Thickness of bed y_b indicates the height of sedimentation over the pipe cross-section. The mean velocity v_a in the discharge area is an area-averaged velocity for the slurry. C_b is the bed concentration, while C_{vab} is the mean spatial concentration in the discharge area. C_{vabc} is the contact-load portion of C_{vab}, or in other words the portion of particles that contribute to contact load within sub-area A_{ab}. The total discharge area is the sum of the sub-areas as showed in Eq. 4-1.

$$A_a = A_{ab} + A_{aw} \tag{4-1}$$

Hydraulic radii of the different areas are given by the following equations:

$$R_{hw} = \frac{A_{aw}}{O_w} \tag{4-2}$$

$$R_{hb} = \frac{A_{ab}}{O_b} \tag{4-3}$$

$$R_{ha} = \frac{A_a}{O_b + O_w} \tag{4-4}$$

The flow boundaries have different hydraulic roughness, and the velocity profile in the vertical cross-section is therefore skewed towards the upper part of the pipe. The bed surface is considered to be hydraulically rough, with the degree of roughness depending on particle size. The pipe wall is considered to be hydraulically smooth for pipes used for particle transportation purposes. Particle concentration will vary over the discharge area, with highest concentration near the bed surface and decreasing towards the uppermost part. The variations of fluid velocity and concentration across the open flow area are strongly affecting frictional pressure drop through the pipe.

Cross-sectional area of sediment bed, A_b is given by Eq. 3-21. Wetted perimeters O_b and O_w are given by Eq. 3-24 and 3-25, respectively.

4.1.1 Continuity equation

The product of the mean delivered mixture velocity and the pipe cross-sectional area is equal to the flow velocity in the discharge area above the bed times the area open to flow above the bed:

$$v_m A = v_a A_a \tag{4-5}$$

The mixture flow rate through the discharge area is:

$$Q_m = v_a A_a \tag{4-6}$$

The solids flow rate through the discharge area is then given by the mean delivered solids concentration as:

$$Q_s = C_{vd} Q_m = C_{vd} v_a A_a \tag{4-7}$$

4.1.2 Momentum equations

The assumption for balancing driving and resisting forces is that the mean velocity and hydraulic gradient for the mixture are the same for both sub-areas of the discharge area:

$$\rho_f g i_m A_a = \tau_w O_w + \tau_b O_b \tag{4-8}$$

$$\rho_f g i_m A_{aw} = \tau_w O_w \tag{4-9}$$

$$\rho_f g i_m A_{ab} = \tau_b O_b \tag{4-10}$$

Where i_m is the hydraulic gradient for the mixture, τ_w is shear stress at pipe wall and τ_b is shear stress at bed surface. According to Eq. 3-42, the shear stresses at the boundaries can be expressed as:

$$\tau_w = \lambda_w \frac{1}{8} \rho_f v_a^2 \tag{4-11}$$

$$\tau_b = \lambda_b \frac{1}{8} \rho_f v_a^2 \tag{4-12}$$

Here λ_w and λ_b are the Darcy-Weisbach friction for the wall and bed, respectively. The hydraulic gradient is then according to Eq. 3-48:

$$i_m = \frac{\lambda_w v_a^2}{2 g D_{hw}} = \frac{\lambda_w v_a^2}{2 g 4 R_{hw}} \tag{4-13}$$

And

$$i_m = \frac{\lambda_b v_a^2}{2 g D_{hb}} = \frac{\lambda_b v_a^2}{2 g 4 R_{hb}} \tag{4-14}$$

4.1.3 Shields parameter and Meyer-Peter Müller Equation

The heart of the model is the utilization of the Meyer-Peter Müller equation (MPM) (Eq. 4-15), which is an empirical law for bed-load transport fitted to an extensive experimental data set[34].

$$\Phi = \alpha(\Theta - \Theta_{cr})^{\beta} \tag{4-15}$$

Here Φ is the Einstein transport parameter, Θ is the Shields parameter, Θ_{cr} the critical Shields parameter, and α and β are coefficients. Einstein parameter can also be expressed as:

$$\Phi = \frac{Q_s}{O_b\sqrt{R_{sd}\,g\,d_{50}^3}} = \frac{q_s}{\sqrt{R_{sd}\,g\,d_{50}^3}} \tag{4-16}$$

Here, q_s is the average solid flux through a unit width of the discharge area. The equation's purpose was originally to describe flow in open channels, but was adopted by Matoušek for use in pipe flow, provided that the coefficients α and β were considered not to be constants. The use of MPM equation has later been defended by further experiments, and the coefficients of the MPM equation are dependent on the particle Reynolds number and can be expressed as[35]:

$$\alpha = \frac{2\omega}{(n+1)(n+2)\tan\varphi} + \frac{58}{\mathrm{Re}_p^{0.62}} \tag{4-17}$$

$$\beta = 1.2 + \frac{1.3}{\mathrm{Re}_p^{0.39}} \tag{4-18}$$

Here, ω is the coefficient for the velocity at top of the sheet flow layer, n is the power of the velocity distribution in the sheet flow layer and φ is the internal friction angle of the particles. Pugh and Wilson give the value $\omega \approx 9.4$ based on their experiments[36, 37]. For the case of the actual sand particle diameter in the field case, the value is found to be close to 9 from the data points presented in their article. The latter value will therefore be used in the modelling, since it is more representative for the particles discussed in the thesis. Matoušek suggests n=1, based on the experimental data presented in his article. For natural sands, the internal friction angle is ~30°[13].

The concept of bed shear velocity u_{*b} was first used by Prandtl[38]. It is an imaginary velocity, describing the shear related motion in the fluid at the bed surface and the velocity profile near the bed boundary.

$$u_{*b} = \sqrt{\frac{\tau_b}{\rho_f}} \tag{4-19}$$

From the experimental data set used by Matoušek, another expression for the bed shear velocity was derived. Here the empirical coefficients are given as K=1.9 and n=1:

$$u_{*b} = \sqrt[2+n]{K v_t^n R_{sd} g C_{vd} \frac{A_a}{O_b}} \tag{4-20}$$

Shields introduced the concept of initiation of particle motion[39]. Shields parameter is the dimensionless shear stress used for describing the erosion of the particle bed. It gives an indication of the erodibility of sediments. To initiate erosion of the bed, a critical value must be exceeded. A high value symbolizes high erosion. The parameter represents the ratio of shear forces to gravitational forces on the particle. The Shields parameter is derived from the following equation:

$$\Theta = \frac{F_{shear}}{F_{gravity}} = \frac{\rho_f u_{*b}^2 d_{50}^2}{\rho_f R_{sd} g d_{50}^3} = \frac{u_{*b}^2}{R_{sd} g d_{50}} \tag{4-21}$$

Combining Eq. 4-19 and Eq. 4-21 yields:

$$\Theta = \frac{\tau_b}{(\rho_s - \rho_f) g d_{50}} \tag{4-22}$$

In the famous Shields diagram, the critical Shields parameter is of implicit nature. An explicit equation has been proposed, which is based on the fluid and particle characteristics through particle Reynolds number[40]. The particle Reynolds number is here defined as:

$$\mathrm{Re}_{p'} = \frac{\rho_f d_{50} \sqrt{R_{sd} g d_{50}}}{\mu_f} \tag{4-23}$$

The critical Shields parameter is given as:

$$\Theta_{cr} = \frac{\left(1+\left(0.0223\,\mathrm{Re}_{p'}\right)^{2.8358}\right)^{0.3542}}{3.0946\,\mathrm{Re}_{p'}^{0.6769}} \tag{4-24}$$

4.1.4 Pipe wall and bed-surface friction

Pipe wall is assumed to be hydraulically smooth in the model. The wall friction is then related to the hydraulic radius of the sub-area influenced by the wall R_{hw}. The bed can be considered to be hydraulically rough, and the bed friction is related to hydraulic radius of the sub-area influenced by the bed surface R_{hb}, and the hydraulic roughness factor k_s. Nikuradse equation modified for the bed surface condition is proposed by Matoušek (Eq. 4-25). Here, κ denotes the Kármán constant (κ=0.4):

$$\frac{v_a}{u_{*b}} = \sqrt{\frac{8}{\lambda_b}} = \frac{1}{\kappa}\ln\frac{3.7*4R_{hb}}{k_s} \tag{4-25}$$

The bed friction factor can be expressed by combining Eq. 4-12 and 4-19:

$$\lambda_b = \frac{8u_{*b}^2}{v_a^2} \tag{4-26}$$

For flow at high shear stress, the top of the bed is sheared off and particles will be transported above the stationary part of the bed. High values of Shields parameter indicates that the flow should not be considered to be of pure sheet flow (i.e. where particles are in permanent contact with each other), and the value for hydraulic roughness factor is calculated from Eq. 4-27. The empirical coefficients x_1, x_2, x_3 and x_4 were chosen by Matoušek for best-fit to the experimental data set (x_1=260, x_2=1.0, x_3=2.5, x_4=1.7).

$$k_s = d_{50}x_1\left(\frac{R_{ha}}{d_{50}}\right)^{x_2}\left(\frac{v_t}{v_a}\right)^{x_3}\Theta x_4 \tag{4-27}$$

4.2 Input parameters for the Matoušek model

Some data for a specific gravel pack operation were given from an NCS operator. Data and parameters are presented in Appendix A. A 5.875 in OD, 26.30 lb/ft drillpipe is assumed for the calculations. This drillpipe has an ID value of 5.045 in[41]. Additional input parameters for the model need to be calculated based on the given pump rate and gravel mass rate. Concentrations, flow rates and mixture velocity also need to be calculated for input to the model. These calculations are also presented in the appendix. The median particle diameter is a vital input parameter for the model and is found from sieve analysis. For the modelling a 20/40 US mesh gravel sand is assumed, as this is a typical size for gravel pack operations. The mesh sizes and corresponding openings are given in Table 4-1[5].

Table 4-1 Mesh sizes and gap dimensions[5]

US mesh	Gap dimension (mm)
18	1.000
20	0.841
25	0.707
30	0.595
35	0.500
40	0.400
45	0.354

The 18 and 45 meshes are added as they will be necessary for the calculations. A presentation of the weight percentages from sieving of a gravel sand sample comes from the gravel sand producer, and was given from the NCS operator as part of the field data. For calculation of bulk density, the approach of Santiso and Müller[29] is used as presented in Chapter 3.4.2. Sieve analysis data and calculations of bulk density and median particle diameter are shown in Appendix B.

Several brine types are available for use as carrier fluid, and the choice is here made from the desired density. Both NaCl and NaBr, and mixtures of these are widely used. The brine types and their related densities are presented in Table 4-2[6]. The carrier fluid density given is valid for surface conditions, and hence needs to be corrected for downhole temperature. One method is to correct it for the difference of surface and the circulating temperature. A generic field case with data and temperature correction is presented in Appendix C.

Table 4-2 Brines and related densities[6]

Brine type	Density range (ppg)	Density range (kg/m^3)
NaCl	8.4 – 10.0	0.983 – 1.171
NaBr	8.4 – 12.7	0.983 – 1.487
NaCl/NaBr	8.4 – 12.7	0.983 – 1.487

To estimate the terminal settling velocity for particles, the Schiller-Naumann equation for drag coefficient is chosen (Eq. 3-11). The drag coefficient is dependent on the particle Reynolds number, which again is dependent on the terminal settling velocity. From combination of the general equation for terminal settling velocity (Eq. 3-8), the expression for particle Reynolds number (Eq. 3-5) and the equation for drag coefficient, it is clear that the expression for terminal velocity is implicit. An iterative process is called for, guessing for the velocity until a close match is reached. Resulting graph is shown in Figure 4-2, while the iteration process itself is presented in Appendix D. Terminal settling velocity is estimated to be about 0.64 m/s.

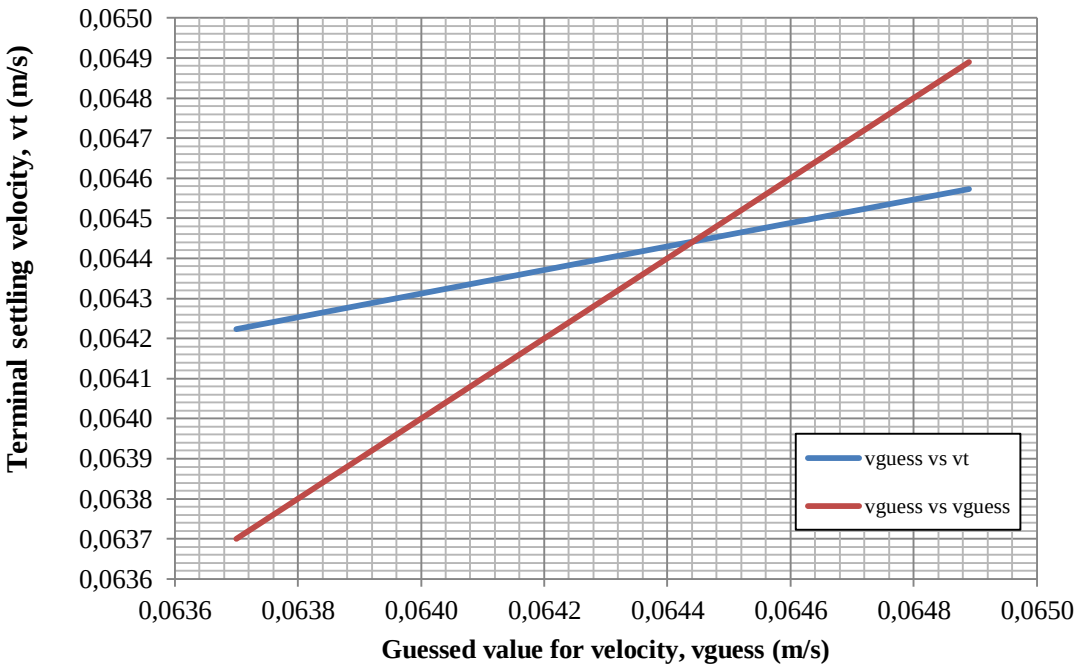

Figure 4-2 Resulting graph from iteration on terminal settling velocity

4.3 Calculation of bed height and weight of sediments

Now, all input parameters are available for modelling of the sedimentation in work string. Input data for the model are presented in Table 4-3. Output parameters of the model are bed height and hydraulic gradient, and they can be solved through iteration of the bed height y_b. The equations presented in this chapter were implemented in Excel. First a value of y_b is guessed for. The size and hydraulic radius of the discharge area and related wetted perimeters are found. This gives information to calculate the mixture velocity in the discharge area, and the solids flow rate is given from Eq. 4-7. Bed friction velocity is calculated to find Shields parameter for the bed. Now it is possible to express the solids flow rate with Eq. 4-16. The iteration goes on until the solids flow rates from the two aforementioned equations match within a decent error margin. All other parameters used in the modelling and their values are shown in Table 4-4.

Table 4-3 Input for work string model

Input parameter	Value
internal diameter pipe, D_p	5.045 in – 0.128143 m
median particle diameter, d_{50}	0.00058 m
volumetric particle concentration, C_{vd}	0.044943396
fluid density, ρ_f @ circulating temp.	1237 kg/m^3
solids density, ρ_s	2650 kg/m^3
fluid viscosity, μ_f	1.6 cP – 0.0016 kg m^{-1}s^{-1}
terminal settling velocity, v_t	0.06444 m/s
mixture flow velocity, v_m	1.486164724 m/s

Table 4-4 Calculated values for modelling

Intermediate parameters and related values			
Areas		Hydraulic radii	
A_t	0.012896731 m^2	R_h	0.03203575 m
A_a	0.011797102 m^2	R_{ha}	0.030003088 m
A_{aw}	0.003470864 m^2	R_{hw}	0.011409157 m
A_{ab}	0.008326238 m^2	R_{hb}	0.093575432 m
A_b	0.001099629 m^2		
Geometrical parameters		Wetted perimeters	
A_{sector}	0.0031509 m^2	O_b	0.088978894 m
$A_{triangle}$	0.00205127 m^2	O_w	0.304217376 m
γ	0.767546657 rad		
Velocities		Reynolds numbers	
v_a	1.624692813 m s^{-1}	N_{Re}	147235.1668
u_{*b}	0.201450466 m s^{-1}	Re_p	28.8957015
		$Re_{p'}$	36.15034465
Shear stresses		Shields parameters	
τ_b	50.20029316 Pa	Θ	6.24406033
τ_w	6.120656092 Pa	Θ_{cr}	0.03322047
Friction factors and roughness		Solids flow rates and flux	
λ_b	0.122994027	q_s	0.009681114 m^2 s^{-1}
λ_w	0.014996011	$Q_s = C_{vd}A_a v_a$	0.000861415 m^3 s^{-1}
k_s	0.0550397 m	$Q_s = q_s O_b$	0.000861415 m^3 s^{-1}
Output			
i_m	0.044208493		
y_b	0.0179646 m		

A value of bed height was found to be approximately 1.8 cm for the data set, corresponding to a cross-sectional area of bed of about 0.0011 m^2. The mass of gravel that have settled out per length unit of pipe is given by Eq. 4-28, where cross-sectional area of bed from modelling and the derived bulk density for the gravel sand are now known.

$$m_b = A_b L \rho_{bulk} \tag{4-28}$$

Choosing a practical unit of kg/100m yields:

$$m_b = 0.001099629\, m^2 * 100\, m * 1643\, \frac{kg}{m^3} \approx 181\, \frac{kg}{100\, m}$$

Based on the slurry transport model presented and the proposed solution for bulk density, there is now a way to quantify the amount of gravel that have settled out inside the horizontal part of the work string. It is most convenient to be able to estimate this during operational planning, and thus have a possibility for avoidance. If, for other operational reasons, the pipe diameter or pump rate cannot be changed, the issue is at least highlighted and the additional gravel consumption should be known.

4.4 Bed friction vs. wall friction

From the output of the modelling, the frictional pressure drop can be seen to be influenced by the friction related to the bed surface λ_b. Friction factor for the sub-area influenced by the bed is over eight times higher than the friction factor of area related to the pipe wall λ_w. This is expected since the pipe wall is much smoother than the bed surface. From Eq. 4-13 and 4-14, an average friction factor can be found that is representative for the pressure loss through the system, using Eq. 4-29. Here λ_a is the friction factor for the entire discharge area A_a above the bed, an average of the friction factors of the two sub-areas.

$$i_m = \frac{\lambda_a v_a^2}{2g4R_{ha}} \tag{4-29}$$

All values except the friction factor is known and presented in Table 4-4. Solving yields a friction factor $\lambda_a \approx 0.039$. Both the bed and wall friction contributes to this average, and it might be interesting to see how the mutual distribution corresponds to the wetted perimeters of the two sub-areas. Lengths of these are found in Table 4-4. The ratio of wetted perimeter of bed, O_b to the total perimeter is:

$$\frac{O_b}{O_b + O_w} = \frac{0.088978894m}{0.088978894m + 0.304217376m} \approx 0.226$$

To find the magnitude of the bed friction influence on the average friction, a simple equation can be solved, where X is the ratio of the bed friction to wall friction.

$$\lambda_b X + \lambda_w (1 - X) = \lambda_a$$
$$0.12294027X + 0.014996011(1 - X) = 0.039435572$$
$$X \approx 0.226$$

This shows that the friction factors for the sub-areas are directly given by the ratio of their characteristic wetted perimeter to total perimeter. An implication of this is that the higher the bed, the more influence the bed friction will have on the friction loss in the open area.

4.5 Sensitivity study

A sensitivity study was conducted, and some of the input parameters influence on the result will be discussed in this chapter. The gravel pack process is not necessarily performed with a constant pump rate throughout the whole operational time, as there might be some variations. It is therefore logical to analyze how different pump rates impact the degree of sedimentation. It is also interesting to see effects form variation of the internal pipe diameter. A selection of the pipe sizes and their related internal diameters used for this study is presented in Table 4-5[41, 42]. Typical pipe sizes used in drilling and well operations are 5 in, 5.5 in and 5.875 in. Depending on the nominal weight, there are several options for internal diameters within each size class.

Table 4-5 Pipe types and related internal diameters[41, 42]

Pipe body diameter (in)	Internal diameter, D_p (in)	Nominal weight (lbm/ft)
5	3.750	32.60
5	4.000	25.60
5	4.276	19.50
5.5	4.670	24.70
5.5	4.778	21.90
5.875	4.595	40.91
5.875	4.625	34.21
5.875	5.045	26.30
5.875	5.153	23.40

For practical reasons, all diameters are given in inches. First the bed height is plotted against pump rate for pipe sizes of commonly used nominal weights in Figure 4-3. Bed height is plotted against pump rates, as this is a common way to express the flow rate. Constant gravel concentration is assumed, and thus the solids flow rate will vary with the pump rate. The curves show a nearly linear relationship between pump rate and height of sediments. For the pipe size used in the field case, the pump rate to avoid sedimentation is nearly 1350 lpm. Going for a slightly smaller internal diameter of 4.778 in the given pump rate of 1150 lpm will give a bed height of 0.3 cm. The plot shows examples of three different pipe OD sizes with a typical ID value. There may be other operational reasons to use the 5.875 in OD pipe, but from Table 4-5 there are other internal diameters for this pipe size that clearly would have been a better choice concerning the risk of sedimentation. The Matoušek model has limitations and will fail for describing scenarios with very thin beds. This is believed to be the reason for the assymptotical behavior graphs are showing before reaching zero bed height. Graphs are indicating that both the flow rate and the internal diameter of the pipe are of high importance to degree of sedimentation.

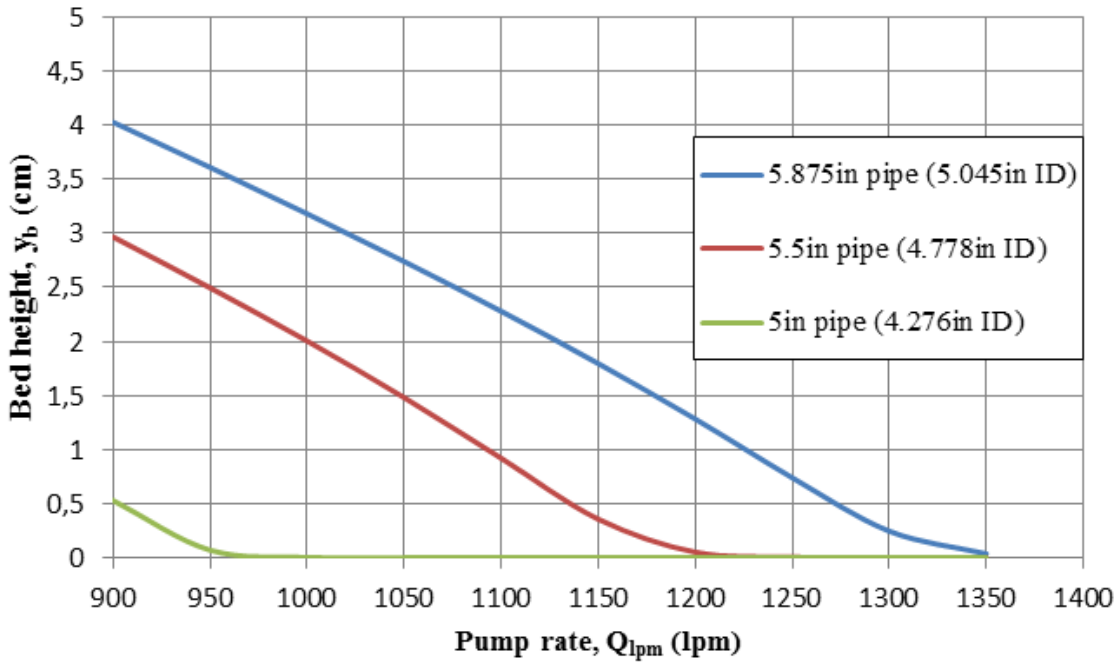

Figure 4-3 Bed height of immobile gravel versus pump rate for three different pipe types

A plot of bed height versus variation in internal diameter is presented in Figure 4-4. Here the discrete diameters for the different pipe types in Table 4-5 are plotted against bed height and connected to show the trend. The plot is a representation of typical internal diameters available and displays the degree of sedimentation for the different flow areas with a pump rate of 1150 lpm and constant gravel concentration. The graph shows an abrupt change in sedimentation going from 4.670 in to 4.778 in ID, and this is indicating a critical corresponding flow velocity in between these internal diameters. For the field case, there might have been possible to avoid the sedimentation if a smaller ID pipe was used instead.

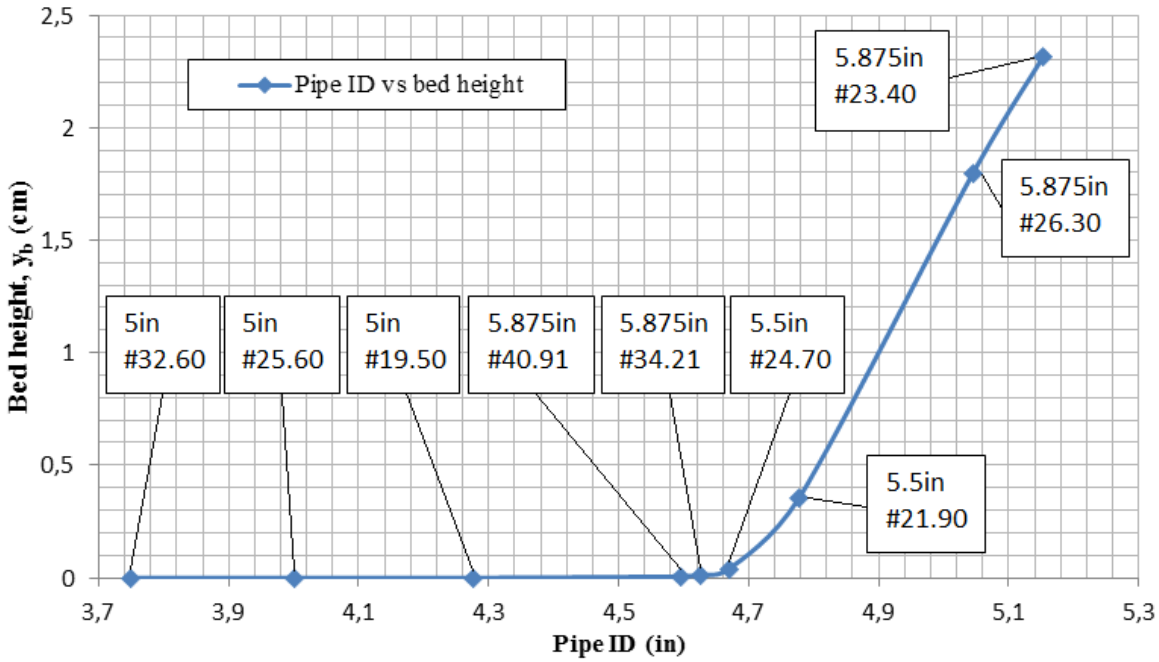

Figure 4-4 Bed height of immobile gravel with varying internal pipe diameter

(This page intentionally left blank)

5 MODELLING OF ALPHA WAVE

For modelling of the alpha wave in gravel packing, Gruesbeck et al. model is chosen[1]. It is commonly used by the industry for this purpose, and is reckoned as the pioneer work for describing the process of gravel packing. Other Master's theses[15, 16, 43] have presented modelling based on other critical velocity models for the gravel packing, like Penberthy et al. and Oroskar and Turian [2, 3]. These models will be presented briefly in this thesis, and resulting values are used for comparison with the results from the modelling. The Gruesbeck et al. model will be presented in Chapter 5.1. Calculations based on field data and generic data used in this thesis will be presented in Chapter 5.2, where also the results will be compared to the other models for critical velocity, and ultimately to the known field data to verify the accuracy. Sensitivity study on a selection of parameters is presented in Chapter 5.3, and in Chapter 5.4 the validity of implementing Swamee-Jain friction equation into the model is discussed.

5.1 The Gruesbeck et al. model

A method for describing the slurry transport in gravel packing was presented by Gruesbeck et al. Based on experimental data and curve fitting of these, an expression for the critical velocity was produced. Both small scale and what was called full scale model were used in experiments, consisting of wire wrapped screen inside acrylic pipe to represent the borehole annulus. A pipe was placed inside the screen to represent a washpipe. Several test were run on the small scale model, with varying inclination and gravel of 20/40 US mesh size. Both tap water and brines were used as carrier fluids. This set-up was used to build the mathematical model, which was in turn verified in the larger scale model. Experiments showed that packing efficiency in deviated wellbores increases with lower gravel concentration, reduced particle density, reduced particle diameter, higher fluid density, higher flow rate of the slurry and increased resistance for fluid flow in washpipe/screen annulus. Gruesbeck et al. holds the latter as the most important variable to achieve successful packing. Reducing the flow through this annulus will reduce the dehydration of the slurry, and therefore minimize the risk of a premature pack. Hence, the packing efficiency can be increased by using a larger diameter washpipe. The experiments showed that having a washpipe diameter to screen internal diameter ratio of greater than 0.6 would optimize gravel packing of deviated wells. The large scale model experiments were made with a range of different particle sizes and brines with density range of 1000 to 1750 kg/m^3, and viscosities from 1 to 100 cP. The experiments did not consider fluid leak-off. Excessive fluid leak-off during the packing process may though be devastating for the outcome, as dehydration of the gravel mixture can lead to higher local gravel

concentration, and therefore increasing the velocity needed to transport gravel above the bed. More gravel settle out, building the height of the bed to a new equilibrium, and it can in worst case lead to total bridging of the annulus and related premature screen-out. Additionally, the increase in concentration and bed height will raise the pressure, leading to more leak-off and possible fracturing of the borehole wall.

The flow of fluid can take two paths; over the sediment bed and through the screen/ washpipe annulus. Flow paths are parallel, and the resistance between them is neglected. The frictional pressure gradients in both annuli are then approximately equal (Eq. 5-1). Here, subscript *o* denotes screen/openhole annulus and w_p denotes screen/washpipe annulus. Mixture of carrier fluid and gravel flows over the bed, and carrier fluid flows in screen/washpipe annulus.

$$\left(\frac{\Delta P}{L}\right)_o \approx \left(\frac{\Delta P}{L}\right)_{wp} \tag{5-1}$$

The pressure gradient in the slurry flowing over the sediment bed is higher than in an equal volume of fluid without solids. The difference in pressure gradient between the two is expressing the energy needed to transport the particles over the bed. Recalling Eq. 3-44 the expression can be written as:

$$\frac{\lambda_* v_*^2 \rho_f}{2D_{h*}} + \psi = \frac{\lambda_{wp} v_{wp}^2 \rho_f}{2D_{hwp}} \tag{5-2}$$

Here, D_{h*} is the hydraulic diameter of the area open to flow above the equilibrium bed, v_* is the equilibrium velocity of the gravel slurry, λ_* is the friction factor related to the fluid flow above bed at equilibrium condition and ψ is a pressure drop increment due to presence of solids. The left hand side of the equation is representing the pressure gradient in solids-free fluid above the equilibrium bed plus the increment from the presence of solids, while right hand side is representing the pressure gradient in screen/washpipe annulus. Originally, Gruesbeck et al. used Blasius equation for the friction factors. As mentioned in Chapter 3, Blasius equation predicts friction factor for smooth pipe. For the modelling of the gravel packing in this thesis, Swamee-Jain equation is used, as the surfaces are considered not smooth (Eq. 3-56). Prediction of the bed height at equilibrium requires a material balance on the fluid and gravel. The scope of work of this thesis is not considering fluid loss, and it is assumed to be zero. An incompressible carrier fluid is also assumed. The material balance equation at equilibrium is given as:

$$(1-C_{vd})Q_m = (1-C_*)Q_* + Q_{wp} + Q_{fl} \tag{5-3}$$

The flow rate split balance through the system at equilibrium, disregarding the fluid loss, can be expressed as:

$$Q_m = Q_* + Q_{wp} \tag{5-4}$$

Then, combining the two equations and rearranging yields:

$$Q_s = Q_m C_{vd} = Q_* C_* \tag{5-5}$$

Actual density of the mixture in screen/openhole annulus at equilibrium conditions can be given as:

$$\rho_m = \rho_s C_* + \rho_f (1 - C_*) \tag{5-6}$$

Eq. 5-3 is expressing the volume balance of the carrier fluid, where Q_m is the initial injected flow rate of mixture, Q_* is the volumetric flow rate in the open area above bed, Q_{wp} is the flow rate in screen/washpipe annulus, Q_{fl} is the rate of fluid loss to formation, C_{vd} is the initial volumetric concentration of gravel, Q_s is the solids flow rate and C_* is the volumetric concentration of the gravel above the bed. Eq. 5-5 is expressing volume balance of the gravel. The equations are only valid when dune has attained an equilibrium height. Gravel is only present in the screen/openhole annulus, so that gravel concentration in the discharge area will be higher than the injected concentration.

5.1.1 Critical velocity

The critical velocity for transport of gravel along the sediment bed is the equilibrium velocity, where the particles attain a dynamic equilibrium and deposition rate equals suspension rate. Gruesbeck et al. states that "The equilibrium velocity is the average slurry velocity required to transport particles along the top of the equilibrium bank". The deposited gravel will build a bed, which restricts flow in annulus and this leads to an increase in slurry velocity above the bed. For a constant flow rate, the slurry flowing above the bed will eventually reach a velocity that prevents further increase of bed height, and the net deposition stops. If flow rate is increased, the slurry velocity increases and the bed is eroded until a new equilibrium is attained. As the bed is deposited along the wellbore, the bed height could increase toward the toe of the well, since fluid loss to formation dehydrates the slurry. This is important to keep in mind if the reservoir section is known to have high loss rate. If so, there are other gravel pack methods to consider, such as alternate path pack.

The equilibrium velocity is dependent upon particle concentration above the bed and the forces acting on the particles. Developing the critical velocity expression, four dimensionless groups including these forces were used, and based on a curve fit of experimental and calculated values an expression for the equilibrium velocity was found (Eq. 5-7). Here, v_t is the terminal settling velocity of the particles, and d_{50} is used to represent the particle diameter.

$$v_* = 15 v_t \left(\frac{D_{h*} v_t \rho_f}{\mu_f} \right)^{0.39} \left(\frac{d_{50} v_t \rho_f}{\mu_f} \right)^{-0.73} \left(\frac{\rho_s - \rho_f}{\rho_s} \right)^{0.17} C_*^{0.14} \tag{5-7}$$

For horizontal particle transport, Gruesbeck et al. found that the incremental pressure difference from particle presence in the slurry when flowing above the bed, compared to an equal volume of solids-free fluid, showed a linear relation when plotted against the product of equilibrium particle concentration and the particle relative submerged density. This relationship enables the possibility to express ψ knowing only the concentration, particle density and fluid density. The plot from the original article is presented in Figure 5-1 and shows the pressure gradient from presence of particles in the slurry flowing over a horizontal bed[1]. The slope shows an approximated value of 50, and ψ can now be estimated from Eq. 5-8. Correlation is valid for carrier fluid dynamic viscosity up to 6cP.

$$\psi \approx 50 \left(\frac{\rho_s - \rho_f}{\rho_f} \right) C_* \tag{5-8}$$

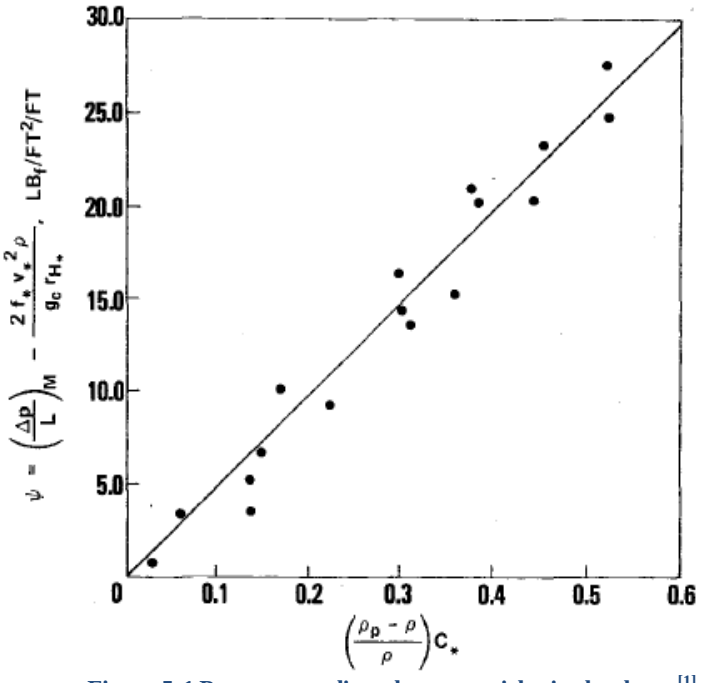

Figure 5-1 Pressure gradient due to particles in the slurry[1]

5.1.2 Flow rate split

The theory of flow rate splitting between the two annuli is the heart of the Gruesbeck et al. model. From the pressure drop balance at equilibrium, given by Eq. 5-2, the flow rate split ratio of the annuli can be deducted. For the modelling, the percentage of flow rate going through screen/washpipe annulus is used for the iteration. An expression for the ratio is derived in this sub-chapter.

Consider a general pressure loss balance equation, not necessarily at equilibrium like presented in Eq. 5-9, where now λ_o is the friction factor of the open area above the bed, v_o is the mixture velocity above the bed and D_{ho} the related hydraulic diameter of the open area:

$$\frac{\lambda_o v_o^2 \rho_f}{2D_{ho}} + \psi = \frac{\lambda_{wp} v_{wp}^2 \rho_f}{2D_{hwp}} \tag{5-9}$$

Rearranging this expression to a ratio of the fluid velocities in the annuli yields:

$$\frac{v_o}{v_{wp}} = \sqrt{\frac{\lambda_{wp} D_{ho}}{\lambda_o D_{hwp}} - \frac{2\psi D_{ho}}{\lambda_o \rho_f v_{wp}^2}} \tag{5-10}$$

Re-expressing Eq. 5-4 on a general form, where Q_o denotes flow rate in screen/openhole annulus gives:

$$Q_m = Q_o + Q_{wp} \tag{5-11}$$

Let R_Q be the ratio between flow rate in screen/openhole annulus and flow rate in screen/washpipe annulus. Expressing the flow rates as area times velocity, where A_o is the cross-sectional area above bed and A_{wp} is the cross-sectional area for flow in screen/washpipe annulus, the following expression can be derived:

$$R_Q = \frac{Q_o}{Q_{wp}} = \frac{A_o v_o}{A_{wp} v_{wp}} \tag{5-12}$$

Combining Eq. 5-10 and 5-12 gives an expression for the flow rate ratio:

$$R_Q = \frac{A_o}{A_{wp}} \sqrt{\frac{\lambda_{wp} D_{ho}}{\lambda_o D_{hwp}} - \frac{2\psi D_{ho}}{\lambda_o \rho_f v_{wp}^2}} \tag{5-13}$$

From Eq. 5-12 an expression for the flow rate in screen/washpipe annulus is found:

$$Q_{wp} = \frac{Q_o}{R_Q} \tag{5-14}$$

Combining Eq. 5-11 and 5-14 yields:

$$Q_m = Q_o + \frac{Q_o}{R_Q} = Q_o\left(1 + \frac{1}{R_Q}\right) \tag{5-15}$$

Then, the ratio of flow rate in screen/washpipe to total flow rate is then:

$$\frac{Q_{wp}}{Q_m} = \frac{1}{1+R_Q} = \frac{1}{1+\frac{A_o}{A_{wp}}\sqrt{\frac{\lambda_{wp}D_{ho}}{\lambda_o D_{hwp}} - \frac{2\psi D_{ho}}{\lambda_o \rho_f v_{wp}^2}}} \tag{5-16}$$

The flow rate split can be seen to vary with variations of the hydraulic diameters and areas of the annuli, the friction factors of the annuli and the flow velocity in screen/washpipe annulus. Through ψ, the flow rate split will also vary with the concentration and density difference of the particles and fluid (Eq. 5-8). As the alpha dune height increases, a lesser percentage of flow will go above the dune as more flow is going through the screen/washpipe annulus. This is intuitive as it is expected that a higher bed poses a larger restriction to the flow above the bed, and that the flow will find less resistance going through the screen/washpipe annulus.

5.1.3 Alternative approach to flow rate split

An alternative to Gruesbeck et al. pressure drop balance exists, and this approach will give a slightly different flow rate split. The equation is similar to that presented in Eq. 5-9, only that now the pressure drop above the alpha dune bed is expressed by the mixture density as presented earlier in Eq. 5-6. The pressure drop balance is:

$$\frac{\lambda_o v_o^2 \rho_m}{2D_{ho}} = \frac{\lambda_{wp} v_{wp}^2 \rho_f}{2D_{hwp}} \tag{5-17}$$

An expression for the flow rate ratio can be derived by using the same method as used for Eq. 5-16:

$$\frac{Q_{wp}}{Q_m} = \frac{1}{1+R_Q} = \frac{1}{1+\frac{A_o}{A_{wp}}\sqrt{\frac{\lambda_{wp}D_{ho}\rho_f}{\lambda_o D_{hwp}\rho_m}}} \tag{5-18}$$

This approach gives a less complex expression compared to the former. The pressure drop balance of Eq. 5-17 is indicating that the entire difference in pressure drop of the two annuli originates from the difference in density of the mixture and the carrier fluid, and thus the concentration. Results from modelling in Chapter 4 indicated that if the bed height is increased, the bed friction will have a larger effect on the total pressure drop. The relation of the pressure increment ψ of Gruesbeck et al. was found from experiments and can be thought of as a collective term for all influence from the presence of solid particles, not only limited to the influence of concentration and density. It is therefore believed that Gruesbeck et al. method is the more representative to use for further modelling of the alpha wave. The screen to OH diameter ratio is larger for the modelled field case than for the Gruesbeck et al. experiment, and there is then some uncertainty to how accurately the slope of the graph in Figure 5-1 resembles the field case. Full-scale experiments are advised.

5.2 Calculations

Determination of alpha wave dune fill percent is the aim for the modelling, as the success of the gravel packing is governed by the successful placement of an alpha dune of adequate height. To low and the result can be a low overall fill percent, to high and there is a risk of premature screen-out. First, the input parameters and the iteration procedure are presented. Calculations for the base case are done using Gruesbeck et al. model for flow split and critical velocity. Two other models for finding critical flow velocity are presented and results compared to what was found earlier. The results from modelling are then compared to pumping time and real alpha dune gravel fill from the operation, using the actual gravel pack job pump chart. An alternative approach to the modelling is presented to conclude this sub-chapter, a method that enables the design of a specific alpha wave fill percent.

5.2.1 Input to model and iteration

Based on data given from an NCS operator, the alpha wave propagation of the gravel pack process will be modelled. Additionally, the generic data used in the modelling of the work string case will be utilized to supplement the unknowns. The data is presented in Table 5-1. For calculations, screen/washpipe wall roughness ε_{wp} is chosen based on Table 3-2, assuming some corrosion, while open hole (borehole wall) roughness ε_{OH} is chosen within

the range of roughnesses for a low competence rock in Table 3-3. Other parameters can be deducted from this data set and were presented in Chapter 4 and the related appendices. They are for convenience also presented in Table 5-1. Screen outer diameter was given from operator and is believed to be an averaged diameter over the screen length, accounting for the OD changes between screen shroud and base pipe. The assumptions are horizontal well configuration, no fluid loss to formation and incompressible carrier fluid.

Table 5-1 Data set for modelling of OHGP

Parameters	Value
Data from operator	
D_w wellbore drilled diameter	8.5 in – 0.2159 m
D_s screen outer diameter	7.154 in – 0.1817116 m
D_{si} screen internal diameter	5.921 in – 0.1503934 m
D_{wp} washpipe outer diameter	5 in – 0.1270 m
Q_{lpm} pump rate	1150 lpm
Gravel mass rate	136.965 kg/min
ρ_f	1250 kg m^{-3}
ρ_s	2650 kg m^{-3}
Generic data	
μ_f	1.6 cP/0.0016 kg $m^{-1}s^{-1}$
d_{50}	0.00058 m
v_t	0.06444 m s^{-1}
ρ_{bulk}	1643 kg m^{-3}
ε_{wp} roughness screen/washpipe annulus	0.0001 m
ε_{OH} roughness screen/openhole annulus	0.01 m
Deducted data	
C_{vd} Mean delivered gravel concentration	0.044943396
Gravel added	1.0175 ppa/119.1 kg m^{-3}
ρ_f Temperature corrected fluid density	1237 kg m^{-3}
Q_m Mixture flow rate	0.019166667 m^3 s^{-1}
Q_f Carrier fluid flow rate	0.018305252 m^3 s^{-1}
Q_s Solids flow rate	0.000861415 m^3 s^{-1}

The modelling process is making use of iteration on the ratio of the total flow rate going through screen/washpipe as input (Eq. 5-16). Flow rate splitting is for the modelling assumed to happen at the heel screen. As gravel slurry is pumped out through the gravel pack tool and into the wellbore, some carrier leaks through the screen and into the annulus between washpipe and screen. As the bed height increases, more flow will be directed into the screen/washpipe annulus when the flow resistance in screen/openhole annulus increases, and gravel concentration in the slurry will increase. Gravel is transported in the annulus between screen and open hole and builds a bed to an equilibrium height when gravel settles out. The goal of the modelling is to balance the pressure gradients in Eq. 5-2. A bed height must first be guessed for to render the area open to flow above bed. As a start,

bed height flush with screen diameter is chosen as this equals the lower value that the proposed model is developed for. Geometrical areas and hydraulic diameters are calculated using equations from Chapter 3.3. This establishes a gravel fill percent from Eq. 3-33. Then the pressure losses in the two annuli are balanced by iteration of the flow rate ratio Q_{wp}/Q_m. Once the balancing is done the output value of velocity above the bed is compared to the critical velocity from Eq. 5-7. If there is no decent match, a new bed height must be chosen and the process is repeated until an equilibrium velocity is accomplished.

Using Eq. 5-9 for flow rate split, the incremental pressure difference ψ is found to be dominating the pressure loss at higher values for the flow rate ratio Q_{wp}/Q_m. Caution should be exercised in the iteration process since the pressure balance at two different flow rates, one lower and one higher. The higher solution was typically found at a ratio of about 0.96, and this was seen to give rise to gravel concentrations exceeding one hundred percent. The higher solution for flow rate split is therefore invalid, and iteration must be done from the lowermost solution.

5.2.2 Calculations based on Swamee-Jain friction equation

In the original Gruesbeck et al. model, Blasius friction equation (Eq. 3-53) is used for calculating the friction factor and pressure losses in both annuli, since the model is developed assuming smooth surfaces and based on experiments using plastic pipe to resemble the borehole wall. This suits well for the screen/washpipe annulus, where the carrier fluid is in contact with the steel inner surface of the screen and outer surface of the washpipe. The utilization is however questionable for the screen/openhole annulus, where the borehole wall roughness could be much higher (Table 3-2 and 3-3). Because this thesis contemplates only alpha wave gravel fill above screen, the involved surfaces are bed and formation wall. This implies expressing the friction factor based on hydraulically rough surfaces. For the case of modelling the alpha wave, the borehole wall and gravel bed can then be considered hydraulically rough. Additionally, the roughness of the screen/washpipe annulus is dependent on the wear and corrosion of the steel surfaces, and another friction equation is preferred. Swamee-Jain equation (Eq. 3-56) is explicit and yields the friction factor directly without the need for iteration. It is as well valid over the range of Reynolds numbers for the flow conditions encountered in the gravel packing process. Absolute roughness ε of the surfaces goes into the equation, and representative values are chosen from Table 3-2 and 3-3. The rock formation is assumed to be of low competence and a conservative value of ε_{OH} = 0.01 m is selected. The internal surface of screen and external surface of the washpipe are assumed to be mildly corroded and a value of $\varepsilon_{wp} = 1.0*10^{-4}$ m is selected.

The base case of 8.5 in OH can now be modelled and calculated values are presented in Table 5-2, while iteration is presented in Appendix E.

Table 5-2 Calculated values and output of modelling using Swamee-Jain friction for 8.5 in OH

Parameters	Values
Screen/openhole annulus	
Q_* equilibrium flow rate in open area	0.003666775 $m^3 s^{-1}$
A_o area open to flow	0.002820977 m^2
A_{so} total area of annulus	0.0106764705 m^2
D_{h*} hydraulic diameter	0.0369537572 m
N_{Re} Reynolds number	37136
λ_* equilibrium friction factor	0.194668899
C_* equilibrium solids concentration	0.2349244472
$(\Delta P/L)_o$ frictional pressure gradient	5505 Pa m^{-1}
ψ incremental pressure drop from solids	2108 Pa m^{-1}
Screen/washpipe annulus	
Q_{wp} equilibrium flow rate	0.015499892 $m^3 s^{-1}$
A_{wp} area of annulus	0.0050965859 m^2
D_{hwp} hydraulic diameter	0.0233934 m
N_{Re} Reynolds number	55004
λ_{wp} equilibrium friction factor	0.031131351
$(\Delta P/L)_{wp}$ frictional pressure gradient	7613 Pa m^{-1}
v_{wp} fluid velocity	3.04 m s^{-1}
Output	
Q_{wp}/Q_m Flow rate split ratio to washpipe/screen annulus	0.80869
γ sector angle	0.7400196208 rad
y_b bed height	0.187666254 m
v_* equilibrium velocity	1.30 m s^{-1}
Volumetric gravel fill percent	73.58
Height fill percent	86.92

Mixture velocity above bed and critical velocity is plotted against volumetric gravel fill percent in Figure 5-2. The crossing point of the two velocity graphs represents the equilibrium velocity, and the gravel fill percentage is the corresponding value on the horizontal axis. Critical velocity shows a near linear relationship with the gravel fill percent, and hence the bed height. Mixture velocity is declining as the increasing bed height will ensure less fluid is flowing through the screen/openhole annulus. The graphs are plotted within the range of gravel fill, which is the scope of this study; from the gravel fill covering the screens and up to about 90 percent volumetric fill. This has been done in accordance to the design criteria 70 to 90 percent given by Bellarby[5]. It was not possible to balance the pressure loss gradients of the two annuli above approximately 85 percent fill, and so this seems to be the limit of the model used for the chosen parameters. The inability to balance the pressure losses above this gravel fill is likely to be caused by interference from the secondary solution discussed in sub-chapter 5.2.1.

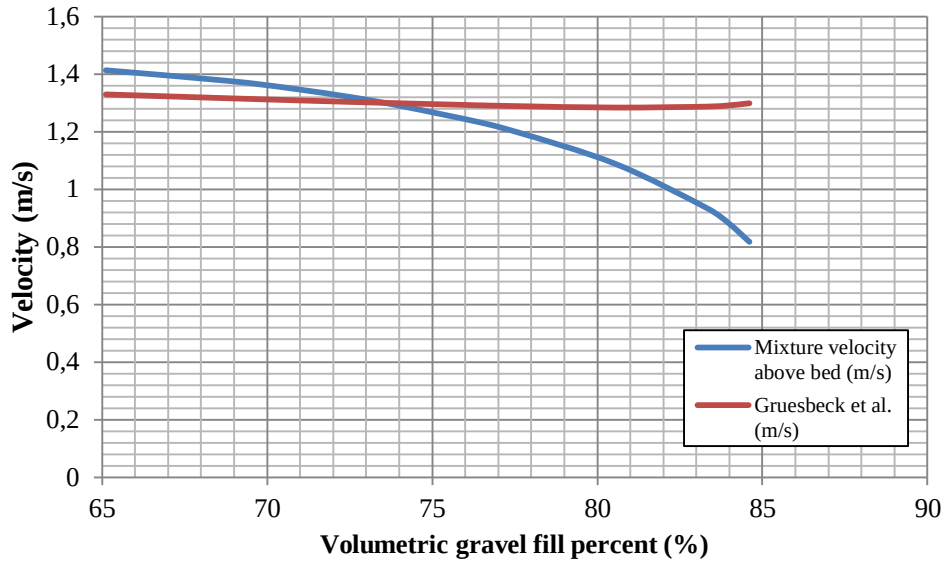

Figure 5-2 Equilibrium velocity and corresponding gravel fill using Swamee-Jain

Resulting graphs show little resemblance to representations of the actual mixture velocity and critical velocity to gravel fill percent found in other Master's theses, where the critical velocity is decreasing with increasing gravel fill and mixture velocity is increasing rapidly at high fill percentages. This is believed to come from handling the flow rate split fixed throughout the calculations, whereas the concept of the modelling in this thesis considers the flow rate split as varying with increased bed height. The slight increase in the critical velocity (red curve) is believed to originate from the rapid increase in gravel concentration, as more and more carrier fluid leaks into screen/washpipe annulus. The higher the concentration, the higher the velocity needed to transport gravel particles will be.

5.2.3 Comparison to other models

Oroskar and Turian presented a model for calculating the critical velocity for slurry flow in pipelines[3]. The model is made for purposes of slurry transport in chemical engineering, and considers only flow through the simple circular pipe geometry. It does not deal with annulus configuration, as it was not developed for gravel packing. Despite this, it has been used for this purpose before. The model is semi-mechanistic and considers both the energy required to suspend particles and the turbulent eddies influencing the transportation of particles, as well as hindered settling due to particle-particle interactions. Regression analysis of 357 data points were done for curve fitting the experimental data. The equation for critical velocity is given as:

$$\frac{v_c}{\sqrt{g d_{50} R_{sd}}} = 1.85\, C^{0.1536} (1-C)^{0.3564} \left(\frac{d_{50}}{D}\right)^{-0.378} N_{\mathrm{Re}}^{-0.09} x^{0.3} \qquad (5\text{-}19)$$

Here, v_c is the critical velocity for settling, C is the volumetric solids concentration, D is the pipe internal diameter and x is the fraction of eddies of velocity higher than the hindered settling velocity of the slurry. For modelling of the gravel pack process, hydraulic diameter must be used instead of the pipe diameter, since the geometry of the annulus differs from that of a circular pipe. The value of x used is 0.96, as this parameter is presented as being close to unity and >0.95. The d_{50} to D ratio is referred to as a characteristic velocity for the flow.

Penberthy et al. developed a model for explaining the gravel placement in horizontal wells. They used a 1500 ft long test rig-up, consisting of 4 in ID casing with 2.0625 in OD centralized screen with ID of 1.7533 in and a 1.315 in OD washpipe. This gave a diameter ratio of washpipe to screen of 0.75. Fluid loss to formation was simulated with perforations along the casing, and this was observed to increase the equilibrium bed height opposite the thief zones. Gravel sizes of 40/60, 20/40 and 12/20 US mesh were used for experiment. Two equations were presented for determination of the critical velocity, where the one giving the maximum value should be selected.

$$v_1 = \left(0.0251\, g_f d_{85} \left(\frac{\rho_s - \rho_f}{\rho_f} \right) \left(\frac{D_h \rho_m}{\mu_f} \right)^{0.775} \right)^{0.816} \tag{5-20}$$

$$v_2 = 1.35 \left(\frac{2 g_f (\rho_s - \rho_f)}{\rho_f} \right)^{0.5} \tag{5-21}$$

Here, g_f is the acceleration due to gravity in ft/s^2, densities are in lbm/ft^3, D_h is the hydraulic diameter of the area above bed in feet, fluid viscosity in lbm/ft-s and d_{85} in feet. The mixture density can be found from Eq. 5-6, using the actual solids concentration above bed. Characteristic particle diameter used in these equations is the diameter representing greater than 85 percent of cumulative weight distribution of the particles. From the cumulative distribution graph in Appendix B, d_{85} is found to be 0.68 mm. Penberthy et al. presented a way of dealing with hydraulic diameter for estimation of the Reynolds number in eccentric annuli. They used what they called *effective diameter*, which is a shape factor times the hydraulic diameter, where the shape factor of the eccentric annulus is dependent on the ratio of the pipe diameters. This shape factor was not intended used in calculation of the hydraulic diameter of the annulus, which has been done in other Master's theses on gravel packing. Calculation of Reynolds number in the screen/openhole annulus is done using the mixture density and fluid viscosity corrected for particle concentration (Eq. 5-22), which differs from the approach of Gruesbeck et al.

$$N_{\mathrm{Re}} = \frac{\rho_m v D_h}{\mu_m} \tag{5-22}$$

The mixture density is given by Eq. 5-6, v is the velocity of the mixture above bed and μ_m is viscosity corrected for solids concentration. The viscosity of the mixture can be calculated using an appropriate equation describing the relationship between the apparent dynamic viscosity and the volumetric concentration of the particles. Here, Thomas equation is presented, which is an expansion of the relationship of Einstein, valid for a broader range of concentrations[44, 45] (Eq. 5-23).

$$\mu_r = \frac{\mu_m}{\mu_f} = 1 + 2.5C + 10.05C^2 + 0.00273e^{16.6C} \tag{5-23}$$

The velocities from these discussed models were plotted against the Gruesbeck et al. model and mixture velocity for the case of 8.5 in OH. From the equations of Penberthy et al. the values of v_2 was found to exceed v_1 at all times, so it was selected for the plot. Resulting graphs are shown in Figure 5-3 and the related data is given in Appendix F.

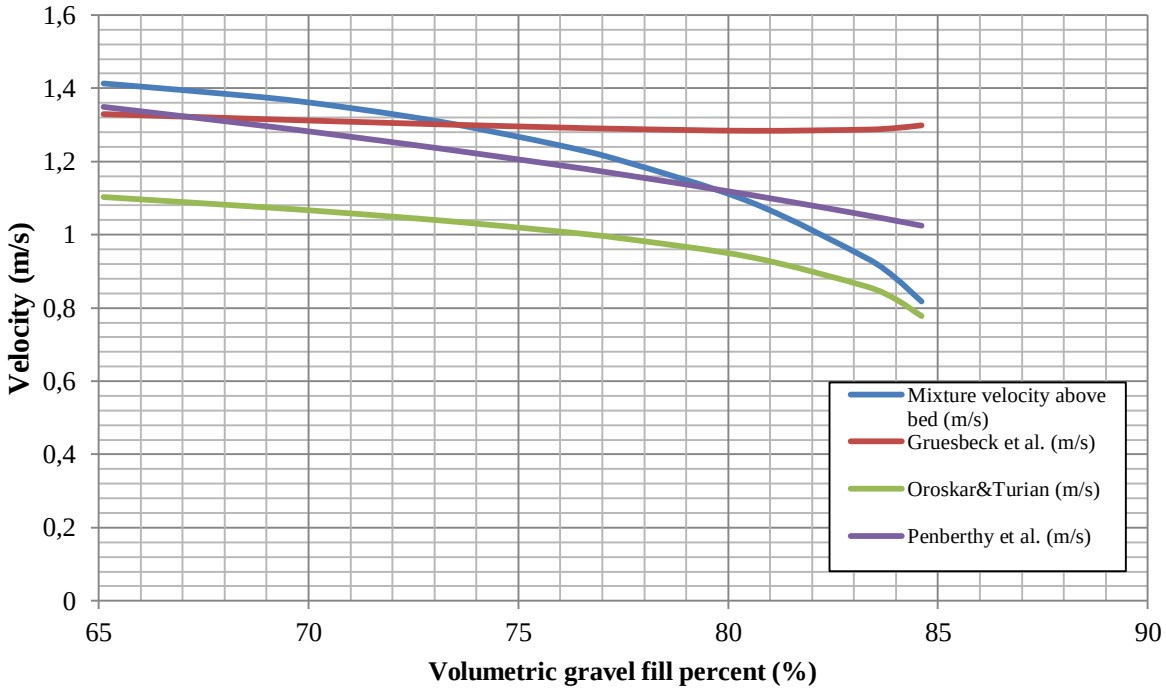

Figure 5-3 Comparison of equilibrium velocities of different models for 8.5 in OH

The graphs are plotted in the range from bed height flush with top of screen ($y_b=D_s$) and up to the point where the model is not able to balance the pressure losses in the two annuli. The critical velocity from Oroskar and Turian seems to equal the mixture velocity somewhere just outside the range of the plot at a gravel fill percent of higher than 85, but this cannot be concluded as it is outside the upper boundary. At the high end of the gravel fill, the graph of Oroskar and Turian shows a marked drop at about the same fill percent where the critical velocity from Gruesbeck et al. model increases distinctly. This can be related to the increasing gravel concentration above the bed, because more carrier fluid leaks through the screens, as discussed in the former sub-chapter for the sudden increase in Gruesbeck et al. critical velocity. As the mixture concentration increases because of the increase of flow through screen/washpipe annulus, the critical velocity of Oroskar and Turian decreases. From Eq. 5-19, the terms involving gravel concentration and the characteristic velocity will be affected. The term of the compliment to the concentration, $1–C$, will dominate and contribute to a reduction of the critical velocity. The critical velocity curve of Penberthy et al. model gives a value of about 79.5 percent, but shows ambiguity, as it seems to also close in on the mixture velocity curve at a second point outside the lower range of the plot. This will be further discussed in the next sub-chapter, when a comparison to field data is made.

5.2.4 Comparison to known field case data

A pumping chart from the actual gravel pack job was received from the NCS operator, together with volumetric data for the work string and directional data for the well. Based on this the modelled gravel fill percent can be compared to reality. First, the pumping time for the slurry to be transported from surface to entering the borehole needs to be calculated. The work string volumetric data is presented in Table 5-3.

Table 5-3 Work string data and total volume

Pipe type	Length (m)	ID (in)	Cross-sectional area (m^2)	Volume (m^3)
5.875 in DP	820m	5.045	0.012896731	10.57531977
8 in DC	145	2.81	0.004001013	0.580146885
5.875 in HWDP	1000	4.00	0.00810732	8.10732
5.875 in DP	1139	5.045	0.012896731	14.68937661
Total volume				33.95216326

A simplified method for approximation of the time it takes to pump gravel from surface to borehole can be used. This does not take into consideration that the solid particles move at higher speed at low inclination angles, due to gravity. Consequently, the real pumping time may be slightly less than the calculated time. The time period for the pumping can be seen on the pumping chart as the drop in pumping pressure before gravel reach the borehole and the alpha wave starts. This pressure drop is related to the density difference of the solid particles and the carrier fluid. Eq. 5-24 is used for approximation of the pumping time, where T_p is the time in seconds for pumping slurry from surface until slurry enters screen/openhole annulus, V_w is the total internal work string volume in m^3 and Q_m is the injected mixture flow rate in m^3/s.

$$T_p = \frac{V_w}{Q_m} \tag{5-24}$$

$$T_p = \frac{33.95216326\ m^3}{0.019166667\ \frac{m^3}{s}} \approx 1771.4\,s \approx 29.5\,\text{min}$$

As mentioned, this assumes no slip velocity for particles transported. The directional data for the well showed that the last thousand meters of the work string has an inclination of >80˚ from vertical. This must be considered when interpreting the pumping chart to find the starting point of the alpha wave. Ideally, there is a clear pressure increase that demarks the beginning of the alpha wave, but as can be seen on the pumping chart presented, the transition is not that clear for this case. This is assumed to be a consequence of the long near horizontal well configuration of the lower part of the work string, and the pressure decline can be seen to stretch out. Pumping chart is presented in Figure 5-4.

Start of beta wave is clearer, and can be seen to begin just before gravel injection on surface is stopped. Start of pumping time 1 is marking the calculated T_p of 29.5 minutes of pumping before slurry enters annulus. Starting point of pumping time 2 is selected where pump pressure shows the first increasing manner. From the calculated pumping time and studying the pressure chart, the volumetric gravel fill percent can be quantified. To utilize this method of deducting the gravel fill percent, some assumptions have to be made. First, the gravel mass rate added to the carrier fluid is assumed to be constant at the value given from operational data (~137 kg/min), and the carrier fluid is assumed to be incompressible. Further assumption is a steady flow rate. Now, the volumetric gravel fill percent can be represented by pumping time only, and the alpha wave fill percent is deduced from the ratio of alpha wave pumping time and total pumping time of alpha and beta wave. The values for both scenarios are given in Table 5-4.

Table 5-4 Pumping times and related volumetric gravel fill percent

	Pumping time 1	Pumping time 2
Alpha	81.3 min	84.0 min
Beta	21.0 min	21.0 min
Fill percent	**79.5**	**80.0**

Modelling shows a volumetric gravel fill percent of 73.58 for Gruesbeck et al. model. This is lower than the actual value deducted from the pumping chart. The reservoir is composed of low competent rock formation, thus some washout and resulting larger wellbore diameter may be encountered. A second attempt can be made assuming a moderate washout at a value of 9 inch wellbore diameter. The calculated values are given in Table 5-5 and the iteration process in Appendix G.

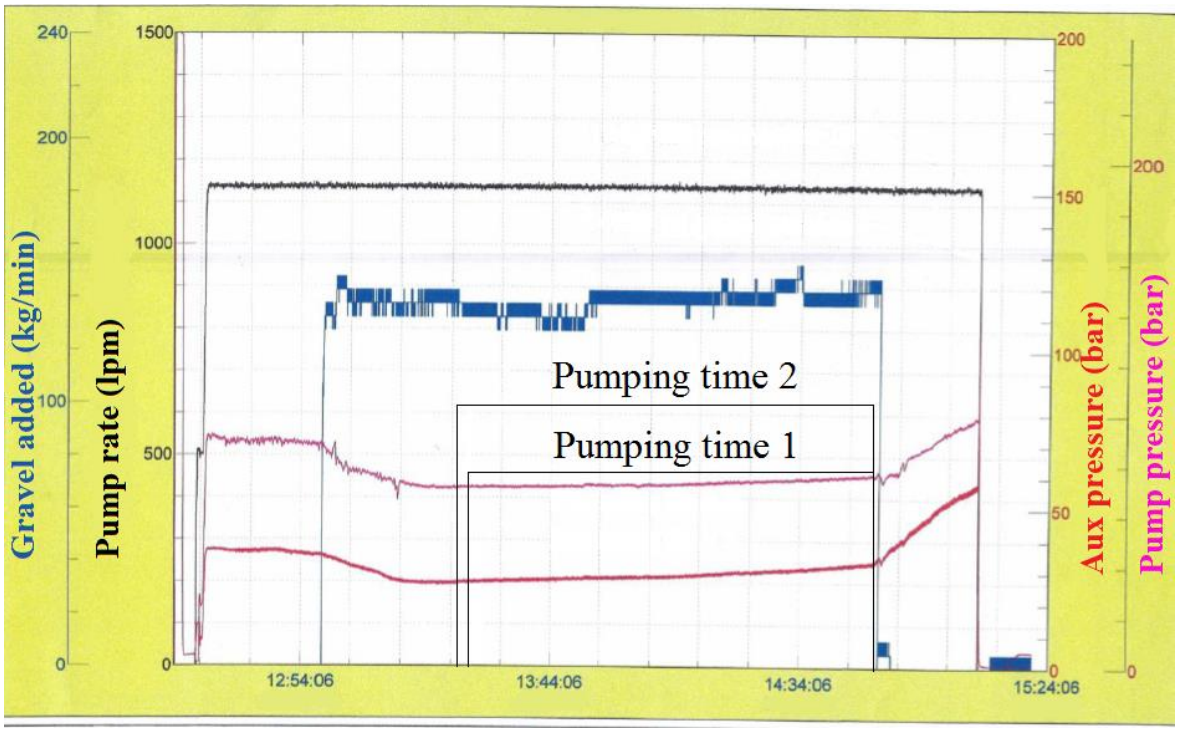

Figure 5-4 Pumping chart for gravel pack job

Table 5-5 Calculated values and output of modelling for 9 in OH

Parameters	Values
Screen/openhole annulus	
Q_* equilibrium flow rate in open area	0.003762417 $m^3 s^{-1}$
A_o area open to flow	0.0029046765 m^2
A_{so} total area of annulus	0.0151101609 m^2
D_{h*} hydraulic diameter	0.0369513414 m
N_{Re} Reynolds number	37004
λ_* equilibrium friction factor	0.194681472
C_* equilibrium solids concentration	0.2289526032
$(\Delta P/L)_o$ frictional pressure gradient	5467.3 Pa m^{-1}
ψ incremental pressure drop from solids	2054.2 Pa m^{-1}
Screen/washpipe annulus	
Q_{wp} equilibrium flow rate	0.01540425 $m^3 s^{-1}$
A_{wp} area of annulus	0.0050965859 m^2
D_{hwp} hydraulic diameter	0.0233934 m
N_{Re} Reynolds number	54664
λ_{wp} equilibrium friction factor	0.031142648
$(\Delta P/L)_{wp}$ frictional pressure gradient	7522 Pa m^{-1}
v_{wp} fluid velocity	3.023 m s^{-1}
Output	
Q_{wp}/Q_m Flow rate split ratio to washpipe/screen annulus	0.8037
γ sector angle	0.7177666549 rad
y_b bed height	0.2003995024 m
v_* equilibrium velocity	1.2953 m s^{-1}
Volumetric gravel fill percent	80.78
Height fill percent	87,66

For the case of a washout of the wellbore to 9 in OH diameter, the volumetric gravel fill percent is calculated to 80.78 percent. This is in good correspondence with the value deducted from the pump chart of the operation, and hence a wellbore diameter of around 9 in is assumed for further work. The resulting graph of mixture velocity and critical velocity according to Gruesbeck et al. is given in Figure 5-5, together with the output from the other models presented in Chapter 5.3.

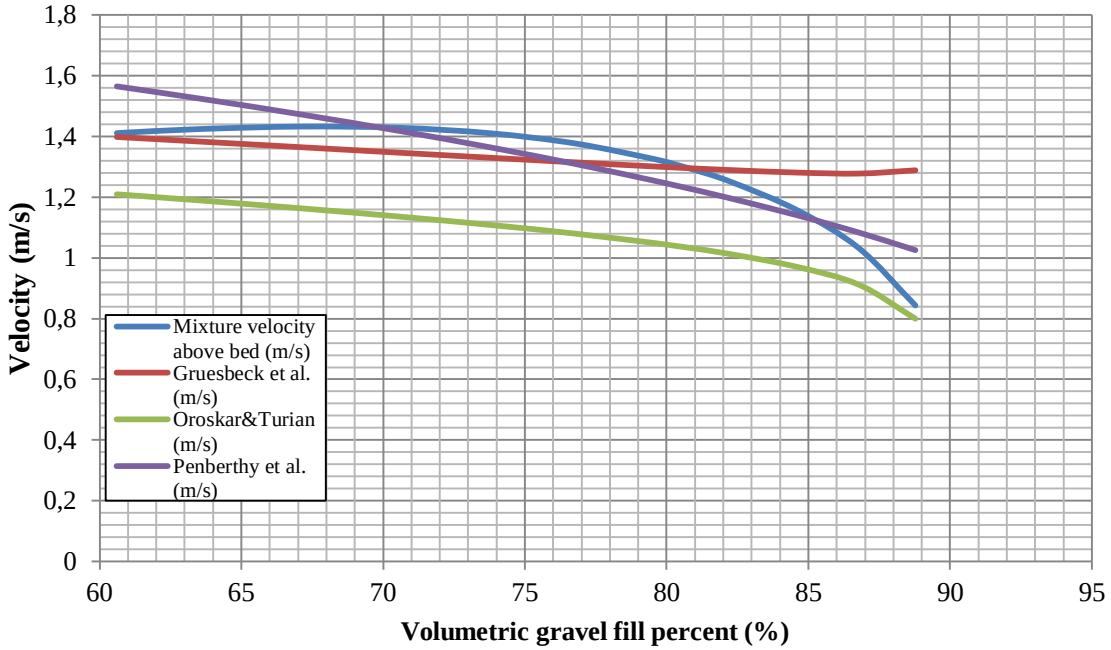

Figure 5-5 Comparison of equilibrium velocities of different models for 9 in OH

The graphs are plotted inside the valid range of the mixture velocity model. The lower boundary is represented by the gravel fill flush with top of screen, and the upper boundary is where there is no longer a solution for the pressure drop balance, as debated earlier. This graph needs some discussion, since it shows two solutions for both Gruesbeck et al. and Penberthy et al. models inside the range of the plot. The one thing that is more or less certain is the gravel fill percent deducted from the pump chart in Figure 5-5, which gives a volumetric fill percent of around 80. Therefore, the lowermost solutions for Gruesbeck et al. and Penberthy et al. are discarded. Penberthy et al. is giving a slightly higher value than Gruesbeck et al. at about 85.3 percent. There is no equilibrium velocity for Oroskar and Turian model inside the plotted range, but there seems to exist a solution outside the upper boundary, at around 90 percent. The graph of critical velocity from Oroskar and Turian makes a marked drop above 86 percent, as the calculation becomes affected by the increasing gravel concentration as discussed in the former sub-chapter.

5.2.5 Alternative approach – design for specific gravel fill

The modelling has so far been done iterating for both the Q_{wp}/Q_m ratio and the bed height simultaneously, while the pump rate has been held constant. Another approach can be used, if we consider a specific volumetric gravel fill percent. This is a practical method for designing the alpha dune to a preferred fill degree. The iteration is now done varying the

pump rate and bringing the pressure drop in the two annuli in balance with the Q_{wp}/Q_m ratio. By doing this, the output will be pump rate needed for a given fill percent. The process was done for three different grades of volumetric fill percent for the case of 9 in OH: 75 percent, 80 percent and 85 percent. The resulting graphs are shown in Figure 5-6 through 5-8.

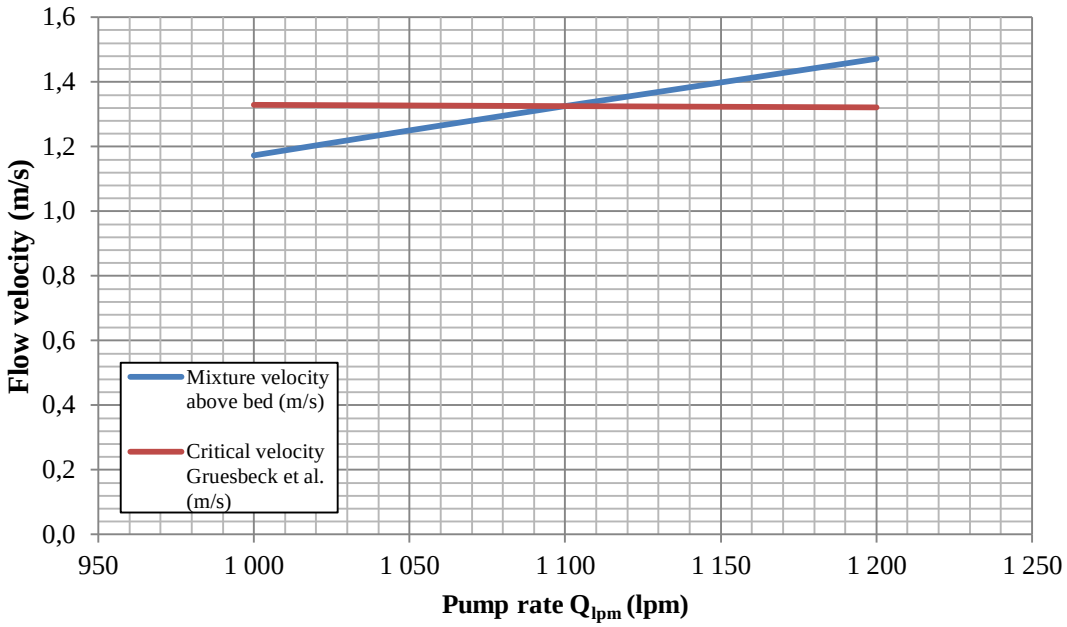

Figure 5-6 Pump rate at equilibrium for 75% fill, 9 in OH

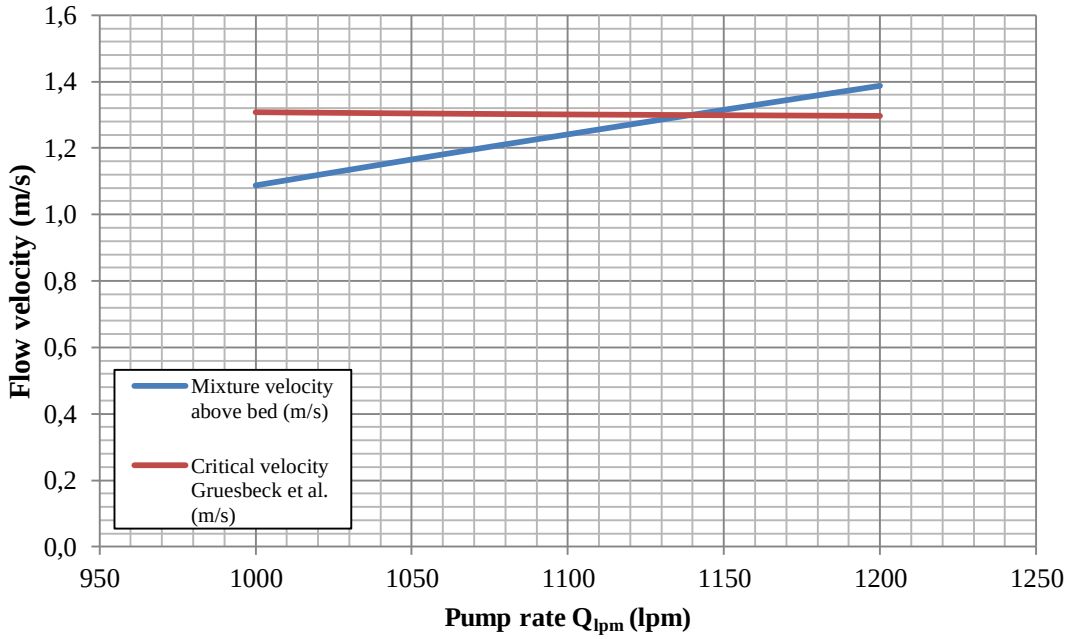

Figure 5-7 Pump rate at equilibrium for 80% fill, 9 in OH

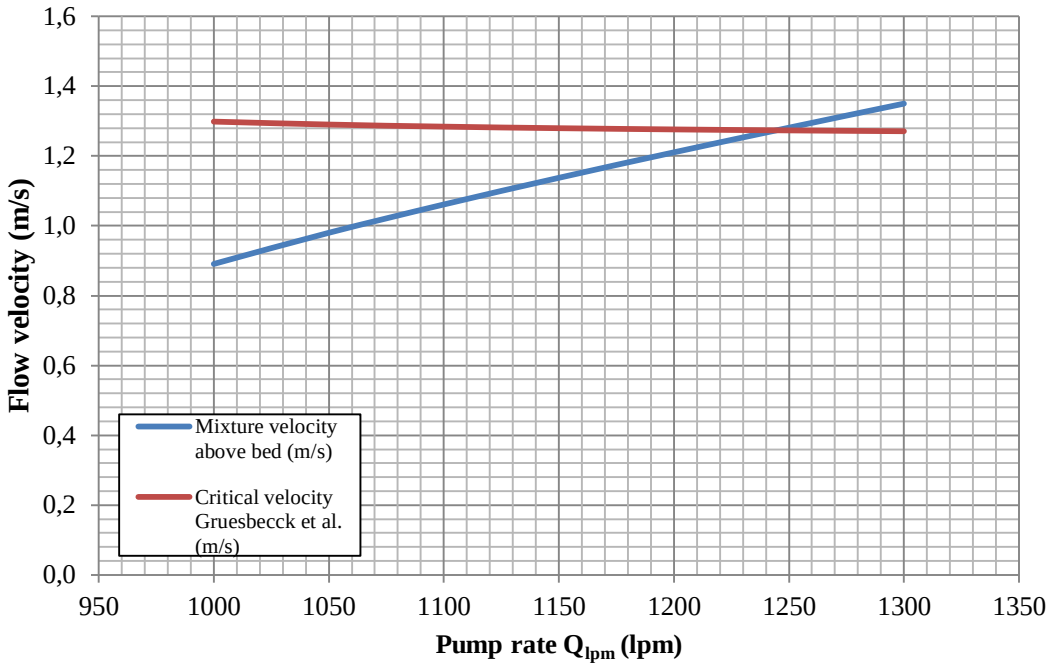

Figure 5-8 Pump rate at equilibrium for 85% fill, 9 in OH

The plots for the three different grades of gravel fill show an increased pump rate needed to reach equilibrium at higher fill. This is an interesting result, as according to Gruesbeck et al. the lowering of the flow rate would cause a higher alpha dune height. It is believed to be related to the varying flow rate splitting and the different friction factors of the two annuli Recall that Gruesbeck et al. model treats both annuli as having the same roughness. At higher gravel fill, more flow will be directed through the screen/washpipe annulus as the flow restriction in the screen/openhole annulus has increased. Then the pump rate must be higher to reach the equilibrium velocity. This might be arguable, but is an implication of handling the flow rate split as changing and operating with large friction factor difference between the annuli flow surfaces. Due to the complexity of the gravel pack process, it cannot be dismissed either. Table 5-6 is presenting data from the iteration on pump rate and flow split ratio.

Calculations on the bed friction in Chapter 4 indicated that its influence becomes more pronounced the higher the sediment bed height is. This was an observation for the case of gravel deposition in the work string, but it could be interesting to examine how this affects the pressure loss in screen/openhole annulus for a variation of bed heights or gravel fill. This might be verified by experiments, preferably full-scale to get a more realistic scenario.

Table 5-6 Iteration for alternative approach

Gravel fill (%)	Q_{lpm} (lpm)	Q_{wp}/Q_m (%)	v_o (m/s)	v_c (m/s)
75	1200	72.203	1.47169	1.32187
	1150	72.431	1.39880	1.32340
	1100	72.698	1.32503	1.32520
	1050	73.020	1.24988	1.32740
	1000	73.405	1.17338	1.33008
80	1200	79.034	1.38754	1.29687
	1150	79.265	1.31508	1.29888
	1100	79.538	1.24123	1.30130
	1050	79.870	1.16569	1.30428
	1000	80.280	1.08757	1.30804
85	1300	85.877	1.35014	1.27107
	1250	86.061	1.28124	1.27341
	1200	86.281	1.21061	1.27625
	1150	86.548	1.13759	1.27977
	1100	86.880	1.06127	1.28425

5.3 Sensitivity study

A short sensitivity study will be executed on the wellbore diameter, due to the uncertainties in this parameter. In addition, it would be interesting to see variations in gravel fill with different washpipe diameter to internal screen diameter around the industry rule-of-thumb 0.8, as mentioned by Bellarby[5].

5.3.1 Influence of the wellbore diameter

Modelling has been done for the base case (8.5 in OH) and the assumed actual wellbore diameter (9 in OH). In the case of more prominent washout, a 9.5 in OH will be modelled for and data is presented in Table 5-7. The corresponding graphs are shown in Figure 5-9, comparing the mixture velocity to the three different critical velocity models used in this thesis. Iteration on the flow split and bed height is given in Appendix H.

Table 5-7 Calculated values and output of modelling for 9.5in OH

Parameters	Values
Screen/openhole annulus	
Q_* equilibrium flow rate in open area	0.00385825 $m^3 s^{-1}$
A_o area open to flow	0.0029883668 m^2
A_{so} total area of annulus	0.0197972051 m^2
D_{h*} hydraulic diameter	0.0369686468 m
N_{Re} Reynolds number	36901
λ_* equilibrium friction factor	0.194614303
C_* equilibrium solids concentration	0.2232657526
$(\Delta P/L)_o$ frictional pressure gradient	5427.4 Pa m^{-1}
ψ incremental pressure drop from solids	2003.2 Pa m^{-1}
Screen/washpipe annulus	
Q_{wp} equilibrium flow rate	0.015308417 $m^3 s^{-1}$
A_{wp} area of annulus	0.0050965859 m^2
D_{hwp} hydraulic diameter	0.0233934 m
N_{Re} Reynolds number	54324
λ_{wp} equilibrium friction factor	0.031154096
$(\Delta P/L)_{wp}$ frictional pressure gradient	7431 Pa m^{-1}
v_{wp} fluid velocity	3.00 m s^{-1}
Output	
Q_{wp}/Q_m Flow rate split ratio to washpipe/screen annulus	0.7987
γ sector angle	0.6976081020 rad
y_b bed height	0.21331138557 m
v_* equilibrium velocity	1.2911 m s^{-1}
Volumetric gravel fill percent	84.91
Height percent fill	88.40

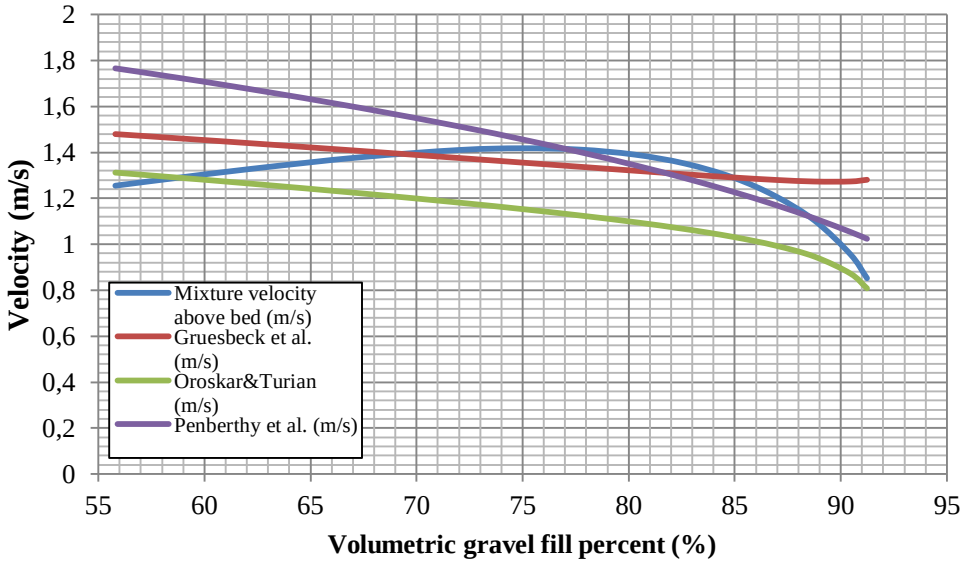

Figure 5-9 Comparison of equilibrium velocities of different models for 9.5 in OH

Mixture velocity curve is crossing critical velocity curves of both Gruesbeck et al. and Penberthy et al. at two points. The curve for Oroskar and Turian is crossed at a low value for gravel fill, and there might be a solution above 91 percent, outside the upper boundary of the plot. A presentation of the output from the different wellbore diameters is given in Table 5-8. Considering now the mixture velocities for the three different wellbore diameters, the velocity decreases with increasing diameter. This is expected as a larger wellbore gives a larger area for the flow of mixture. A larger diameter will also pose less restriction on the mixture flow, and more flow will go through the screen/washpipe annulus. This can be seen from the reduction in Q_{wp}/Q_m at equilibrium with increasing wellbore diameter.

Table 5-8 Results from modelling of different wellbore diameters

Output	Wellbore diameter		
	8.5 in	9 in	9.5 in
Q_{wp}/Q_m at equilibrium	0.80869	0.8037	0.7987
v_* equilibrium velocity (m/s)	1.30	1.2953	1.2911
Volumetric gravel fill percent (%)	73.58	80.78	84.91
Height fill percent (%)	86.92	87.66	88.40

The flow rate split ratio shows a linear relationship to change in wellbore diameter, and for larger diameter less flow will go through screen/washpipe annulus (Figure 5-10). Only a 1.2 percent drop in flow rate is experienced when increasing the wellbore diameter 1 inch. The relationship is also linear for equilibrium velocity, which will decrease with increasing wellbore diameter (Figure 5-11), and also here the influence of wellbore diameter is marginal.

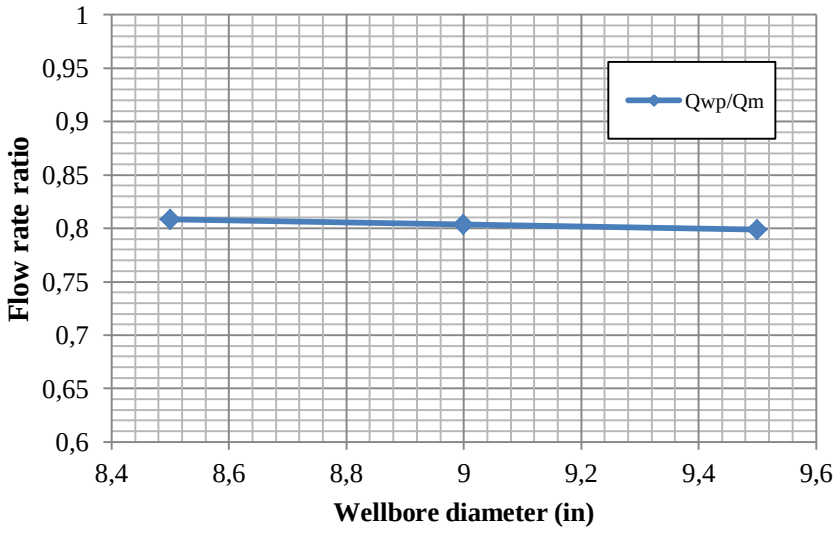

Figure 5-10 Flow rate split ratio for different wellbore diameters

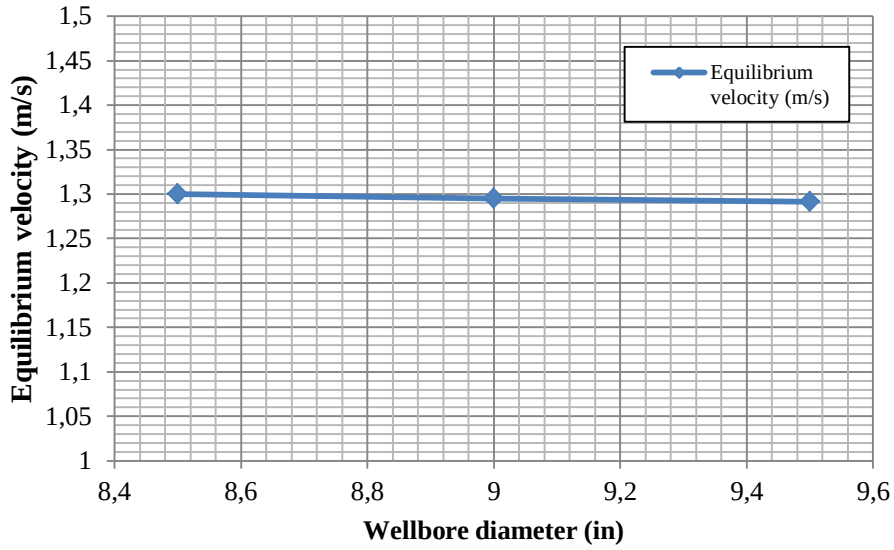

Figure 5-11 Equilibrium velocities for different wellbore diameters

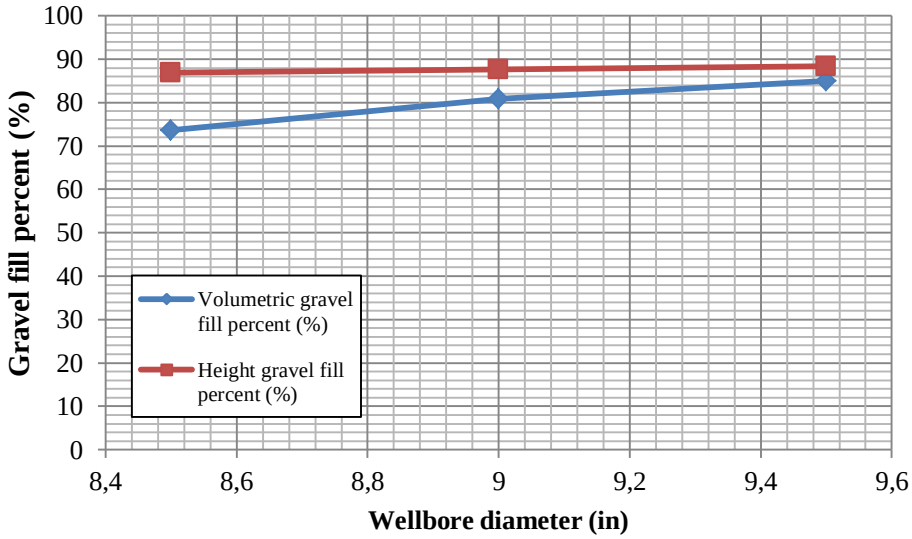

Figure 5-12 Gravel fill percent for different wellbore diameters

Plotting the gravel fill percent for the three different scenarios (Figure 5-12), one can observe that the height fill percent increases strictly linear to the increasing wellbore diameter, and increases 1.7 percent from 8.5 to 9.5 inch diameter. The volumetric gravel fill percent is increasing over the interval in a declining trend, due to the geometry of the open flow area above the bed, and increases 15.4 percent over the same interval. This is caused by the contribution from a larger area available for gravel above screens when the borehole size increases.

5.3.2 Influence of the washpipe size

It would be interesting to verify how sensitive the gravel fill is to change of washpipe diameter. The "0.8 rule" of washpipe external diameter to screen internal diameter has been mentioned earlier. In the gravel pack operation presented in this chapter, a 5 in washpipe was used. This corresponds to a ratio of about 0.84, well above the recommended value. A washpipe of 4.75 in would give a ratio of about 0.80 and so would be at the recommended minimum. Resulting plot is shown in Figure 5-13.

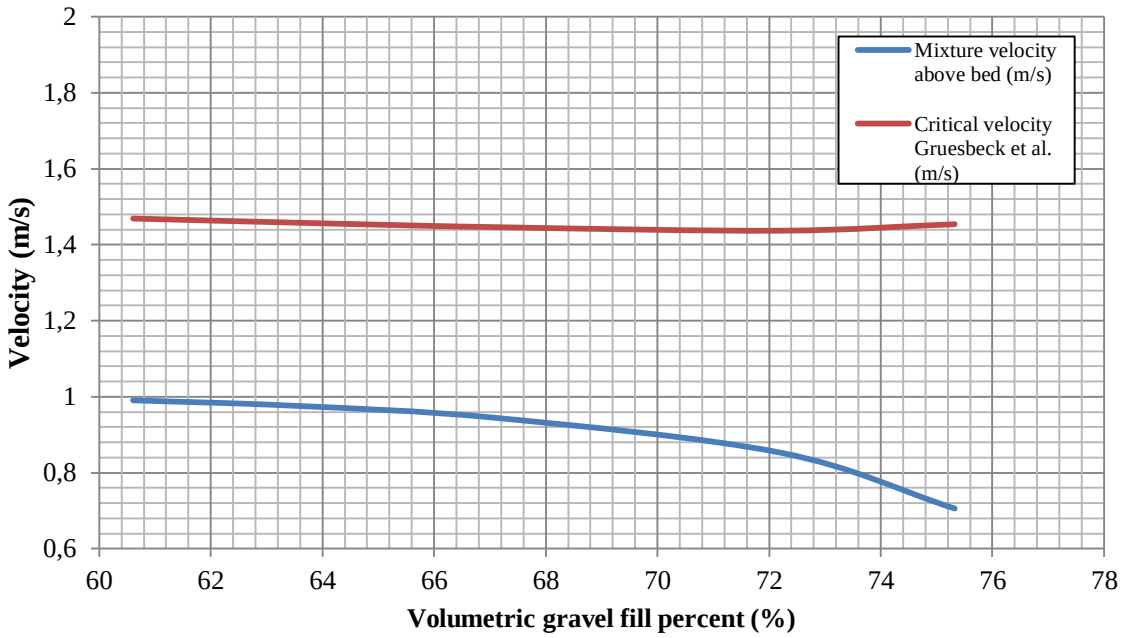

Figure 5-13 Equilibrium velocity and related gravel fill for 9 in OH and 4.75 in washpipe

The lower boundary for the plot is gravel fill corresponding to just covering screens. There is no solution inside the range of the plot, so an equilibrium alpha dune height is believed to exist below the screens. The two graphs show only a minute convergence towards each other in the direction of lower gravel fill. It is not certain that the method of modelling handles the implications of a larger screen/washpipe annulus very well, because of the sensitivity to the washpipe diameter. The influence of the washpipe diameter should be tested experimentally to verify the effect on the fill percent, preferably with a full-scale experiment.

5.3.3 Influence of viscosity

The correct value of the brine viscosity is not known, due to uncertainties in the correct circulation temperature. Therefore, a test of the sensitivity to this parameter is needed. Gravel fill percent will be modelled for two different values of viscosity for the 9 in OH case, one lower and one higher than the generic value of 1.6 cP. Change of viscosity affects the terminal settling velocity, and iterations were performed for the three different viscosities to find the related values. Schiller-Naumann equation was used to calculate drag coefficients, and iteration process was done similarly as for the carrier fluid in the base case. For carrier fluid density of 1 cP v_t = 0.07706 m/s. For a fluid density of 1.6 cP v_t = 0.06444 m/s, and for 2.2 cP v_t = 0.05598 m/s. The corresponding plots for mixture velocities and critical velocities are shown in Figure 5-14 and 5-15, whilst the iteration data will be given in Appendix I. Table 5-9 presents the results.

Table 5-9 Resulting values for different viscosities

Viscosity (cP)	Volumetric gravel fill (%)	Q_{wp}/Q_m (%)	v_* (m/s)	λ_*	ψ (Pa/m)
1.0	82.07	82.48	1.239	0.202	2301
1.6	80.78	80.37	1.295	0.195	2054
2.2	80.67	79.98	1.314	0.194	2014

The gravel fill percent can be seen to be quite insensitive to change in viscosity in general. The most pronounced difference is from the low to the mid value of viscosity, where the gravel fill reduces by 1.6 percent, split ratio decreases 2.6 percent and equilibrium velocity increases 4.5 percent. Changing from 1.6 to 2.2 cP, the gravel fill is reduced by 0.14 percent, split ratio decreases 0.5 percent and equilibrium velocity increases 1.5 percent. The resulting gravel fill percent is not much affected by change in viscosity, and is therefore believed to be quite insensitive to moderate temperature changes during circulation. As the fluid viscosity is increased, the equilibrium velocity also increases. One could intuitively believe that a more viscous fluid required less flow velocity to keep the gravel in suspension. However, the effects of fluid viscosity on the transport of solid particles are not fully understood or agreed upon[46]. A full- scale experiment might bring clarity to the matter.

The equilibrium friction factor in screen/openhole annulus, the flow rate ratio and the incremental pressure drop is following the same trend; for a higher viscosity they will all be lower. Increasing the viscosity, the difference will largely affect the Reynolds number, but the higher hydraulic diameter from the decrease in gravel fill will be dominant in the

friction factor equation (Eq. 3-56), and the overall effect will be a slightly lower friction factor for the flow above the bed. A lower friction implies less resistance, and thus more flow will go above the bed. This can be read from the lower Q_{wp}/Q_m ratio in Table 5-9. The incremental pressure drop ψ is also decreasing with increase of viscosity. This is due to its dependency on the gravel concentration. Less flow in screen/washpipe annulus means less dehydration of the slurry and hence a lower solids concentration.

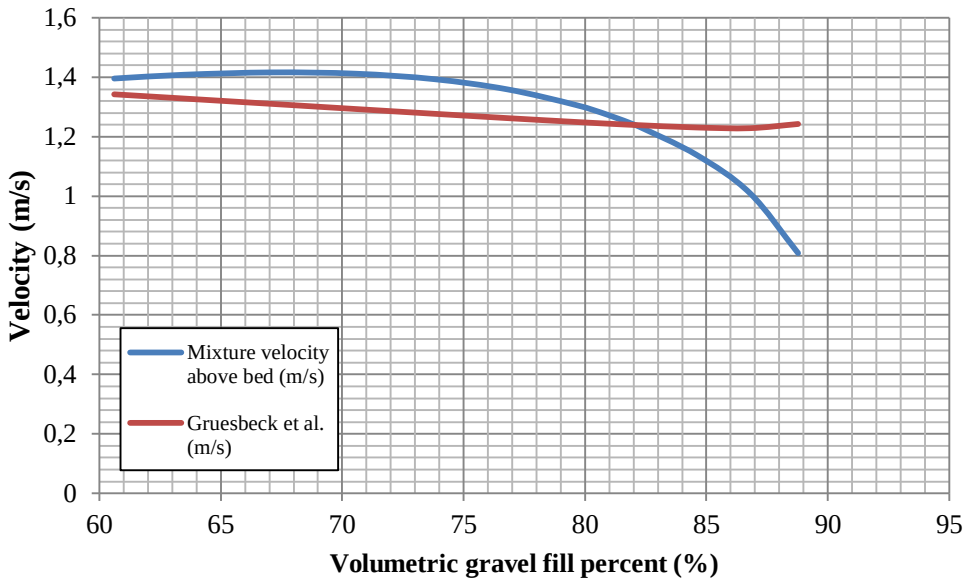

Figure 5-14 Equilibrium velocity and related gravel fill for 1.0 cP carrier fluid

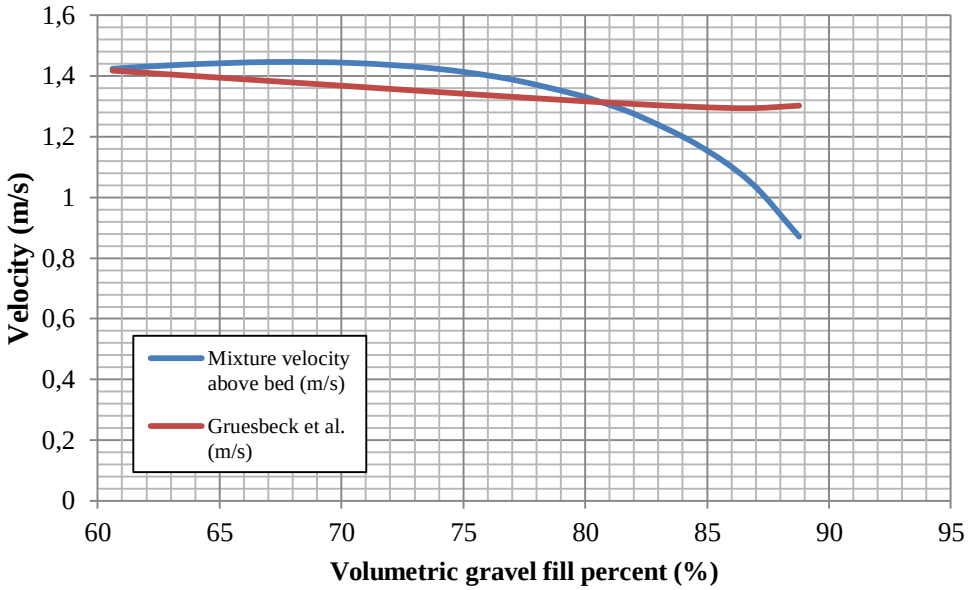

Figure 5-15 Equilibrium velocity and related gravel fill for 2.2 cP carrier fluid

5.4 Discussion of friction factor and roughness using Swamee-Jain

It is clear that there is some uncertainty about the roughness chosen to represent the screen/openhole annulus. From Table 3-3, a conservative value for a poor competence, high fracture rock was picked. The value of the absolute roughness is 1 cm, and this might be disputable. Having found hydraulic diameter, friction factor and Reynolds number at equilibrium for the alpha dune, it would be interesting to cross-check this data with the Moody diagram (Figure 3-8). The relative roughness at equilibrium is approximately 0.27. The maximum relative roughness from the Moody diagram is 0.05. Hence, the calculated value is out of the chart. Moody's data comprises pipes of various materials and roughnesses, but the plots are limited in the range. Using Swamee-Jain equation (Eq. 3-56) for friction factor and plotting it against a range of Reynolds numbers for the turbulent region, a self-made extension to the Moody diagram is presented (Figure 5-16), and the conditions at equilibrium can be compared to the original Moody diagram. Lines for various values of roughness are plotted to check correspondence.

The lower line resembles a relative roughness of 0.05, which is the maximum value from the original Moody diagram. A relative roughness of 0.05 corresponds to a roughness of 0.00185 for the actual hydraulic diameter of the discharge area at equilibrium, which is lower than any values of rock surface in Table 3-3, even for high competence formations. As the alpha dune increases in height, the equivalent diameter of the open area reduces significantly. This will eventually render a high relative roughness, much higher than shown in the original Moody diagram. In the article by Moody[47], the validity of the diagram is discussed. The values of the roughness are solely for new pipe, and aging and use will affect this parameter. Flow of water in circular pipes are the basis for the friction charts, and the charts can be applied as an approximation to not too eccentric configuration, or forms not too different from a circular section, by using hydraulic diameter as an equivalent diameter. In the case discussed in Chapter 5, the geometry of the discharge area is at equilibrium not at all circular, and it is therefore uncertainty about how well this case is resembled by the Moody diagram. The flow is not only influenced by the roughness of the formation wall, but also by the surface of the bed, which is in constant motion as particles are picked up and deposited. From modelling of the sedimentation in work string in Chapter 4, there were indications that the bed surface could be a considerable contributor to the overall frictional pressure loss and not only the wall surface, and that this will be more pronounced as the open area above the bed becomes more confined. That means, as the alpha dune fill percent increases.

The value used for absolute roughness of the borehole wall seems to make a good fit and gives a decent match between modelled and field case volumetric gravel fill percent. Therefore, the absolute roughness used is believed to produce a friction factor that is in

good correspondence with the actual friction factor, and so is representing the overall picture rather than the physical surface of the wall itself. Friction factor of the screen/openhole annulus and the bed surface influence need to be verified, and experiments might be helpful.

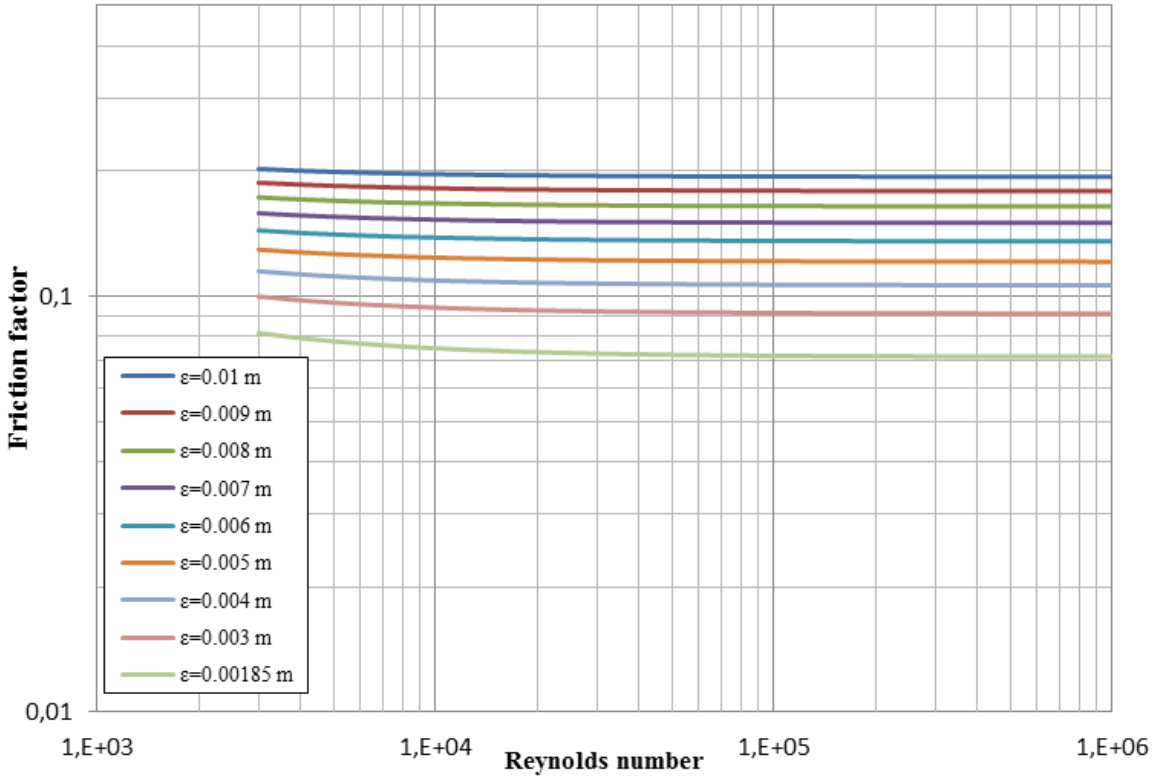

Figure 5-16 Moody diagram for different wall roughnesses, 9 in OH

(This page intentionally left blank)

6 PROPOSAL FOR FULL-SCALE EXPERIMENT

Two different experiments are proposed; work string case and alpha wave case. The work string case will be based on the problem described in Chapter 4, where the experiment will focus on the sedimentation in a pipe resembling the drillpipe work string. The results from modelling can be compared to experimental data to quality check the model, and a sensitivity study on the changeable parameters can be conducted. The alpha wave experiment will be based on findings in Chapter 5. Results from modelling of the alpha wave in the former chapter suggest that a full-scale experiment should be run to verify the proposed flow rate splitting and also check the pressure losses through the system, to examine how the wall roughness affects the flow split. The empirical models made for gravel packing are based on small-scale experiments, small-scale in the meaning that no known models have been developed using real-life diameters for borehole, screens and washpipe. A real full-scale experiment could be fruitful for study of the influence of washpipe size and other important parameters, and also study the flow rate splitting between the two annuli to verify the proposed method used for modelling in this thesis.

6.1 Basis for experiments

IRIS - International Research Institute of Stavanger is an independent research center located close to the University of Stavanger. IRIS can host experiments of this size. A jar test bench, originally made to test drilling jars, can be used for the purpose of supporting the rig-up of tubulars involved. It is situated outdoors and has a length of 45 m, with the possibility for extension up to 70 m. A picture of the structure is presented in Figure 6-1.

Figure 6-1 Jar test bench at IRIS

In both experiments (work string case and alpha wave case) the system will be open to atmosphere in outlet end. Slurry is pumped in at one end and exits at the other, where the exiting fluid and slurry mixture is received. Fluid and gravel will be gathered in a tank and the fluid pumped back to a brine storage tank. Both experiments will be limited to horizontal scenario.

6.1.1 Fluids and gravel

To bring the experiment closer to reality, brine is chosen for carrier fluid rather than water. This may restrict the possibilities of disposal during and after the experiments. HSE considerations must also be a part of the planning, as brines can pose a risk to both the environment and to those involved in handling the fluids during experiments. Sensitivity study in Chapter 5 indicates that the resulting gravel fill percent of the alpha wave is not affected much by density changes. This is reassuring, as the prevailing air temperature can vary considerably from day to day. Gravel for the experiments will be ordinary 20/40 US mesh gravel sand, preferably well rounded and with low angularity, as the models used for calculations assume spherical particles.

6.2 Work string experiment

The data and parameters from Chapter 4 will make the basis for the experiment. The parameters that need to be measured are fluid viscosity and density, which will vary with the air temperature. The brine used will be chosen to have a density and viscosity equal to the bottomhole conditions of field case presented in Chapter 4. A closer approximation to the correct values can be done in a simulation program like WellCat, but for the calculations in this chapter the earlier deducted values are used.

6.2.1 Equipment and set-up

Transparent acrylic pipe with internal diameter of 5 in and 0.25 in wall thickness will be used for this experiment, to enable the possibility to observe the sedimentation process and measure bed height. The pipe length will consist of several pipes connected to each other by flanges with gaskets in between. Preferably a “dead” material should be used for this purpose as it will not protrude into the internal pipe void when flanges are bolted together. Cork gaskets are a suitable choice, since the expected pressure in the system will be low. Flanges of the same acrylic material will be glued onto the pipe ends. At the inlet of the pipe, a steel end-cap with coupling for a hose will be bolted to a plastic flange with a gasket in between.

The acrylic pipe will be supported inside the jar test bench showed in Figure 6-1, which consists of a metal structure about 36 m long. Inlet point for flow to the pipe will be at one end, and in the other the flow is let to exit to an open return tank. Brine can then be pumped back to the brine storage tank, and the gravel collected and reused. The main pump for the experiment will be a centrifugal type, to minimize fluctuations and deliver a smooth and even flow at steady rate. Pump is fed from a brine storage tank. The gravel is introduced to the flow via a hopper to the preferred concentration. The flow goes through a hose of a certain length to stabilize the flow upon entering the acrylic pipe. At the other end of the pipe, flow is collected in an open vessel of a size that will let the gravel settle out, so that solids-free brine can be pumped back to the storage tank. A vessel of 2*3 m base and 1 m height will hold a maximum of 6.0 m^3 and suits the experiment well. The vessel will be reused for the alpha wave experiment, where this size is required. Brine is transferred back to the storage tank through a return hose, and through a filtering device just above the tank top. A total of 40 m 3 in ID hose from feeding pump to the inlet of the acrylic pipe is assumed.

Transfer pumping can be done with two air operated diaphragm pumps, which are excellent for pumping slurry and represent a low cost option. Two times (two return pumps) 10 m 2 in ID hose from return tank to storage tank is assumed. The pumping capacity of the return pumps must equal the pump rate of the experiment for a possible continuous operation. The base case is 1150 lpm, but experiments with higher rates can be expected. The idea behind dual pumps is easier handling, since a single diaphragm pump with capacity to deliver the required pump rate will be quite large. Figure 6-2 gives a simplistic representation of the experimental set-up.

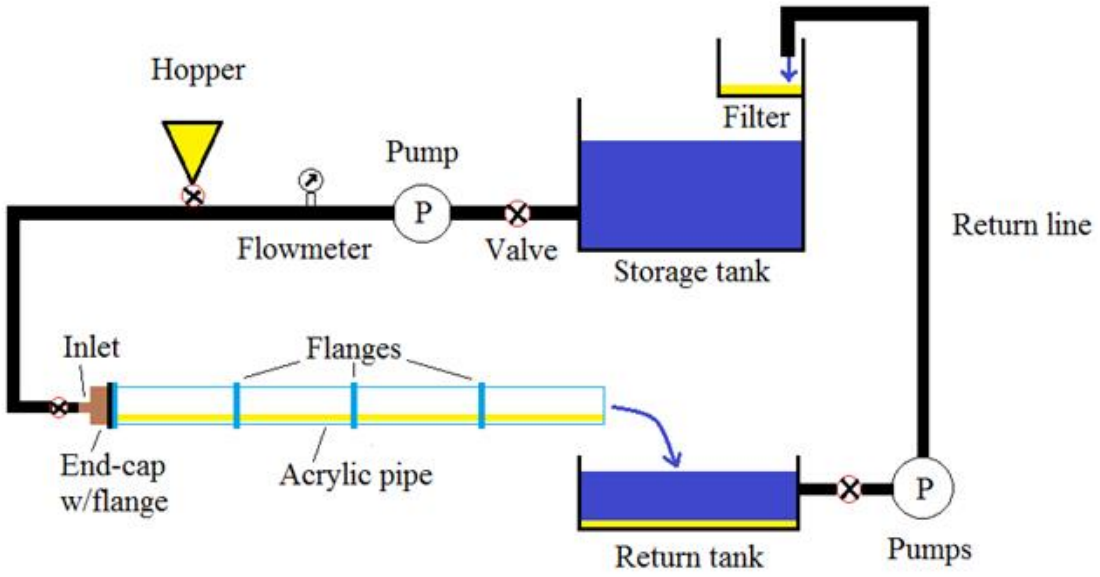

Figure 6-2 Experimental set-up for work string case

6.2.2 Calculations using Matoušek model

Changing only the internal pipe diameter and mean flow velocity from the field case, the input values for the experiment are given in Table 6-1. Resulting values for intermediate calculations and output are given in Table 6-2.

Table 6-1 Input for work string experiment

Input parameter	Value
internal diameter pipe, D_p	5.0 in – 0.1270 m
median particle diameter, d_{50}	0.00058 m
gravel added	136.965 kg/min
gravel concentration	1.0175 ppa
pump rate, Q_{lpm}	1150 lpm
volumetric particle concentration, C_{vd}	0.044943396
fluid density, ρ_f	1237 kg m^{-3}
solids density, ρ_s	2650 kg m^{-3}
bulk density gravel, ρ_{bulk}	1643 kg m^{-3}
fluid viscosity, μ_f	1.6 cP – 0.0016 kg $m^{-1}s^{-1}$
terminal settling velocity, v_t	0.06444 m s^{-1}
mixture flow velocity, v_m	1.513036042 m s^{-1}

The mass of sediments inside the pipe section can now be quantified from the bed height and the bulk density of the gravel. Bulk density is given from calculations in Appendix B. Over the length of the pipe section L_p, the mass of gravel accumulated will now be given by Eq. 4-28:

$$m_b = A_b L_p \rho_{bulk} = 0.000898181\, m^2 * 36\, m * 1643\, \frac{kg}{m^3} \approx 53.13\, kg$$

The pressure loss over the pipe section can be calculated combining Eq. 3-45 and 3-46:

$$dP = i_m g \rho_f L_p = 0.04565137 \frac{m}{m} * 9.81 \frac{m}{s^2} * 1237 \frac{kg}{m^3} * 36m \approx 19940 Pa = 0.2 bar$$

Table 6-2 Calculated values for work string experiment

Intermediate parameters and related values			
Areas		Hydraulic radii	
A_t	0.012667687 m^2	R_h	0.03175 m
A_a	0.011769506 m^2	R_{ha}	0.030074944 m
A_{aw}	0.003885421 m^2	R_{hw}	0.012624639 m
A_{ab}	0.007884085 m^2	R_{hb}	0.094336206 m
A_b	0.000898181 m^2		
Geometrical parameters		Wetted perimeters	
A_{sector}	0.002896151 m^2	O_b	0.083574327 m
$A_{triangle}$	0.00199797 m^2	O_w	0.307764928 m
γ	0.718246746 rad		
Velocities		Reynolds numbers	
v_a	1.628502232 m s^{-1}	N_{Re}	148560.2807
u_{*b}	0.205542017 m s^{-1}	Re_p	28.8957015
		$Re_{p'}$	36.15034465
Shear stresses		Shields parameters	
τ_b	52.26018308 Pa	Θ	6.50027551
τ_w	6.993772498 Pa	Θ_{cr}	0.03322047
Friction factors and roughness		Solids flow rates and flux	
λ_b	0.127442563	q_s	0.010307174 m^2 s^{-1}
λ_w	0.017055131	$Q_s = C_{vd}A_a v_a$	0.000861415 m^3 s^{-1}
k_s	0.058692162 m	$Q_s = q_s O_b$	0.000861415 m^3 s^{-1}
Output			
i_m	0.04565137		
y_b	0.015687 m		

6.2.3 Pressure rating of acrylic pipe

An acrylic pipe of 5 in ID and a wall thickness of 0.25 in will be proposed for the experiment. The burst pressure rating can be deducted from Barlow's equation (Eq. 6-1), as the criteria for thin walled cylinder is fulfilled; wall thickness is less than a tenth of the inner radius. Here, P_{br} is the burst pressure, σ_y is the yield stress rating of the material, t is wall thickness and D_e is external diameter of the pipe.

$$P_{br} = \frac{2\sigma_y t}{D_e} \tag{6-1}$$

Yield strength of acrylic plastic is found in literature to be 10000 psi[48], and this yields a burst pressure tolerance of nearly 63 bar. This is well above the expected pressure loss of 0.2 bar through the pipe. The selected thickness will also make the pipe more sturdy and resistant to breaking during transport and installation.

6.2.4 Amount of fluid and gravel needed

Duration of the experiment is governing the amount of fluid and gravel needed, and can be calculated from the values found in Table 6-2. First, the expected time to finish the experiment is calculated. The assumption for the calculation is that the sediment process is happening at an equilibrium state similar to that of the gravel packing. First, the volume of the sediments must be calculated from Eq. 6-2, where V_g is volume of gravel sediment and A_b is the cross-sectional area of the bed found in Table 6-2 to be around 0.0009 m^2. Pipe length L_p is 36m. Bulk density was calculated as 1643 kg/m^3 in Appendix B. Note that the calculation must consider the porosity of the packed gravel particles. This yields a gravel volume of about 0.02 m^3 from Eq. 6-2.

$$V_g = A_b L_p \phi = A_b L_p \frac{\rho_{bulk}}{\rho_s} \tag{6-2}$$

Pumping time for a bed to form along the pipe length after slurry enters the pipe is now given by Eq. 6-3. Here Q_s is the solids flow rate above the bed, which was found to be around 0.00086 m^3/s (Table 6-2). Pumping time is then 23.3 s to form a bed along the whole pipe length.

$$T_p = \frac{V_g}{Q_s} \tag{6-3}$$

Bed velocity, v_b is now found from the pipe length and the pumping time as:

$$v_b = \frac{L_p}{T_p} = \frac{36m}{23.3s} = 1.55m/s$$

Fluid volume needed just for the sediment process is found from the pumping time and carrier fluid flow rate Q_f, which was calculated in Appendix A and is valid also for this case.

$$V_f = Q_f T_p = 0.018305252 \frac{m^3}{s} * 23.3s \approx 0.427m^3$$

An excess is necessary to account for volume in lines up to inlet point at acrylic pipe and for uncertainties. Furthermore, the experiment will be initiated by a constant and stable flow of brine through the pipe before the gravel is introduced into the system, and therefore a higher volume of fluid is needed. Table 6-3 shows an overview of the assumed fluid volumes needed in the system during pumping. The storage tank needs to hold enough fluid to act as a buffer in case problems occur. The volumes of hoses and acrylic pipe are for completely fluid filled scenario. The return tank should be filled to some degree before starting pumping, to serve as a buffer in case the level in the storage tank should run low.

Table 6-3 Expected brine volume in system when pumping, work string experiment

System part	Fluid volume (m^3)
Storage tank	2.0
Hose, 40m 3 in ID	0.182
Acrylic pipe, 36m 5 in ID	0.456
Return tank	1.0
Return hoses, 2*10 m 2 in ID	0.041
Total Volume	**3.68**

Amount of required gravel can then be approximated. The time for sediment process of the pipe was estimated to 23.3 seconds from the slurry enters the acrylic pipe. To account for uncertainties in this estimate, there should at least be enough gravel to pump slurry for 1 minute. This amount can easily be found in Table 6-1 as gravel added (kg/min), but can also be calculated as:

$$m_g = \frac{Q_{lpm}}{1000} C_{vd} \rho_s = 1.15m^3 * 0.044943396 * 2650 \frac{kg}{m^3} = 136.965kg$$

6.3 Alpha wave experiment

Data and parameters from Chapter 5 will make the basis for this experiment. The same brine and gravel is used for this experiment as that for the work string, and the density and viscosity is representing downhole conditions of the field case. The experiment is considering 8.5 in OH and 6.625 in screens, which was the base case of Chapter 5. The experiment aims to verify the flow rate split from the modelling and bring clarity to the friction in the screen/openhole annulus, especially the bed friction influence.

6.3.1 Equipment and set-up

The alpha wave experiment will use the same set-up and equipment as the work string experiment, except the acrylic pipe is now changed to a full-scale gravel pack configuration. The experimental rig is meant to represent full-scale diameters of tubulars, as a means to bring the experiments closer to reality, both in dimensions and pump rates. The borehole wall will be replicated by tubulars of 8.5 inches internal diameter. Screens of size 6.625 inches OD base pipe will be chosen, with the opportunity to use different washpipe sizes. A 9.625 in casing with nominal weight of 53.5 lbm/ft and 8.535 in ID suits the chosen internal diameter very well[49]. One casing joint of about 40ft length (range 3) joined together with around 80 ft transparent acrylic pipe will make up the outer pipe wall ("borehole wall") in the experiment. This will give a total length of around 36 m (120 ft). Inside, three screen joints will be situated on the low side for eccentric annulus configuration. Joints of tubulars will be placed inside the screen basepipe to simulate a washpipe, also fully eccentric.

The absolute wall roughness of the acrylic pipe must be altered, as it is to smooth compared to the real surface of drilled formation rock. The inside of the acrylic pipe can be applied a layer of resin to add texture to it and still be transparent, with the intention to increase the hydraulic roughness and bring it closer to a real borehole wall. Another solution is to attach a coarse sand paper to the lower half of the pipe. It is believed that the bed surface area eventually will become more dominant to the frictional pressure loss, so that an exact match to the roughness of the wall is not strictly necessary.

The acrylic pipe section will like for the work string experiment be made up of several shorter lengths of pipe, and this will make the job of modifying the inside surface easier. Screens and washpipe inside the plastic tubular will put a lot of force on it, and care has to be taken during the installation process to avoid damage or breakage. A trolley made for lifting purposes runs along the steel structure of the jar test bench (Figure 6-3). Manual chain hoists can be attached to the trolley and aid in the installation process.

Figure 6-3 Trolley and chain hoists

In Figure 6-3, one can also see the attachment point for the jars. The experimental arrangement will be fixed to this point to provide stability. The casing joint and the first screen joint will be connected to form an assembly, where an end cap is welded onto the casing and the box end of the screen is let to stick out. A blind flange is welded to this end, which allows the assembly to be fixed to the jar test bench structure. The inlet point for the flow will be through the high side of the end cap, where a connection for the hose will be installed. Figure 6-4 shows the assembly.

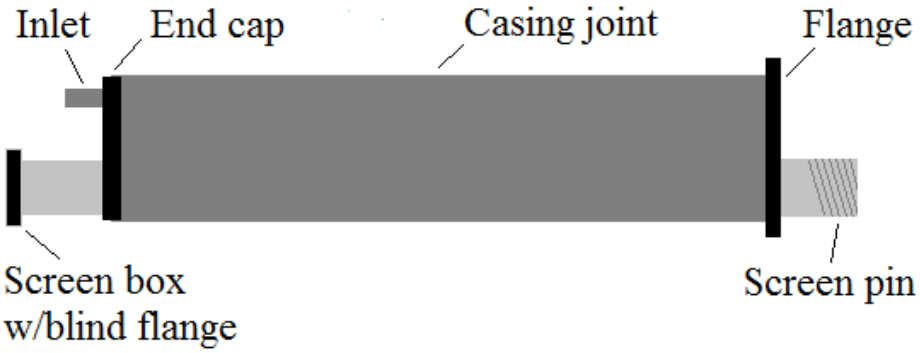

Figure 6-4 Casing/screen assembly

After the assembly has been installed onto the jar test bench, the next screen joint is connected. Then the screens can be lifted by the lifting equipment mounted on the trolley, and the acrylic pipe sections can be connected. The process repeats until all screen joints and acrylic pipe sections are in place. Finally, the washpipe can be slid into the screen base pipe. Changing the washpipe size between experiments will by this solution be a quick and effortless operation.

To quantify the flow rate split between the annuli, the flow contribution through the system for each annulus will have its own return tank. These tanks will be dimensioned to each receive all expected fluid for the duration of each experiment, and their specific capacity will be estimated in sub-chapter 6.3.4. When alpha wave reaches the outlet, the volume in each tank will be used to calculate the flow rate split for the actual bed height.

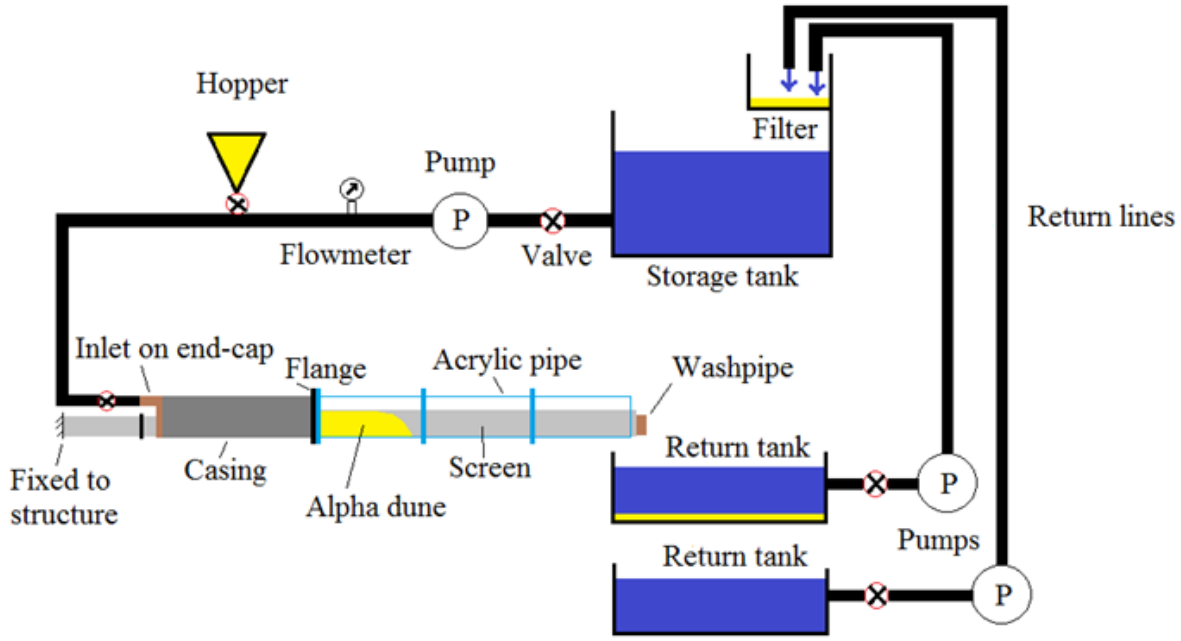

Figure 6-5 Experimental set-up for alpha wave case

6.3.2 Compressive loading on the acrylic pipe

Special care must be taken when introducing acrylic pipe for the full-scale experiment. Screen joints and washpipe will inflict a considerable load on the plastic tube. The acrylic pipe will see some load from the tubulars, and this load needs to be supported to protect the plastic from potential breakage. A method to relieve as much of this load as possible is proposed. The main idea is to support the outlet end to take away some of the weight from

the inside of the plastic tube, and to ensure that the weight of the screen section is distributed to a greater area by resting the screen section on rubber or elastomer elements inside the plastic tube. The plastic tube itself will rest in a number of cradles over the total length. Figure 6-6 shows the experimental set-up and the load supports.

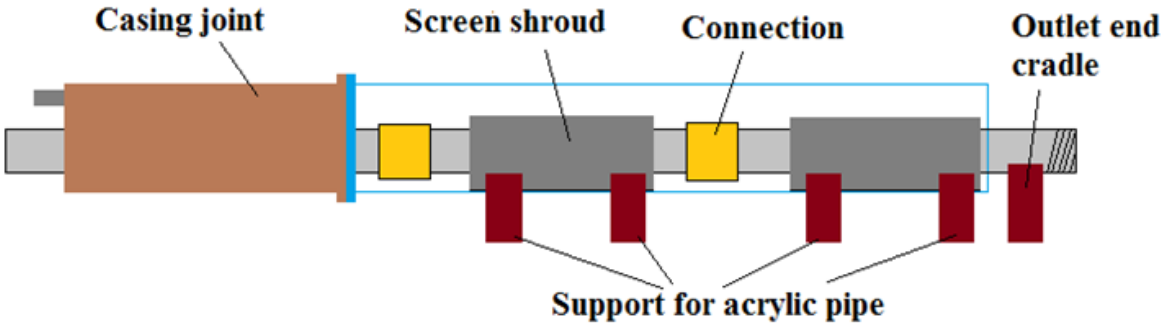

Figure 6-6 Supports for acrylic pipe and outlet

The washpipe used in the experiment will be a 5 in tubular just like in the base case. Other sizes will also be used for experiments, but 5 in will probably be the largest, and so load calculations will be based on this. To save weight, a 5 in tubing with nominal weight of 11.50 lbm/ft is chosen, and the data can be found in API specifications for casing and tubing[49]. Screens used are 6.625 in 33.50 lbm/ft[50]. Screen section will as well be supported inside the casing joint, near the transition to plastic pipe. Therefore, the plastic pipe will only experience loading from screens and washpipe along its length. The remaining length (40 ft) sits inside the 9.625 in casing assembly. In total, the weight both screen and washpipe joints will pose on the inside of the acrylic pipe is:

$$Weight\ of\ screens\ and\ washpipe = 80\ ft * (33.5 + 11.5)\frac{lbm}{ft} = 3600 lbm$$

Over the length of the acrylic pipe, only the shrouded portion of the screens will be in contact with the plastic pipe wall. The outer diameter of the screen is at maximum at the shrouded part . It is reasonable to believe that the loads will be transmitted through the contact points between plastic and the shroud.

Two full lengths of screen joints will be situated inside the length of the acrylic pipe, and this means that a total of 60 ft of the screens will make contact with the plastic pipe, if assuming a 30 ft length of shroud per joint. A rubber/elastomer element will be attached to the full length of the bottom of each shroud. They will be made to transfer the load to an adequately sized area, and safeguard the integrity of the plastic. The element will have a

width of 3 in, but for upcoming calculations it is assumed that only a third of this width will transfer the loads. It is important that the element is wide enough to ensure sufficient load support, but also small enough to influence minimally on the slurry flow.

The acrylic pipe also needs to be supported. Opposite each shroud end, a steel cradle with elastomer/rubber lining will encompass a portion of the outside of the acrylic pipe. This makes sure that the combined load of the screen and washpipe is evenly spread over the support area. Figure 6-7 shows both the internal load support and the external cradle.

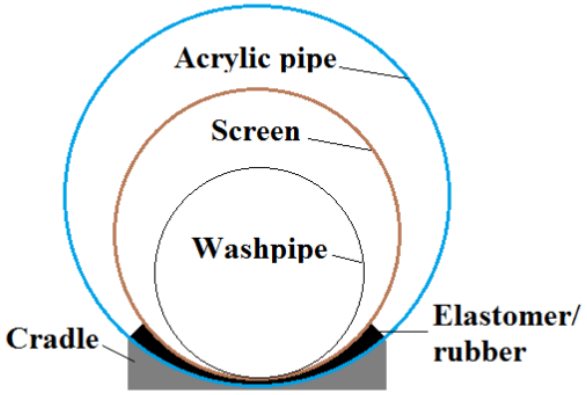

Figure 6-7 Cross-sectional view of annular configuration and load supports

The maximum load the acrylic pipe will experience needs to be calculated. The worst case scenario is a fully gravel packed screen/openhole annulus and carrier fluid present in screen/washpipe annulus and pack voids. The combined mass of gravel and fluid is quantified with background in data from the base case in Chapter 5 (Table 5-1 and 5-2). First, volume of sand fill in annulus is given by:

$$V_{so} = A_{so} L_p \tag{6-4}$$

Here, V_{so} is volume of the screen/openhole annulus for a given length of pipe, A_{so} is the cross-sectional area of the annulus and L_p is length of the acrylic pipe of 80 ft (24.384 m). This yields a volume of about 0.26 m^3. Then the mass of the gravel m_g is:

$$m_g = \rho_{bulk} V_{so} = 1643 \frac{kg}{m^3} * 0.26 m^3 \approx 427 kg$$

The pores of the gravel pack will be saturated with carrier fluid. Porosity ϕ is found from calculations in Appendix B, and the mass of fluid in screen/openhole annulus m_{fso} is:

$$m_{fso} = \rho_f V_{so} \phi = 1237 \frac{kg}{m^3} * 0.26 m^3 * 0.38 \approx 122 kg$$

At last, the mass of fluid in screen/washpipe annulus is calculated. Volume of the annulus V_{wp} for a given pipe length is found using Eq. 6-5, where A_{wp}:

$$V_{wp} = A_{wp} L_p \tag{6-5}$$

This yields a volume of $0.124 m^3$, and the mass of fluid in screen/washpipe annulus is then:

$$m_{fwp} = V_{wp} \rho_f = 0.124 m^3 * 1237 \frac{kg}{m^3} \approx 153 kg$$

The total mass of gravel and fluid inside the acrylic pipe is:

$$m_{gf} = m_g + m_{fso} + m_{fwp} = 702 kg \approx 1548 lbm$$

The maximum total extra weight the plastic pipe can experience is now the sum of the weight of screens and washpipe, and the weight of gravel and fluid:

$$Total\ weight = 3600 lbm + 1548 lbm = 5148 lbm$$

For the load calculations for the screen supports, 30ft of shroud is assumed for each screen joint. As mentioned, the rubber/elastomer elements will have a width of three inches, and a conservative assumption that only a third of this width will transfer the load to the acrylic pipe was made. The total load transferring area can then be approximated. The total weight of the tubulars inside the plastic pipe is divided between the two lengths of shrouds, 60 ft in total. The pressure exerted in psi on the plastic pipe is then, for the combined length of the two shrouds and the element width of one inch:

$$\text{Pressure} = \frac{5148 lbm}{1 in * 60\, ft * 12 \frac{in}{ft}} \approx 14.3 psi$$

The stress on the plastic material is considered to be sufficiently small to proclaim that a 3D stress analysis is not necessary, and the proposed counteractive methods of load support are acceptable.

6.3.3 Calculations using Gruesbeck et al. model

Calculations for the alpha wave experiment are based on the field case of 8.5 in OH, 6.625 in screen and 5 in washpipe from Chapter 5. Pump rate and gravel concentration are similar to the base case, and fluid density and viscosity is assumed to be unchanged for the calculations. Under the assumption that the absolute roughness of the borehole wall is reproducible for the inside of the acrylic pipe, the calculated values from Chapter 5 will still be valid.

Table 6-4 Calculated values and output of modelling using Swamee-Jain friction for 8.5in experimental set-up

Parameters	Values
Screen/openhole annulus	
Q_* equilibrium flow rate in open area	0.003666775 $m^3 s^{-1}$
A_o area open to flow	0.002820977 m^2
A_{so} total area of annulus	0.0106764705 m^2
D_{h*} hydraulic diameter	0.0369537572 m
N_{Re} Reynolds number	37136
λ_* equilibrium friction factor	0.194668899
C_* equilibrium solids concentration	0.2349244472
$(\Delta P/L)_o$ frictional pressure gradient	5505 Pa m^{-1}
ψ incremental pressure drop from solids	2108 Pa m^{-1}
Screen/washpipe annulus	
Q_{wp} equilibrium flow rate	0.015499892 $m^3 s^{-1}$
A_{wp} area of annulus	0.0050965859 m^2
D_{hwp} hydraulic diameter	0.0233934 m
N_{Re} Reynolds number	55004
λ_{wp} equilibrium friction factor	0.031131351
$(\Delta P/L)_{wp}$ frictional pressure gradient	7613 Pa m^{-1}
v_{wp} fluid velocity	3.04 m s^{-1}
Output	
Q_{wp}/Q_m Flow rate split ratio to washpipe/screen annulus	0.80869
γ sector angle	0.7400196208 rad
y_b bed height	0.187666254 m
v_* equilibrium velocity	1.30 m s^{-1}
Volumetric gravel fill percent	73.58
Height fill percent	86.92

Amount of gravel in alpha dune at the calculated volumetric gravel fill percent can be found from a slightly modified Eq. 4-28, using A_g as the gravel filled cross-sectional area of the annulus:

$$m_b = (A_{so} - A_o) L_p \rho_{bulk} \approx 465\, kg$$

Pressure loss through the annuli is found to be 7613 Pa/m. The total pressure loss over the full annuli lengths, from inlet point to outlet is then:

$$dP = 7613\, \frac{Pa}{m} * 36\, m * 10^{-5}\, \frac{bar}{Pa} \approx 2.74 bar$$

6.3.4 Pressure rating of acrylic pipe

An acrylic pipe of 8.5 in ID and a wall thickness of 0.5 in will be proposed for the alpha wave experiment. The burst pressure rating can also for this case be deducted from Barlow's equation (Eq. 6-1), as the criteria for thin walled cylinder is fulfilled.

Burst pressure tolerance is calculated to nearly 73 bar. This is well above the expected pressure loss through the system that was found to be 2.74 bar. The selected wall thickness will warrant resistance to possible impacts during installation, and ensure adequate support of the loads from the screen and washpipe joints.

6.3.5 Amount of fluid and gravel needed

Like for the work string experiment, it is now possible to estimate fluid volume and amount of gravel needed. First, gravel volume in the fully evolved alpha dune is calculated using Eq. 6-2, and then the pumping time for alpha wave to propagate to the outlet is calculated using Eq. 6-3.

$$V_g = (A_{so} - A_o) L_p \frac{\rho_{bulk}}{\rho_s} \approx 0.175 m^3$$

$$T_p = \frac{V_g}{Q_s} = \frac{0.175334615\ m^3}{0.000861415\ \frac{m^3}{s}} \approx 203.5 s$$

Velocity of the alpha wave, v_α is now:

$$v_\alpha = \frac{36m}{203.54s} \approx 0.177m/s$$

The amount of gravel for the actual bed height was calculated in Chapter 6.3.2. The total amount of gravel for the experiment should include an excess in case the actual gravel fill or pumping time is higher than expected. A margin of 50% is proposed, and this yields:

$$m_g = 1.5 * m_b = 1.5 * 464.6kg \approx 700kg$$

For the estimation of fluid volume, the execution of the experiment must first be clarified. Gravel will first be introduced into the system after a stable flow of brine is flowing through and filling the annuli. The return pumps are stopped as gravel is added into the flow, and the volume in both return tanks are noted (level should be as low as possible). This will be done to have volume control of the flow contribution from the individual annuli, and the possibility to estimate the flow rate split after the experiment is finished. As for the gravel calculation, an excess of 50% is recommended. Carrier fluid flow rate, Q_f was calculated in Appendix A, and in combination with the pumping time and margin the volume of fluid needed is:

$$V_f = 1.5Q_f T_p = 0.018305252 \ \frac{m^3}{s} * 203.54s \approx 5.59m^3$$

This is the minimum volume of brine that should be in the storage tank at the moment gravel is introduced and the return pumps are stopped. For practical purposes this is rounded off to 6.0 m^3.

Table 6-5 Overview of brine volumes in system when pumping, alpha wave experiment

System part	Fluid volume (m^3)
Storage tank	6.0
Hose, 40m 3 in ID	0.182
Screen/pipe annulus	0.384
Screen/washpipe annulus	0.184
Return tanks combined	1.0
Return hoses, 2*10m 2 in ID	0.041
Total Volume	**7.8**

Table 6-5 shows the volumes in each part of the system during pumping and gives the grand total brine volume needed as 7.8 m^3. Volume of fluid in the return tanks needs to be as low as possible when return pumps are stopped, because the tanks afterwards will accumulate all the fluid for the remainder of the experiment. It is reasonable to believe that some fluid will be left in the tanks when pumps are stopped, so a total of 1.0 m^3 is suggested. The return tanks must be scaled to hold the estimated volume V_f = 5.59 m^3. As the real flow rate split is not known, each of the tanks must be able to hold the entire volume. Then two tanks of 2*3 m base and 1 m height are proposed, as they have a capacity of 6.0 m^3.

(This page intentionally left blank)

7 CONCLUSIONS

A practical slurry transport model was used to quantify the amount of sedimentation in the horizontal part of the work string during gravel packing. Based on this semi-mechanistic model, the amount of sediments was estimated from the bed height, and the bulk density derived from a proposed particle packing model for the gravel.

Sensitivity study indicates that the internal diameter of the work string should be carefully selected to avoid sedimentation. Pump rate is also governing the degree of sedimentation. The lower the rate, the more gravel is accumulated. Sedimentation in work string is believed to be highly affected by both the internal diameter of the pipe and the pump rate.

Friction in the discharge area above bed is believed to become more affected by the bed surface and near bed area as the bed height increases, directly proportional to the ratio of wetted perimeters for wall and wetted perimeter for bed surface.

Modelling for the alpha wave was done using varying flow rate split, as opposed to what has been seen in earlier theses. The plotted values of mixture velocity above bed and critical velocities from the different models showed little resemblance to what have been seen in the other theses on gravel packing. It is believed that the way flow rate split is implemented in this thesis is truer to the intention of Gruesbeck et al., and is more descriptive for the flow pattern.

The resulting plots of actual mixture velocity above the bed and the critical flow velocities from the different models gave ambiguous results, as up to two equilibrium solutions was found for both Gruesbeck et al. and Penberthy et al. models (their critical velocity curves crossed the mixture velocity curve at two points in some cases). From the pump chart for the gravel pack job, the real gravel fill percent could be approximated. Comparison of this gravel fill to the results from the models indicated that the higher solution of each model was the best match. Resulting gravel fill indicates good correspondence between output from Gruesbeck et al. model and data from the real gravel pack operation.

Gruesbeck et al. model shows good correspondence with field case when assuming a light washout. Penberthy et al. is constantly predicting higher gravel fill than Gruesbeck et al. The model of Oroskar and Turian gave no clear results but is believed to over-predict the gravel fill when applying the presented flow rate split technique, as it is constantly indicating an equilibrium velocity outside the upper boundary of the modelling range.

Frictional pressure drop through a conduit, when transporting slurry over a sediment bed, seems to be more dominated by the bed surface friction when the open area reduces. This is also believed to be the case for flow in screen/openhole annulus during alpha wave propagation. The alpha wave is modelled using a friction factor based on an absolute roughness for the borehole wall, which appears to give a decent match to the actual gravel packing job. It is uncertain if the method of using the wellbore wall roughness gives the best representation of the real friction factor in the screen/openhole annulus. The resulting friction factor is though representing the overall friction, and an effort should be made to implement the concept of bed friction into the equations.

The model used is sensitive to change in washpipe size, and it was not possible to get conclusions for how the change in size affects the gravel fill percent. Washpipe to screen diameter ratio is an important design criteria for the gravel pack operation and is believed to have major influence on the success of packing. A full-scale experiment is advised to investigate the influence further.

Existing critical velocity models developed for gravel packing are based on small-scale experiments. Oroskar and Turian model is used in other Mater's theses, but this model was not made specifically for the purpose of gravel packing. It might not be descriptive for eccentric annuli configurations, as it was developed for flow in circular conduits.

Findings from modelling both the work string and alpha wave cases, indicates that verification from experiments is required. Gruesbeck et al. model is based on small-scale experiments. Carrying out a real full-scale diameters experiment is not known to been done, and it is believed to bring clarity to the process of slurry transport in gravel packing.

REFERENCES

[1] C. Gruesbeck, W. M. Salathiel, and E. E. Echols, "Design of Gravel Packs in Deviated Wellbores," *Journal of Petroleum Technology*, vol. 31, pp. 109-115, 1979.
[2] W. L. Penberthy, Jr., K. L. Bickham, H. T. Nguyen, and T. A. Paulley, "Gravel Placement in Horizontal Wells," *SPE Drilling and Completion*, vol. 12, pp. 85-92, 1997.
[3] A. R. Oroskar and R. M. Turian, "The Critical Velocity in Pipeline Flow of Slurries," *AIChE Journal*, vol. 26, pp. 550-558, 1980.
[4] V. Matoušek, "Predictive model for frictional pressure drop in settling-slurry pipe with stationary deposit," *Powder Technology*, vol. 192, pp. 367-374, 2009.
[5] J. Bellarby, *Well Completion Design*, 1st ed. vol. 56. Oxford: Elsevier, 2009.
[6] W. K. Ott and J. D. Woods, *Modern Sandface Completion Practices Handbook*, 2nd ed. Houston, Texas: World Oil, 2005.
[7] R. J. Saucier, "Considerations in Gravel Pack Design," *Journal of Petroleum Technology*, vol. 26, pp. 205-212, 1974.
[8] American Petroleum Institute, "ANSI/API Recommended Practice 19C," ed. Washington, USA: API Publishing Services, 2008.
[9] F. M. White, *Viscous Fluid Flow*, 2nd ed.: McGraw-Hill International Editions, 1991.
[10] R. B. Bird, W. E. Stewart, and E. N. Lightfoot, *Transport Phenomena*: John Wiley & Sons, 1960.
[11] E. Loth, "Drag of non-spherical solid particles of regular and irregular shape," *Powder Technology*, vol. 182, pp. 342-353, 2008.
[12] A. D. Salman and A. Verba, "New Aproximate Equations to Estimate the Drag Coefficient of Different Particles of Regular Shape," *Periodica Polytechnica. Chemical Engineering*, vol. 32, p. 261, 1988.
[13] S. A. Miedema, *Slurry Transport: Fundamentals, a historical overview and the Delft Head Loss & Limit Deposit Velocity Framework*, 1st ed.: Delft University of Technology, 2016.
[14] R. Clift, J. R. Grace, and M. E. Weber, *Bubbles, Drops and Particles*. New York, USA: Academic Press, Inc., 1978.
[15] H. Chen, "Flow and Pressure Profile Distributions in Gravel Pack Equipments," MSc, Faculty of Science and Technology, University of Stavanger, Stavanger, 2008.
[16] Y. R. Costamte, "Modelling of Open-Hole Gravel Packing on Longer Blank Pipe and Screen Sections," MSc, Faculty of Science and Technology, University of Stavanger, Stavanger, 2010.
[17] S. M. Peker and Ş. Ş. Helvacı, *Solid-Liquid Two Phase Flow*, 1st ed. Netherlands: Elsevier Science, 2008.
[18] H. Blasius, "Das Aehnlichkeitsgesetz bei Reibungsvorgängen in Flüssigkeiten," in *Mitteilungen über Forschungsarbeiten auf dem Gebiete des Ingenieurwesens*, ed Berlin, Heidelberg: Springer, 1913, pp. 1-41.
[19] H. D. Beggs, *Production Optimization Using NODAL™ Analysis*, 2nd ed. Tulsa, Okla: OGCI and Petroskills publ., 2003.
[20] D. C. Rennels and H. M. Hudson, "Surface Friction," in *Pipe Flow: A Practical and Comprehensive Guide*, ed. Hoboken: Wiley, 2012, pp. 77-87.
[21] W. C. Lyons, B. Guo, R. L. Graham, and G. D. Hawley, *Air and Gas Drilling Manual: Applications for Oil and Gas Recovery Wells and Geothermal Fluids Recovery Wells*, 3rd ed. Amsterdam ; Boston: Elsevier/Gulf Professional Publishing, 2009.

[22] J. Nikuradse, "Strömungsgesetze in rauhen Rohren. vDI Forshungsheft, 361," *English, in Technical Memorandum*, vol. 1292, 1933.
[23] C. F. Colebrook, "Turbulent Flow in Pipes, With Particular Reference to the Transition Region Between the Smooth and Rough Pipe Laws," *Journal of the ICE*, vol. 11, pp. 133-156, 1939.
[24] P. K. Swamee and A. K. Jain, "Explicit Equations for Pipe-Flow Problems," *Journal of the Hydraulics Division, ASCE*, vol. 102, pp. 657-664, 1976.
[25] P. Glover. (2002, Petrophysics MSc Course Notes. Available: http://homepages.see.leeds.ac.uk/~earpwjg/PG_EN/CD%20Contents/GGL-66565%20Petrophysics%20English/Chapter%202.PDF
[26] T. Aste and D. Weaire, *The Pursuit of Perfect Packing*, 1st ed. Bristol: Institute of Physics Publishing, 2000.
[27] A. V. Anikeenko, N. N. Medvedev, and T. Aste, "Structural and entropic insights into the nature of the random-close-packing limit," *Physical review E, Statistical, nonlinear, and soft matter physics*, vol. 77, pp. 031101-1-031101-9, 2008.
[28] G. Y. Onoda and E. G. Liniger, "Random Loose Packings of Uniform Spheres and the Dilatancy Onset," *Physical Review Letters*, vol. 64, pp. 2727-2730, 1990.
[29] E. Santiso and E. A. Müller, "Dense packing of binary and polydisperse hard spheres," *Molecular Physics*, vol. 100, pp. 2461-2469, 2002.
[30] V. Matoušek and J. Krupička, "On Equivalent Roughness of Mobile Bed at High Shear Stress," *Journal of Hydrology and Hydromechanics*, vol. 57, pp. 191-199, 2009.
[31] V. Matoušek, "Interaction of slurry pipe flow with a stationary bed," *Journal of the Southern African Institute of Mining and Metallurgy*, vol. 107, pp. 365-372, 2007.
[32] F. J. Pugh, "Bed-load velocity and concentration profiles in high shear stress flows," PhD, Department of Civil Engineering, Queen's University at Kingston, Ontario, Canada, 1995.
[33] F. N. Nnadi, "Bed-load transport at high shear stress: with application to friction in rivers and sand waves," PhD, Department of Civil Engineering, Queen's University at Kingston, Ontario, Canada, 1992.
[34] E. Meyer-Peter and R. Müller, "Formulas for bed-load transport," in *International Association for Hydraulic Structures Research 2nd meeting*, Stockholm, Sweden, 1948, pp. 39-64.
[35] V. Matoušek, "Solids Transport Formula in Predictive Model for Pipe Flow of Slurry above Deposit," *Particulate Science and Technology*, vol. 29, pp. 89-106, 2011.
[36] F. J. Pugh and K. C. Wilson, "Role of the interface in stratified slurry flow," *Powder Technology*, vol. 104, pp. 221-226, 1999.
[37] F. J. Pugh and K. C. Wilson, "Velocity and Concentration Distributions in Sheet Flow Above Plane Beds," *Journal of Hydraulic Engineering*, vol. 125, p. 117, 1999.
[38] L. Prandtl, "Über Flüssigkeitsbewegung bei sehr kleiner Reibung," *Verhandlungen des III Internationalen Mathematiker-Kongresses, Heidelberg, 1904*, pp. 484-491, 1905.
[39] A. Shields, "Anwendung der Ähnlichkeitsmechanik und der Turbulenzforschung auf die Geschiebebewegung," *Mitteilungen der Preussischen Versuchsanstalt für Wasser-, Erd- und Schiffbau*, vol. 26, pp. 1-26, 1936.
[40] Z. Cao, G. Pender, and J. Meng, "Explicit Formulation of the Shields Diagram for Incipient Motion of Sediment," *Journal of Hydraulic Engineering*, vol. 132, pp. 1097-1099, 2006.
[41] Odfjell Well Services. (05.05.2017). *Drillpipe specifications*. Available: http://www.odfjellwellservices.com/rental-services/tubulars/drillpipe-specs/
[42] International Organization for Standardization, "Petroleum and natural gas industries: Steel drill pipe (ISO 11961:2008)," vol. NS-EN ISO 11961:2008, ed. Lysaker: Standard Norge, 2008.

[43] R. Bergkvam, "Parametric sensitivity studies of gravel packing," MSc, Faculty of Science and Technology, University of Stavanger, Stavanger, 2015.
[44] A. Einstein, "Über die von der molekularkinetischen Theorie der Wärme geforderte Bewegung von in ruhenden Flüssigkeiten suspendierten Teilchen," *Annalen der Physik*, vol. 322, pp. 549-560, 1905.
[45] D. G. Thomas, "Transport characteristics of suspension: VIII. A note on the viscosity of Newtonian suspensions of uniform spherical particles," *Journal of Colloid Science*, vol. 20, pp. 267-277, 1965.
[46] F. B. Soepyan, S. Cremaschi, C. Sarica, H. J. Subramani, and G. E. Kouba, "Model parameter fine-tuning and ranking methodology to improve the accuracy of threshold velocity predictions for solid particle transport," *Journal of Petroleum Science and Engineering*, vol. 110, pp. 210-224, 2013.
[47] L. F. Moody, "Friction factors for pipe flow," *Trans. Asme*, vol. 66, pp. 671-684, 1944.
[48] J. A. Brydson, *Plastics Materials*, 6th ed. Kent: Elsevier Science, 2013.
[49] International Organization for Standardization, *Specification for casing and tubing : API Specification 5CT/ISO 11960:2004, Petroleum and natural gas industries - steel pipes for use as casing and tubing for wells*, 8th ed. Washington, D.C: American Petroleum Institute, 2005.
[50] Pro-Quip. (06.26.2017). *Screen specifications*. Available: http://ic.pro-quip.no/Equipments/Details/10199

(This page intentionally left blank)

APPENDIX A – Field data for modelling of work string case

Table A-1 Data for work string modelling

Parameters	Value
Pipe ID, D_p	5.045 in = 0.128143 m
Carrier fluid density, ρ_f	1250 kg/m^3
Particle density, ρ_s	2650 kg/m^3
Gravel mass rate	136.965 kg/min
Pump rate, Q_{lpm}	1150 lpm

Mixture flow rate:

$$Q_m = \frac{1150\,\frac{litres}{\min}}{1000\,\frac{litres}{m^3} * 60\,\frac{s}{\min}} = 0.019166667\,\frac{m^3}{s}$$

Solids flow rate:

$$Q_s = \frac{136.965\,\frac{kg}{\min}}{2650\,\frac{kg}{m^3} * 60\,\frac{s}{\min}} = 0.000861415\,\frac{m^3}{s}$$

Carrier fluid flow rate:

$$Q_f = Q_m - Q_s = 0.018305252\,\frac{m^3}{s}$$

Gravel concentration:

Given mixture flow rate as cubic meters per minute, the mass rate of the solids needs to be expressed in the same time unit to calculate gravel concentration.

$$\dot{m} = \frac{136.965\,\frac{kg}{\min}}{60\,\frac{s}{\min}} = 2.28275\,\frac{kg}{s}$$

$$Gravel\ conc = \frac{\dot{m}}{Q_m} = \frac{2.28275\ \frac{kg}{s}}{0.019166667\frac{m^3}{s}} * 0.003875\frac{m^3}{gal} * 2.204622622\ \frac{lbs}{kg} \approx 1.0175\ ppa$$

Mean delivered gravel concentration:

$$C_{vd} = \frac{Q_s}{Q_m} = \frac{0.000861415\frac{m^3}{s}}{0.019166667\frac{m^3}{s}} = 0.0044943396$$

Velocity of mixture:

Mixture velocity is given as mixture flow rate through the full cross-sectional area of the drillpipe.

$$A_p = \frac{\pi D_p^2}{4} = 0.012896731 m^2$$

$$v_m = \frac{Q_m}{A_p} = 1.486164724\frac{m}{s}$$

APPENDIX B – Calculations of median particle diameter and bulk density

Table A-2 Sieve analysis data

Mesh	Gap dimension (mm)	Weight percentage	Percent passing
18	1.000		
20	0.841	0.6	99.4
25	0.707	7.3	92.1
30	0.595	36.7	55.4
35	0.500	39.9	15.5
40	0.400	15.0	0.5
45/Pan	0.354	0.5	

Table A-2 gives the weight percent left on top of the respective mesh after the sieving process. The sand content in the pan is a mix of finer particles that have gone through the arrangement. Some assumptions have to be made, as the sizes of the samples left in pan and the first sieve are not further investigated. The weight percent of these two samples are low compared to the others. Therefore the assumption is made that the diameter range of the sample received on the top sieve (20 mesh – 0.841 mm) is between this sieve and the next consecutive standard mesh size (18 mesh – 1.000 mm). A similar assumption is made for the sample received in the pan; all particles are assumed to be larger than the next standard sieve (45 mesh – 0.354 mm). These assumptions seem reasonable, as the weight percentages of the samples in question are quite low.

Based on the values in the table and values for the additional mesh sizes, a cumulative distribution can be made, showing a continuous particle diameter distribution and passing percent expressed as probability (Figure A-1).

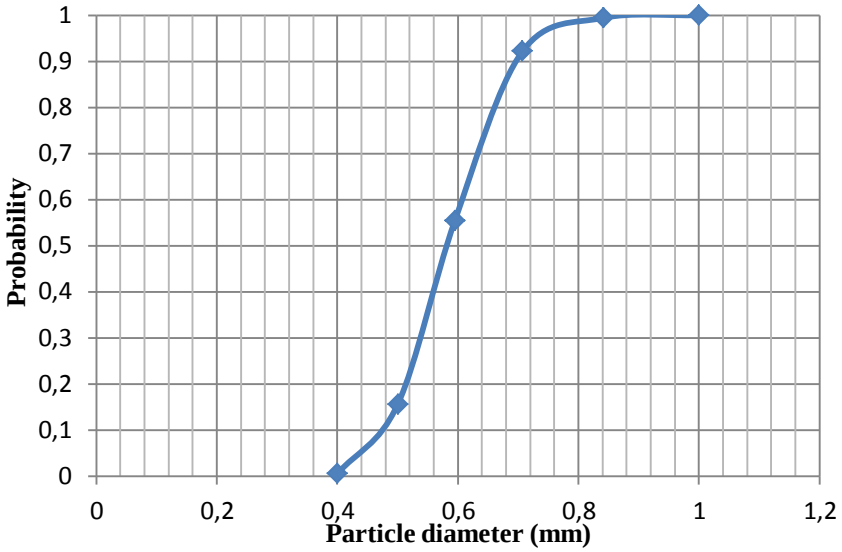

Figure A-1 Exceedance curve showing cumulative particle distribution

The value of the median particle diameter d_{50} is read directly from the graph as the particle diameter at probability of 0.5. The value is approximately 0.58 mm.

$$d_{50} \approx 0.58mm$$

To find the bulk density of the gravel, the approach explained in Chapter 3.4.2 is used. For this, a value for the standard deviation of the distribution is needed. Particle distribution graph plotted as particle diameters and respective probabilities are shown in Figure A-2. Here, the mid-point between the sieves are chosen to represent the probability of the particle diameter, and it may therefore not be an exact presentation. The plotted graph indicates a lognormal distribution. To find the standard deviation, the mean particle diameter needs to be calculated. For a lognormal distribution, the following equation gives the mean particle diameter as the expected value:

$$E(X) = e^{\mu_d + \frac{\sigma^2}{2}} = \int_0^\infty (1 - F(x))dx$$

Here, μ_d is median particle diameter, σ is standard deviation and $F(x)$ is a function describing the cumulative particle distribution. Mean is given by the value of the area above the graph. Solving this can be done by numerical integration to find the area under the graph, and then subtract it from the total area within the boundaries. Total area has the value of 1. The area below the graph can be handled as six sub-areas given by the ranges between the sieves. Each sub-area can be represented by a trapezoid, which will give a close enough match to the curve. Calculation gives a value of 0.4112205. Mean particle

diameter is then 0.5887795 mm. Knowing both the median and mean diameter, the equation above can be used to solve for the standard deviation. A value of 0.173 is found. According to Table 3-5, this yields a packing density of 0.62, and hence a porosity of 0.38. With a particle density is 2650 kg/m^3, Eq. 3-59 yields the bulk density:

$$\rho_{bulk} = 0.62 * 2650 \frac{kg}{m^3} = 1643 \frac{kg}{m^3}$$

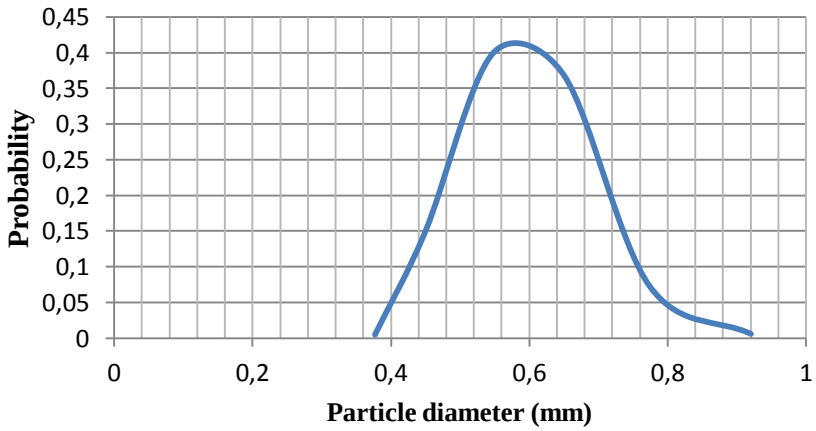

Figure A-2 Particle distribution

(This page intentionally left blank)

APPENDIX C – Generic field case data

Table A-3 Generic data

Parameter	Value
Pore pressure	210 bar
Reservoir temperature	85˚C/185˚F
Surface temperature	15˚C/59˚F
TVD	2000 m
Brine density, ρ_f	1250 kg/m^3
Brine viscosity, μ_f	1.6 cP/0.0016 kg m^{-1}s^{-1}
Circulating temperature	40˚C/104˚F

Conversion from Celsius to Fahrenheit:

$$˚F = ˚C*1.8 + 32$$

Static temperature gradient:

$$(85˚C - 15˚C)/2000m = 0.035˚C/m$$

Fluid density converted to field units:

$$\rho_f = 1250\ \frac{kg}{m^3} * 2.20462262\ \frac{lbm}{kg} * 0.003875\ \frac{m^3}{gal} = 10.679\ ppg$$

The fluid density is then corrected for circulating temperature, using a simple density reduction per temperature relationship for brines. For brines in the range 9.1 to 11.0 ppg, there is a density reduction of 0.0025 ppg/˚F. The difference between circulating and surface temperature is 45˚F. This yields a density reduction of 0.1125 ppg. The corrected fluid density for temperature in SI units is now:

$$\rho_f = (10.679 - 0.1125) * 0.45359237\ \frac{kg}{lbm} * \frac{1}{0.003875}\ \frac{gal}{m^3} = 1237\ \frac{kg}{m^3}$$

(This page intentionally left blank)

APPENDIX D – Iteration on the terminal settling velocity

vguess (m/s)	v_t (m/s)	Rep	C_D
0 063700	0.064223	28.5639	2.1010
0 063710	0.064226	28.5684	2.1008
0 063720	0.064229	28.5728	2.1006
0 063730	0.064232	28.5773	2.1004
0 063740	0.064235	28.5818	2.1002
0 063750	0.064238	28.5863	2.1000
0 063760	0.064241	28.5908	2.0998
0 063770	0.064244	28.5953	2.0996
0 063780	0.064247	28.5997	2.0994
0 063790	0.064250	28.6042	2.0992
0 063800	0.064253	28.6087	2.0990
0 063810	0.064256	28.6132	2.0989
0 063820	0.064259	28.6177	2.0987
0 063830	0.064262	28.6222	2.0985
0 063840	0.064265	28.6267	2.0983
0 063850	0.064268	28.6311	2.0981
0 063860	0.064271	28.6356	2.0979
0 063870	0.064274	28.6401	2.0977
0 063880	0.064277	28.6446	2.0975
0 063890	0.064280	28.6491	2.0973
0 063900	0.064283	28.6536	2.0971
0 063910	0.064286	28.6580	2.0969
0 063920	0.064288	28.6625	2.0967
0 063930	0.064291	28.6670	2.0965
0 063940	0.064294	28.6715	2.0963
0 063950	0.064297	28.6760	2.0962
0 063960	0.064300	28.6805	2.0960
0 063970	0.064303	28.6849	2.0958
0 063980	0.064306	28.6894	2.0956
0 063990	0.064309	28.6939	2.0954
0 064000	0.064312	28.6984	2.0952
0 064010	0.064315	28.7029	2.0950
0.064020	0.064318	28.7074	2.0948
0.064030	0.064321	28.7119	2.0946
0.064040	0.064324	28.7163	2.0944
0.064050	0.064327	28.7208	2.0942
0.064060	0.064330	28.7253	2.0940
0.064070	0.064333	28.7298	2.0938
0.064080	0.064336	28.7343	2.0937

vguess (m/s)	v_t (m/s)	Rep	C_D
0.064090	0.064339	28.7388	2.0935
0.064100	0.064342	28.7432	2.0933
0.064110	0.064345	28.7477	2.0931
0.064120	0.064347	28.7522	2.0929
0.064130	0.064350	28.7567	2.0927
0.064140	0.064353	28.7612	2.0925
0.064150	0.064356	28.7657	2.0923
0.064160	0.064359	28.7701	2.0921
0.064170	0.064362	28.7746	2.0919
0.064180	0.064365	28.7791	2.0917
0.064190	0.064368	28.7836	2.0915
0.064200	0.064371	28.7881	2.0914
0.064210	0.064374	28.7926	2.0912
0.064220	0.064377	28.7971	2.0910
0.064230	0.064380	28.8015	2.0908
0.064240	0.064383	28.8060	2.0906
0.064250	0.064386	28.8105	2.0904
0.064260	0.064389	28.8150	2.0902
0.064270	0.064392	28.8195	2.0900
0.064280	0.064395	28.8240	2.0898
0.064290	0.064397	28.8284	2.0896
0.064300	0.064400	28.8329	2.0894
0.064310	0.064403	28.8374	2.0893
0.064320	0.064406	28.8419	2.0891
0.064330	0.064409	28.8464	2.0889
0.064340	0.064412	28.8509	2.0887
0.064350	0.064415	28.8553	2.0885
0.064360	0.064418	28.8598	2.0883
0.064370	0.064421	28.8643	2.0881
0.064380	0.064424	28.8688	2.0879
0.064390	0.064427	28.8733	2.0877
0.064400	0.064430	28.8778	2.0875
0.064410	0.064433	28.8822	2.0874
0.064420	0.064436	28.8867	2.0872
0.064430	0.064439	28.8912	2.0870
0.064440	0.064441	28.8957	2.0868
0.064450	0.064444	28.9002	2.0866
0.064460	0.064447	28.9047	2.0864
0.064470	0.064450	28.9092	2.0862

(This page intentionally left blank)

APPENDIX E – Gruesbeck et al. equilibrium velocity for 8.5 in OH using Swamee-Jain friction factor

Qwp/Q	Gravel fill %	Mixture velocity (m/s)	Gruesbeck (m/s)
72.538	65.114	1.41318	1.32948
76.122	68.849	1.37609	1.31601
77.975	70.721	1.35045	1.30949
79.795	72.526	1.32026	1.30344
80.692	73.404	1.30329	1.30062
80.869	73.578	1.29982	1.30006
83.311	75.938	1.24514	1.29303
84.999	77.545	1.19930	1.28890
88.223	80.563	1.08775	1,28383
91.3185	83.323	0.93455	1.28717
92.1179	83.973	0.88292	1.29118
92.99	84.608	0.81760	1.29875

(This page intentionally left blank)

APPENDIX F – Gruesbeck et al. equilibrium velocity and comparison to other models for 8.5 in OH using Swamee-Jain friction factor

Qwp/Q	Gravel fill %	Mixture velocity (m/s)	Gruesbeck (m/s)	O&T (m/s)	Penberthy (m/s)
72.538	65.114	1.41318	1.32948	1.10289	1.34907
76.122	68.849	1.37609	1.31601	1.07581	1.29856
77.975	70.721	1.35045	1.30949	1.06070	1.27175
79.795	72.526	1.32026	1.30344	1.04478	1.24480
80.692	73.404	1.30329	1.30062	1.03643	1.23128
80.869	73.578	1.29982	1.30006	1.03472	1.22857
83.311	75.938	1.24514	1.29303	1.00931	1.19050
84.999	77.545	1.19930	1.28890	0.98887	1.16316
88.223	80.563	1.08775	1.28383	0.93820	1.10811
91.3185	83.323	0.93455	1.28717	0.85758	1.05259
92.1179	83.973	0.88292	1.29118	0.82500	1.03864
92.99	84.608	0.81760	1.29875	0.77776	1.02466

(This page intentionally left blank)

APPENDIX G – Gruesbeck et al. equilibrium velocity and comparison to other models for 9 in OH using Swamee-Jain friction factor

Qwp/Q	Gravel fill %	Mixture velocity (m/s)	Gruesbeck (m/s)	O&T (m/s)	Penberthy (m/s)
56.189	60.608	1.41077	1.39799	1.20934	1.56467
59.00	63.477	1.42393	1.38318	1.18950	1.52518
62.878	67.122	1.43220	1.36423	1.16293	1.47196
66.85	70.560	1.42832	1.34631	1.13599	1.41812
70.859	73.789	1.41024	1.32959	1.10836	1.36366
74.836	76.807	1.37624	1.31426	1.07943	1.30862
78.718	79.614	1.32423	1.30066	1.04824	1.25302
79.666	80.283	1.30818	1.29757	1.03990	1.23904
80.042	80.547	1.30142	1.29638	1.03649	1.23343
80.23	80.679	1.29791	1.29579	1.03477	1.23063
80.37	80.777	1.29530	1.29535	1.03347	1.22853
82.44	82.212	1.25223	1.28921	1.01300	1.19689
85.955	84.603	1.15709	1.28080	0.97021	1.14024
89.26	86.790	1.03125	1.27755	0.91128	1.08310
92.538	88.776	0.84327	1.28827	0.79969	1.02551

(This page intentionally left blank)

APPENDIX H – Gruesbeck et al. equilibrium velocity and comparison to other models for 9.5 in OH using Swamee-Jain friction factor

Qwp/Q	Gravel fill %	Mixture velocity (m/s)	Gruesbeck (m/s)	O&T (m/s)	Penberthy (m/s)
42.7	55.798	1.25503	1.47965	1.31197	1.76586
44.94	58.612	1.28796	1.46227	1.29115	1.72689
48.16	62.222	1.32852	1.43950	1.26348	1.67430
53.47	67.325	1.37866	1.40653	1.22216	1.59407
59.265	72.040	1.41052	1.37531	1.18093	1.51230
63.331	74.964	1.41800	1.35571	1.15331	1.45698
67.49	77.710	1.41203	1.33728	1.12530	1.40103
71.675	80.276	1.39035	1.32022	1.09648	1.34448
75.806	82.664	1.35113	1.30474	1.06611	1.28736
79.87	84.905	1.29109	1.29104	1.03241	1.22881
83.622	86.906	1.21000	1.28025	0.99460	1.17148
87.199	88.766	1.10316	1.27310	0.94602	1.11278
90.572	90.455	0.95625	1.27335	0.87255	1.05361
92.286	91.237	0.85221	1.28068	0.80821	1.02385

(This page intentionally left blank)

Appendix I – Gruesbeck et al. equilibrium velocity and comparison to other models for 9 in OH with different viscosities

Viscosity 1.0 cP:

Qwp/Q	Gravel fill %	Mixture velocity (m/s)	Gruesbeck (m/s)	O&T (m/s)	Penberthy (m/s)
56.65	60.608	1.39592	1.34276	1.26310	1.56467
59.442	63.477	1.40858	1.32858	1.24237	1.52518
63.285	67.122	1.41650	1.31042	1.21457	1.47196
67.225	70.560	1.41216	1.29326	1.18639	1.41812
71.2	73.789	1.39374	1.27727	1.15745	1.36366
75.145	76.807	1.35934	1.26265	1.12712	1.30862
78.994	79.614	1.30706	1.24970	1.09435	1.25302
80.863	80.939	1.27355	1.24399	1.07650	1.22502
82.478	82.067	1.23942	1.23946	1.05954	1.20016
82.687	82.212	1.23462	1.23890	1.05722	1.19689
86.1805	84.603	1.13851	1.23116	1.01187	1.14024
89.4775	86.790	1.01036	1.22879	0.94857	1.08310
92.847	88.776	0.80835	1.24289	0.81967	1.02551

Viscosity 2.2 cP:

Qwp/Q	Gravel fill %	Mixture velocity (m/s)	Gruesbeck (m/s)	O&T (m/s)	Penberthy (m/s)
55.774	60.608	1.42413	1.41787	1.17392	1.56467
58.607	63.477	1.43758	1.40282	1.15468	1.52518
62.511	67.122	1.44636	1.38355	1.12890	1.47196
66.513	70.560	1.44284	1.36532	1.10280	1.41812
70.5515	73.789	1.42512	1.34829	1.07604	1.36366
74.56	76.807	1.39134	1.33267	1.04806	1.30862
78.47	79.614	1.33966	1.31875	1.01793	1.25302
79.979	80.669	1.31377	1.31379	1.00505	1.23083
80.368	80.939	1.30649	1.31256	1.00158	1.22502
82.217	82.212	1.26814	1.30696	0.98398	1.19689
85.754	84.603	1.17365	1.29814	0.94296	1.14024
89.067	86.790	1.04978	1.29420	0.88710	1.08310
92.294	88.776	0.87085	1.30244	0.78628	1.02551